PERSONAL CLASSIFICATION SYSTEMS AIDED BY FUZZY LOGIC

TAKAHIRO TAKEDA

MARCH 2014

PERSONAL CLASSIFICATION SYSTEMS AIDED BY FUZZY LOGIC

BY

TAKAHIRO TAKEDA

A dissertation submitted in partial fulfillment of the requirement for the degree of

DOCTOR OF ENGINEERING

UNIVERSITY OF HYOGO, JAPAN

MARCH 2014

To my mother, father, and sister for helping me bold the foundations in my life and allowing me to give my studies.

Acknowledgments

I would like to appreciate, first of all, Professor Yutaka Hata of University of Hyogo for giving me the opportunity to study under him. I am grateful to Associate Professor Syoji Kobashi of University of Hyogo, and Associate Professor Kei Kuramoto of University of Hyogo that they guide my education to a direction I may not have otherwise considered. Their wise counsels and supports are invaluable.

I would like to thank Doctor Kazuhiko Taniguchi and Tadahito Egawa of Kinden Corporation, Mister Kazunari Asari of The Kansai Electric Power Company Inc. and Mister Toshiyuki Sawayama of New Sensor Incorporated for providing an experimental environment, and helpful discussion in the field of sensor.

I would like to thank Professor Yoshitada Sakai of Division of Rehabilitaion Medicine, Kobe University Graduate School of Medicine and Doctor Hiroshi Nakajima in OMRON Corporation for helpful discussion in the field of health monitoring.

The author also would like to thank to all volunteers. I must also thank all members in Information Systems Laboratory for their encouragement and fruitful discussions.

PREFACE

This dissertation introduces personal classification systems aided by fuzzy logic. The classification systems are used in our daylily lives such as vending machine, security system, heath management system and so on. Especially, the biometric security and health condition estimation are important to our society. Generally speaking, human movements are individually different by our physical function such as gender, age, height and so on and physiological function such as health condition, mental state, habit and so on. It is considered that by measuring the movement, we are able to know the functions of a person. The dissertation describes four classification methods based on movement measurement; an object classification method to adults, children, toddlers and other object from distance distribution data, a foot-age estimation method from sole pressure distribution data, a walking ability evaluation method from sole pressure distribution data, and a biometric personal authentication method from sole pressure distribution data.

In the object classification method using time-of-flight (TOF) principal camera, the system classifies moving objects to adults, children, toddlers and other objects such as animals or baggage. The TOF camera acquires distance distribution images. The moving objects are detected from the images by fuzzy *k*-means clustering method. The classification system extracts height, thickness, aspect ratio and occupancy of a silhouette as features of the detected object to classify it. These features are gnomically calculated from distance information and camera installation parameters. For classification, the system determines fuzzy degree of adult, child, toddler and objects, and the object. In experiment, the method classified subjects with good classification rate.

In the foot-age estimation method from sole pressure distribution, we estimate a foot-age by classifying the walker to young age, middle age and elderly group. The sole pressure distribution while walking is acquired by mat-type load distribution sensor. The method extracts step length, step center-of-sole-pressure (COP) width, CSP trajectory and time of double support period. The fuzzy degree of young, middle and elderly are calculated by statistically determined fuzzy membership function, and the foot-age is estimated from these fuzzy degrees by fuzzy MIN-MAX center-of-gravity method. In addition, an automated diagnosis and advice system based on foot-age is proposed.

In the walking ability evaluation method from sole pressure distribution data, we develop a gait level index which is quantitative index to evaluate gait level by classifying the data to patients or commons. The method extracts gait speed, time of double support and gait balance as gait features. The gait level index is estimated by fuzzy MIN-MAX center-of-gravity method. In experiment, we took sole pressure data from 10 patients and 90 commons. As the results this method estimated gait level index.

The biometric security system based on walking authenticates person by gait features extracted from shape of sole and white shift from sole pressure distributions. The fuzzy degree of similarities are decided by using statistically learned fuzzy membership functions for right and left sole, independently. The fuzzy degree of sole pressure data is calculated by combining fuzzy degrees of right and left sole. In experiment, the system authenticated person with better accuracy than other method based on walking.

Finally, we conclude this classification methods for security and healthcare system.

Contents

1 Introduction

In our life, classification systems are used for various fields. Here, the classification system is defined as a system which classifies something to categories provided in the common characteristics. For example, a vertebrate animals are categorized into “Mammals”, “Aves”, “Amphibian” , “Reptile”, and “Fish”. And, they are classified by their birth, living space, shape, respiration and so on. Moreover, security systems classify us to administrated person or not, and vending machines also classify monies with high accuracy. Therefore, the classifications are important in our society. However, the systems sometimes request us to manual inputs and manual classifications. Representative examples are as follows; the age of a chopper is checked when the shopper is trying to buy liquor or cigarettes, medical doctors determine health condition of a patient by their subjective experience. The manual classifications induce problems such as low user-friendliness, false classification and high human costs. Recently, a necessity of automated classification system is increase with incensement of automation system and subdivision of categories. There are three types automated classification system. As the first type, the system uses manual inputted information such as network authentication, diagnosis based on medical interview sheet and so on. Generally said, it has higher accuracy and lower user-friendliness. Second type automated classification system uses a property which records information of the person. For example, an identification (ID) card, a key and a clinical record are used for personal authentication or diagnosis. It has middle accuracy and user-friendliness. As the third, the system measures classification target directory. It is used for vending machine and biometric authentication. In this study, we focus on the classification system based on directory measurement for their user user-friendliness. When classification target is standardized objects, the system can be developed by simple pattern matching method, because a time unchangeableness of the target is high. However, the human beings and other living bodies might vary at measurement date and time. Therefore, it is difficult to develop a classification systems for human by their time variability and individuality.

There are many sensors to measure human and living bodies. The camera which is one of non-contact sensors acquires appearance body from single shot photograph, and it obtains motions and activities of the body from moving images. The non-contact sensors can measure targets with long range and wide view. In generally, the obtained images include background, noise, and non-target object. It is needed to extract the body from image by background subtraction and clustering method. However, because sometimes noisy object interrupts by an occluding, it is difficult to extract the target. To improve extraction rate, distance information is used for human detection. By using the distance information, we can find the occluded person. The distance information is acquired by stereoscopic vision camera, laser triangulation camera and time-of-flight (TOF) principal camera. The force plate which is one of contact sensors acquires center-of-gravities among human standing. The contact sensors obtain information at a surface of a human body. For example, pressure sensor acquires a pressure between the sensor and contacted point of the body, and the thermal sensor measures a body temperature. A measurement area of the type sensor is narrow, but it can mea rue the information certainly.

This study proposes classification systems for human based on fuzzy logic. The fuzzy logic is one of soft computing method to treat ambiguous values such as “Tall”, “Fast”, “Big”, “Long” by multi-valued logic, and it is widely used for human-related sciences and successfully solves these problems. Biometrics is one of these attractive applications. It requires feature extraction and matching tasks. Especially, fuzzy logic has been successfully applied to many biometric matching systems. In the applications, fuzzy logic achieved higher robustness, adaptively and precision. Here, fuzzy rules are derived from human experiences and knowledge to understand fuzzy values of characteristics. To classify human, fuzzy degrees are obtained from developed fuzzy rules and fuzzy membership functions. In this study, the fuzzy degree is treated as a similarity degree of a category. Then, our systems classifies target objects by the fuzzy degree. One of merits of using the fuzzy logic, it can be feed backed by human experiences and knowledge, therefore, the system is comprehensible for human.

This article describes four personal classification systems. In the Chapter 2, an object classification method from distance distribution images is proposed. The method is proposed as night vision security system by classifying moving objects. In the system, a TOF camera measures distance distribution image. The TOF camera is one of active infrared camera, and it is able to measure distance information at daytime and nighttime. The target objects are detected and extracted by background subtraction and fuzzy k-means clustering method. Fuzzy if-then rules and fuzzy membership functions are derived from human characteristics and average heights of generations. The system classifies target object to adults, children, toddlers and the other object. Here, other objects is considered as animal, baggage, car and so on. In the Chapter 3, a walking ability estimation method from sole pressure distribution is proposed. The sole pressure distribution is pressure distribution at sole of subject while walking, and it is acquired by mat-type lad distribution sensor. The method is proposed as a diagnosis system for walking ability. In the system, a foot-age which is one of age related indexes is developed to evaluate the walking of subject. By using the foot-age, we are able to know our walking abilities without medical knowledge. To estimate the foot-age, the system classifies the subject to young age, middle age and elderly groups based on fuzzy inference. Then, the fuzzy MIN-MAX center-of-gravity method estimates foot-age of the subjects. In the Chapter 4, a gait level estimation method from sole pressure distribution is proposed. The method is proposed as a diagnosis support system for rehabilitation. In the rehabilitation field, an personalized rehabilitation program is made for each patients related to their gait level. Now, medical doctors or physical therapists evaluate the gait level by their experience and subjectively. To make a quantitative index to evaluate the gait level of a patient, our system estimates gait level index by classifying the acquired sole pressure data to patient or commons. In Chapter 5, a biometric security system is proposed. The biometric system authenticates person from their sole pressure distribution. The walking is most natural motion in our daily motions, and the system do not retardation us. The shape and weight shift related features are extracted, and fuzzy degrees are calculated as an authentication score. From the fuzzy degree, the biometric system identifies and verifies the walking person. Finally, the Chapter 6 conclude this article.

2 Fuzzy Object Classification Method from Distance Distribution Images

This chapter proposes a fuzzy logic based object classification method from distance distribution images acquired by laser infrared time-of-flight (TOF) camera. The method classifies detected objects to adults, children, toddlers and other objects form appearance based features. Section 2.1 introduces the object classification system. Section 2.2 explains TOF principle and our sensor system. Section 2.3 shows fuzzy aided object detection method from a distance distribution image. Section 2.4 shows fuzzy logic based object classification method. Section 2.5 describes experimental results. Section 2.6 discusses the object classification system. Section 2.6 concludes this chapter.

2.1 Introduction

A detection system of people distribution situations has received much considerable attention over the years in various fields. For example, these detection systems are used for energy-saving, security, navigation, amusement and computer vision fields [1]-[3]. In energy-saving fields, the system monitors or counts a number of people in the room to optimize air-conditioning or illumination control [4]. In amusement or computer vision fields, motion capture systems are used to control machine or reconstruct movements of people [5], [6]. In security fields, surveillance camera investigates and prevents crimes by monitoring the people distribution [7]. Security systems need a high accuracy and environmental stability. There are a lot of wide challenges to detect people distribution from the visible image by an imaging device. Generally, most of them employ CCD camera, thermo-graphic image and infrared laser camera. The CCD camera acquires visible moving image, and the general infrared sensor acquires thermal image. These images are strongly influenced on illumination environment or temperature environment. It makes increasingly difficult to extract restrictive characteristics like texture, edge and change in signal value with robust and cost-efficiency. Thus, it is under-qualified for the security system in night. On the other hand, thermo-graphic and infrared laser cameras are used in night-vision systems. These cameras form an image using infrared radiation. The thermo-graphic camera is a passive infrared camera, and it measures infrared thermal emission from humans or animals. The camera is adapted to living body. However, because a resolution of this camera is low, the camera sometimes detects falsely a warm object as human. For example, it detects concrete road heated up by strong sunshine. Moreover, a high temperature objects may cause the afterimage. Meanwhile, human senses 3-dimensional (3D) information such as distances by psychological factors and physiological factors. Therefore, it is very important to obtain the distance information for intelligent complex system like human's sense. The stereo vision system is able to acquire distance information [8], but it needs much processing for calibration of two cameras. The infrared laser camera is an active sensing camera, and it measures distance distribution by time-of-flight (TOF) principle. The TOF principle is a possible method for fast optical acquisition of distance information. The principle measures distance from phase delay of radiated and received infrared waves. The phase delay is occurred from the distance between

target and camera. Thus, the infrared TOF camera is able to acquire distance information, and it forms surfaces of objects. The infrared TOF camera provides the objects by 3D position and configuration of the object obtained from distance distribution. The camera is also available to night. On the past works, Ikemura *et al.* [9] proposed a human detection method by Haar-like filters from distance distribution image acquired a TOF camera. These filters find a difference between top of head and shoulders of human. Since the TOF camera is set to install on ceiling of room, it is not applicable to outdoor usage. On the other hand, K. Ho *et al.* [10] proposed object detection method by background subtraction and clustering based on fuzzy inference. The method is able to use outdoor. However, it did not classify objects to human or not. This method extends the human detection system proposed by Ref. [10].

In this method, we propose an object estimation method by using the infrared TOF camera. The method detects moving objects, and it classifies them to humans or other objects. The system classifies humans to adults, children and toddlers depending on their height. The height is primary factor to classify human, and it can be estimated by using the TOF camera. We aim to develop a method for any TOF camera and security system. Several security systems are limited the sampling intervals. Thus, we do not employ dynamic features such as human behaviors which depend on sampling intervals. In this method, a *k*-means clustering method [10] detects moving objects. To classify them, height, thickness, aspect ratio and occupancy of the objects are calculated as features. The method estimates the objects based on fuzzy logic aided by human characteristics and average height in Japan. In our experiments, we employed seven volunteers and two dogs. Animals such as dog are hard to measure by TOF camera, because their pelage is strong noise source. As the results, the method measured height of subjects with low estimation error. We tested out method for animal, single target and multiple targets. The method estimated subjects with 84.9 ± 16.3% (mean ± standard deviation) in classification rate.

2.2 Time of Flight Camera

In this study, we acquire a distance distribution by using infrared time-of-flight (TOF) camera. The infrared TOF camera measures distance based on phase-measuring TOF principle. The TOF principle is a possible method for fast optical acquisition of distance. According to the distance between the target and the camera, reflected waves are delayed in phase compared to the source radiated wave. Where, the distance corresponding to on full cycle d_{max} is given by Equation 2.1 from speed of light c and modulation frequency f_M.

$$d_{\max} = \frac{c}{2 f_M} \quad [\mathrm{m}] \tag{2.1}$$

As the equation, camera range is depends on the modulation frequency. For example, at a modulation frequency of 30 MHz, the d_{max} is 4.997 m at a speed of light 299792458 m/sec. To measure a distance between camera and object, infrared LED array of the camera emit modulated light pulses. The modulated signal can be thought of a sinusoidal signal as shown in Figure 2.1. In the figure, the vertical lines shows refracted signal of 4 period phase shifts. The camera system measures its precise time of arrival and phase delay between emitted and received signal. The target distance d can be calculated from the delay $\Delta\phi$ by Equation 2.2.

$$d = d_{\max} \times \frac{\Delta\phi}{2\pi} \quad [\mathrm{m}] \tag{2.2}$$

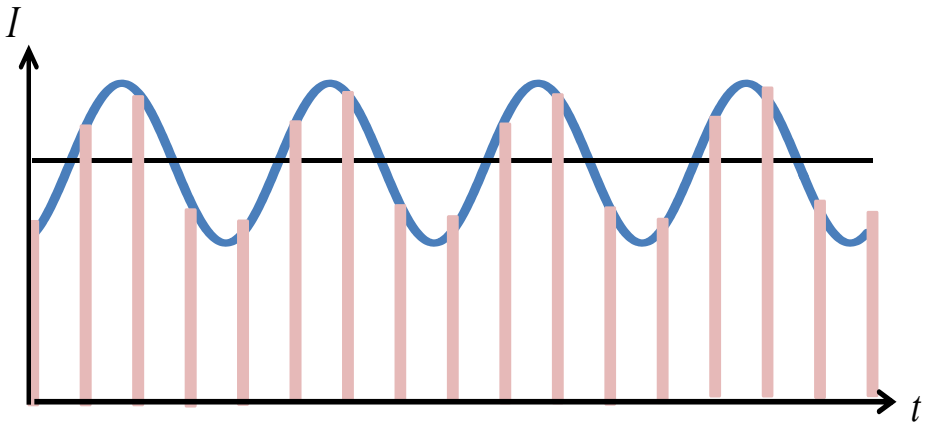

Figure 2.1. Time of flight sampling of reflected modulated signal.

Table 2.1 Specification of TOF cameras.

TOF camera	SR-4000	D-IMager
Dimension ($H \times W \times D$)	65 × 65 × 68 mm	54 × 170 × 49 mm
Frame rate	max 54fps	15, 20, 25, 30 fps
Spherical distance (range)	14 bit (0 ~ 16381)	11 bit (0 ~ 1500)
Field of view	43.6° × 34.6°	30° × 44°
Pixel array size ($w \times h$)	176×144 pixels	160 × 120 pixels
Focus length	10 mm	-
Detection range	0.3 ~ 5.0 m	1.2 ~ 9.0 m
Absolute accuracy	±10 mm	±30 mm

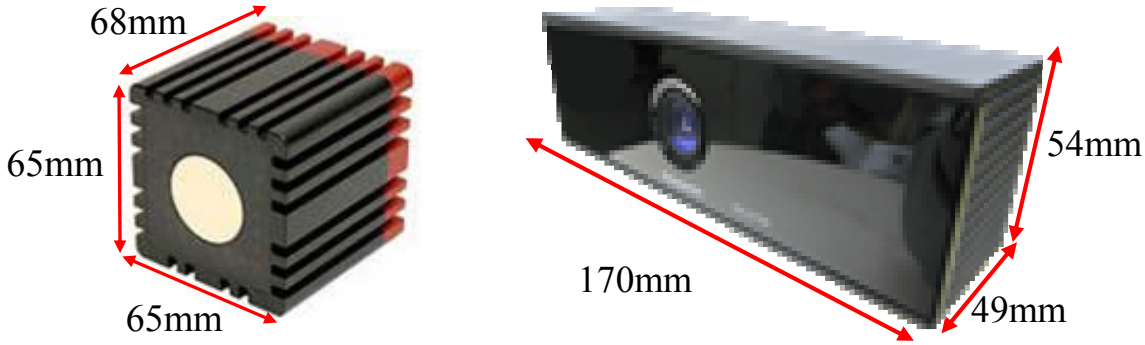

(a) SR-4000 (b) D-IMager

Figure 2.2. Appearances of TOF cameras.

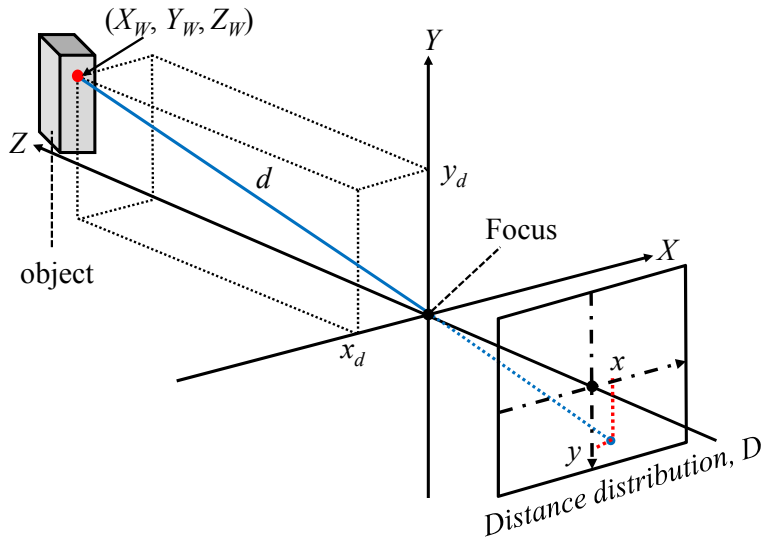

Figure 2.3. Camera coordinate systems of TOF cameras.

In this article, we employ two infrared TOF cameras "SwissRanger SR-4000, MESA imaging AG" and "D-IMager EKL3104, Panasonic Corporation" to test the availability of our developed algorithm. Table 2.1 shows specification of SR-4000 and D-IMager. SR-4000 measures distance distribution for the range from 0.8 m to 5.0 m, and the image resolution is 176 × 144 pixels. D-IMager measures distance distribution for the range from 1.2 m to 9.0 m, and the resolution is 160 ×120 pixels. The SR-4000 has higher accuracy than D-IMager. On the other hand, the D-IMager is able to measure wider area than SR-4000. Figure 2.2 shows appearances of these cameras. These cameras reconstruct the incoming light wave and image the distance distribution as depth map image in real-time. Figure 2.3 shows camera coordinate system. In this paper, the notation $D(x, y, t)$ denotes the distance distribution data of a sampling time t. The notation x and y are local coordinate value. The distribution D is quantified by measurement of 3D position $P(X_W, Y_W, Z_W)$ as shown in Figure 2.3, and it consists of distance distribution image $d(x, y)$. Figure 2.4 and Figure 2.5 show examples of distance distribution images acquired by SR-4000 and D-IMager, respectively. Left figure shows 2D distance distribution as shown in Figure 2.6. And right figure shows 3D position of the distribution as shown in Figure 2.7.

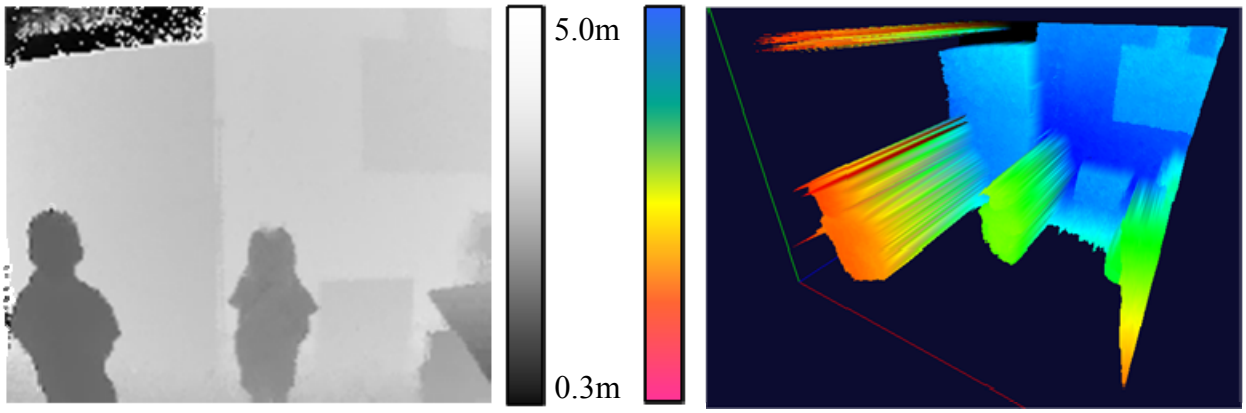

(a) 2D view (b) 3D view

Figure 2.4. Examples of distance distribution image of SR-4000.

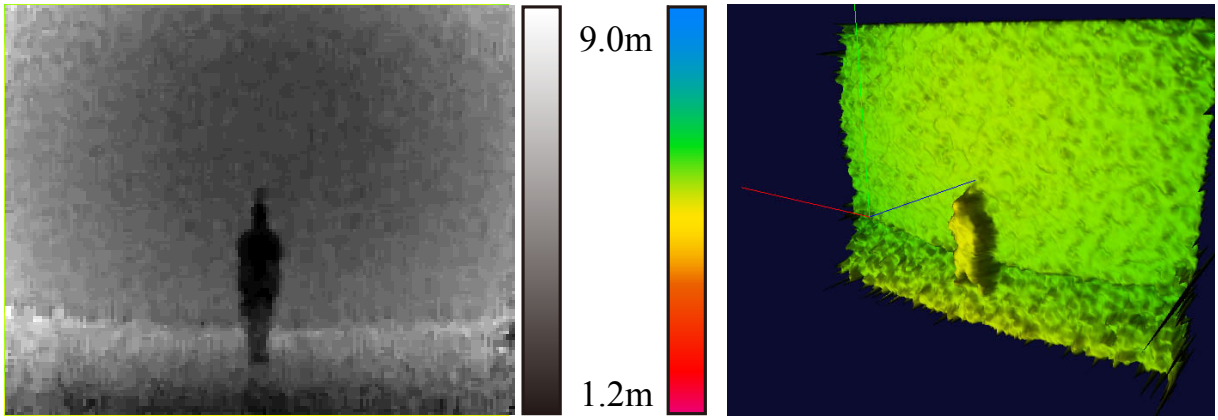

(a) 2D view (b) 3D view

Figure 2.5. Examples of distance distribution image of D-IMager.

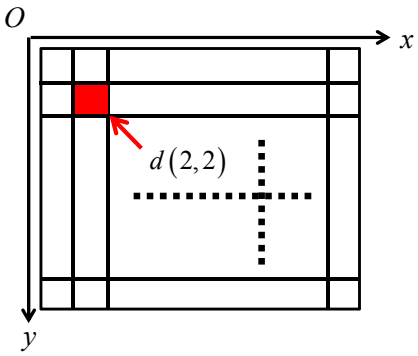

Figure 2.6. Explanation of 2D view.

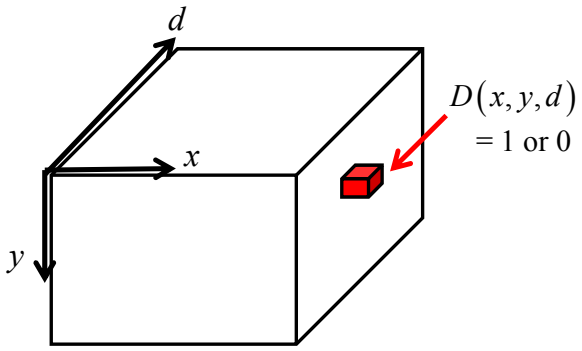

Figure 2.7. Explanation of 3D view.

Figure 2.8 shows proposed experimental system. In this figure, the notation H denotes camera installation height, and the θ dose a depression angle. In our system, to estimate human height, the H is set from 1.6 m to 2.5 m, and the θ is limited to less than 30 degree. The measurement range is set as 5 m for both cameras. The camera continuously monitors acquisition area and sends the distance distribution image data to personal computer by wired connection. The frame rate of the experimental system is 15 fps.

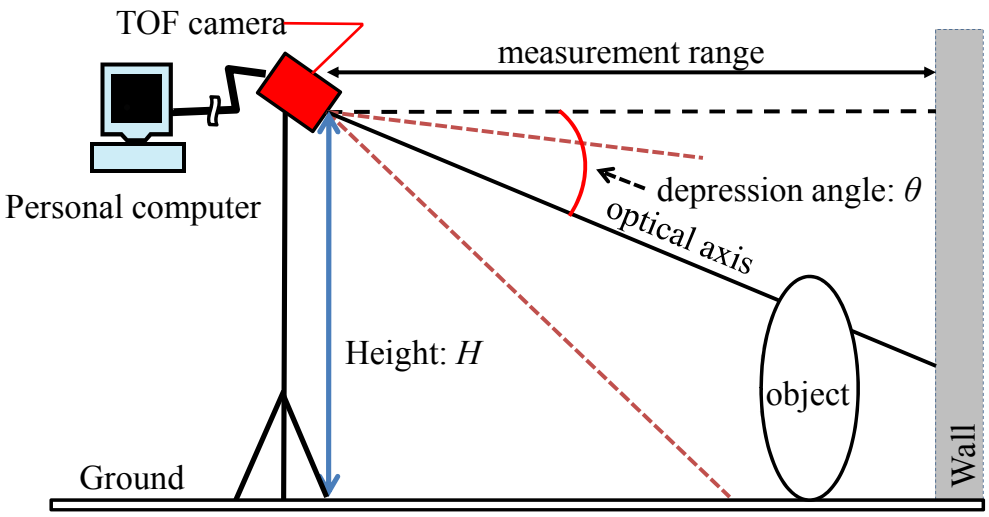

Figure 2.8. Camera installation of our system.

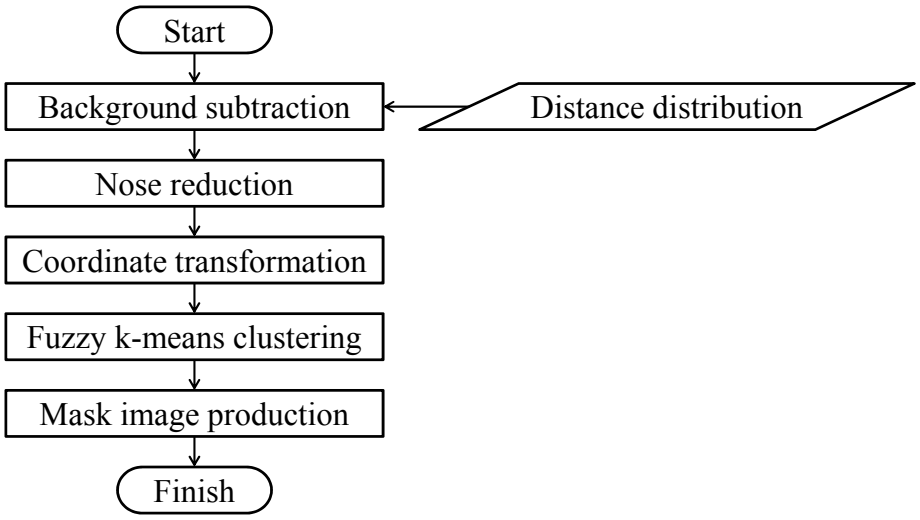

Figure 2.9. Procedure of object detection method.

2.3 Object Detection

The estimation system detects moving objects from distance distribution image $D(x, y, t)$ acquired by the infrared TOF camera. For detection, background subtraction, noise rejection and transformation are performed as the pre-processing. Then, the system detects human by fuzzy *k*-means clustering. Figure 2.9 shows procedure of pre-processing and human detection.

The acquired image includes background objects and some noises. The system performs background subtraction to separate interest objects from the acquisition image $d_{RAW}(x, y)$ by background model $d_B(x, y)$. In this system, the background model $d_B(x, y)$ is developed from statistics information of background [11], and it is defined by Equation 2.3.

$$d_B(x,y) = \overline{d_B}(x,y) \pm \sigma_B(x,y) \pm \kappa\zeta \quad \text{[m]} \tag{2.3}$$

Here, the notation $\overline{d_B}(x,y)$ denotes a mean value of the pixel in background data, and $\sigma_B(x,y)$ denotes a deviation of the pixel (x, y). These mean and deviation values are calculated from distance distribution data at camera installation. Moreover, the notation κ

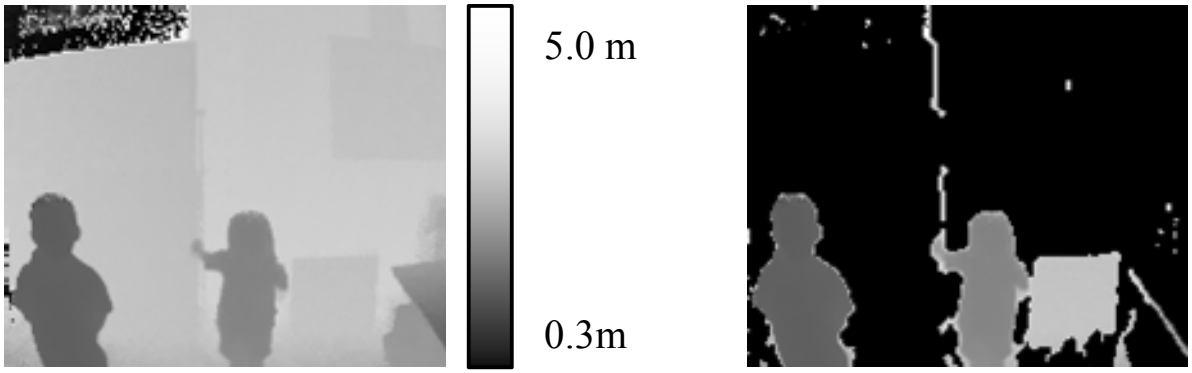

(a) raw data (b) background subtracted image

Figure 2.10. Example raw data and background subtracted image.

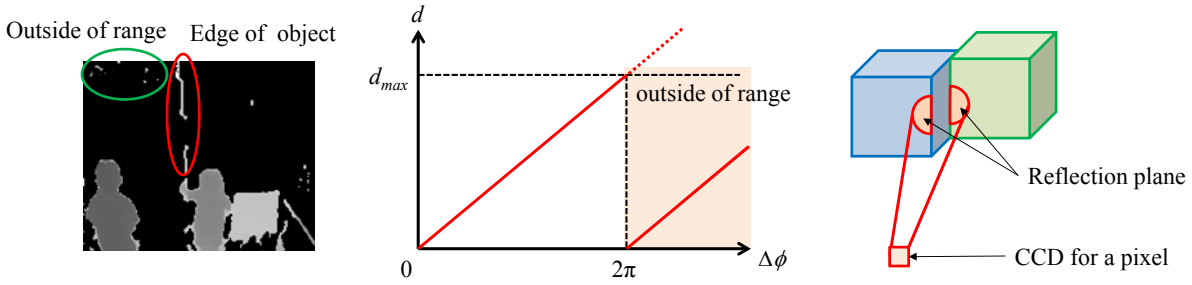

(a) examples of noise (b) outside of range (c) edge of object

Figure 2.11 Major noise sources of TOF camera.

denotes coefficient and ζ does maximum noise value of the distance distribution. In this paper, these parameters are experimentally determined, and we set κ= 1.0 and σ_B = 0.075 m (1.5% in detection range). Then, the subtracted distance $d_{SUB}(x, y)$ is obtained by Equation 2.4.

$$d_{SUB}(x,y)=\begin{cases}0 & if\ \overline{d_B}(x,y)-\sigma_B(x,y)-\kappa\zeta \le d_{RAW}(x,y) \le \overline{d_B}(x,y)+\sigma_B(x,y)+\kappa\zeta \\ d_{RAW}(x,y) & otherwise\end{cases} \text{ [m]} \quad (2.4)$$

Figure 2.10 shows an example of acquisition image $d_{RAW}(x, y)$ and background subtracted image $d_{SUB}(x, y)$. Then, the system reduces noises from background subtracted image $d_{SUB}(x, y)$. Figure 2.11 illustrates major noise sources of TOF principal cameras. When objects exist outside range of the TOF camera, the reflected wave delays over one cycle. Thus, the TOF camera confuses the distance of outside objects with inside objects. By the confusing, noises are generated. As shown in Figure 2.11(c), when the radiated wave reflects at edge of object, border of objects, human hair and pelage, the noises are generated. To reduce these noises, the system applies median filter and labeling process to background subtracted image $d_{SUB}(x, y)$. And if an area of labeled pixels is less than 1.0%, we reject the pixels as the noise. We obtain the noise reduced distance distribution $d_{DN}(x, y)$. Figure 2.12 shows an example of background subtracted image $d_{SUB}(x, y)$ and noise reduced image $d_{DN}(x, y)$. In this method, the TOF camera is installed with depression angle. For feature extraction, the system corrects the camera installation angle θ by coordinate transformation. The 3D position of noise reduced data P_{DN} is rotated around the x-axis by rotational transform matrix of Equation 2.5.

(a) background subtracted image (b) noise reduced image

Figure 2.12. Example background subtracted image and noise reduced images.

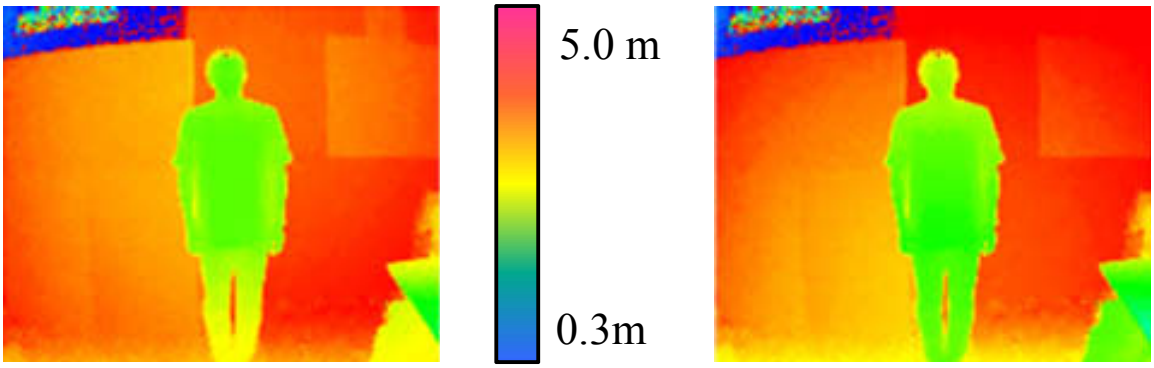

(a) source image (b) transformed image

Figure 2.13 An example of correct camera installation depression angle.

$$P_{SRC}{}^{T} = \begin{pmatrix} X_S \\ Y_S \\ Z_S \end{pmatrix} = \begin{pmatrix} 1 & 0 & 0 \\ 0 & \cos\theta & -\sin\theta \\ 0 & \sin\theta & \cos\theta \end{pmatrix} P_{SUB}{}^{T} \tag{2.5}$$

Here, the notation P_{SRC} is rotated 3D position and (X_S, Y_S, Z_S) denote world coordinate values of the rotated image. Figure 2.13 shows an example of coordinate transform process.

To detect moving objects, the system performs the clustering method using fuzzy inferences which like ISODATA clustering algorithm [10], [12]. The algorithm based on *k*-means clustering, and it automatically decides the number of clusters *k*. The system clusters moving objects from the 3D position P_{SRC}. The *k*-means method clusters the 3D position data to clusters $c = \{c_1, c_2, \ldots, c_k\}$. We consider the distance of each cluster d_{ij} is short, when the method divides an object to two or more clusters. Here, the notation d_{ij} denotes a Euclidean distance between centroids of c_i and c_j in the *X*-*Y*-*Z* space. The notation $d_{min}(k)$ denotes the shortest distance among all d_{ij} for the *k*. For example, when the *k* is 3, the $d_{min}(3)$ is minimum value among d_{12}, d_{23} and d_{31}. Moreover, we consider small clusters are generated from noises. The size of cluster s_i is calculated from c_i, and $s_{min}(k)$ denotes the size of the smallest cluster. From the knowledge, we obtained following fuzzy if-then rules.

Rule 1 : IF a minimum distance $d_{min}(k)$ is *LONG*, THEN a fuzzy degree $\mu_D(k)$ of distance is high.

Rule 2 : IF a size of the smallest cluster $s_{min}(k)$ is *MANY*, THEN a fuzzy degree $\mu_S(k)$ of the cluster size is high.

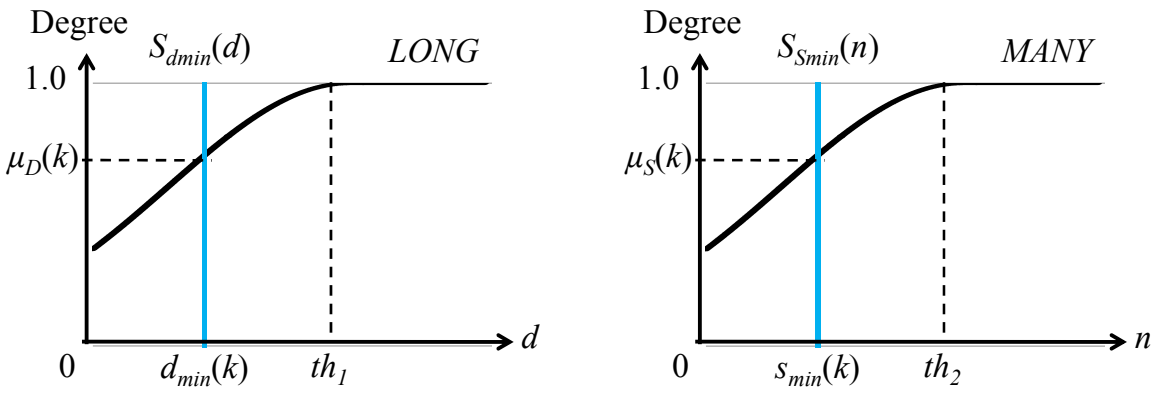

(a) LONG (b) MANY

Figure 2.14. Fuzzy membership functions of clustering method.

Here, the fuzzy membership function *LONG* and *MANY* shown in Figure 2.14 are defined as Equations 2.6 and 2.7, respectively. Here, the th_1 of *LONG* is determined as 20% of measurement range. The th_2 of *MANY* is determined as 5% of pixel array size of the TOF camera.

$$LONG = \begin{cases} \exp\left\{-\dfrac{(d-th_1)^2}{th_1{}^2}\right\} & if\ d < th_1 \\ 1.0 & otherwise \end{cases} \tag{2.6}$$

$$MANY = \begin{cases} \exp\left\{-\dfrac{(n-th_2)^2}{th_2{}^2}\right\} & if\ n < th_1 \\ 1.0 & otherwise \end{cases} \tag{2.7}$$

Fuzzy degrees $\mu_D(k)$ and $\mu_S(k)$ are calculated as Equations2.8 and 2.9, respectively.

$$\mu_D(k) = \min\left(LONG, S_{d_{\min}(k)}(d)\right) \text{ [degree]} \tag{2.8}$$

$$\mu_S(k) = \min\left(MANY, S_{S_{\min}(k)}(n)\right) \text{ [degree]} \tag{2.9}$$

Here, fuzzy singleton function $S_\alpha(\beta)$ is defined by Equation 2.10.

$$S_\alpha(\beta) = \begin{cases} 1 & if\ \beta = \alpha \\ 0 & otherwise \end{cases} \text{ [degree]} \tag{2.10}$$

From these fuzzy degrees, a fuzzy degree $\mu_{Class}(k)$ of appropriateness of current number k is calculated by Equation 2.11.

$$\mu_{Class}(k) = \mu_D(k) \times \mu_C(k) \text{ [degree]} \tag{2.11}$$

Here, the fuzzy degree $\mu_{Class}(k)$ has higher value when the number of cluster k is smaller than the number of objects. When k is bigger than the number of objects, the degree is low. The cluster number k is decided by the fuzzy degree $\mu_{Class}(k)$ as following process.

1. The number of clusters k is initialized as 2.
2. System performs k-means clustering method for k =2.
3. A fuzzy degree $\mu_{Class}(k)$ is calculated.
4. If the fuzzy degree $\mu_{Class}(k) \geq 0.5$, then, the number k is updated as k+1.

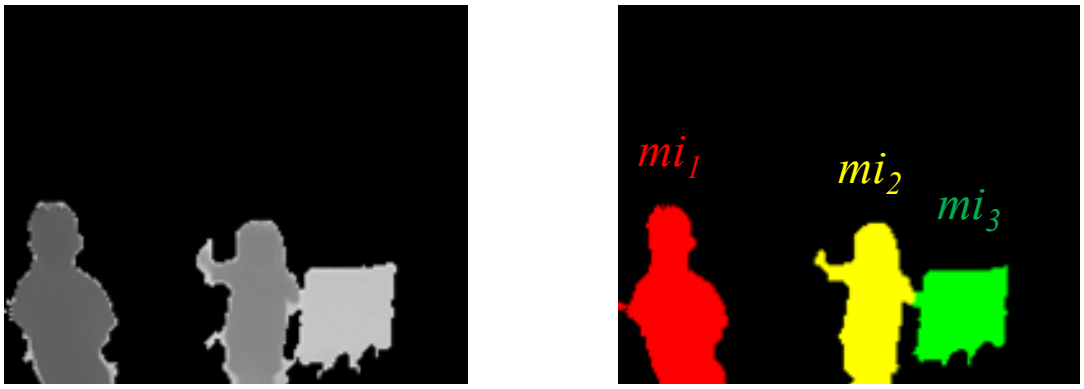

(a) noise reduced image (b) 2D mask image

Figure 2.15. Examples of 2D mask images obtained by fuzzy clustering process.

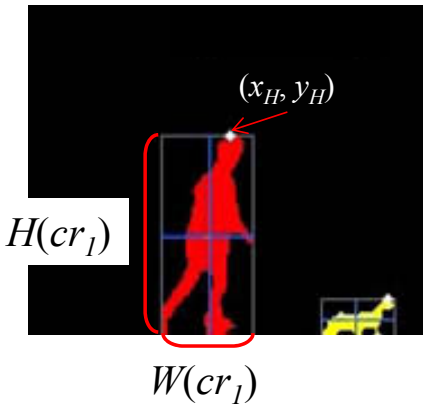

Figure 2.16. Examples of circumscribe rectangle and heat point of a mask image.

5. The system repeats the calculation while the fuzzy degree $\mu_{Class}(k) \geq 0.5$. If the fuzzy degree $\mu_{Class}(k) < 0.5$, then, we the number of cluster k is decided as k-1.

The system executes k-means clustering method by using the decided number k. Then, the system obtains the number of clusters. Moreover, the system detects moving objects $\boldsymbol{o} = \{o_1, o_2, \ldots, o_i, \ldots, o_k\}$ as clusters, and it obtains 2D mask images $MI = \{mi_1, mi_2, \ldots, mi_i, \ldots, mi_k\}$ of these objects. Here, the notation i means index of objects. Figure 2.15 shows an example of the 2D mask images (k=3).

2.4 Object Classification

2.4.1 Feature Extraction

To classify clusters, we extract features form each cluster. In our method, the system calculates a height, thickness, aspect ratio and occupancy as human body characteristics. To extract these features, we make a circumscribe rectangle cr_i for the mask image mi_i as shown in Figure 2.16. Here, the notation $H(cr_i)$ and $W(cr_i)$ denote height and width of the circumscribe rectangle, respectively. .

The height of object h_i is calculated from camera installation parameter (H, θ) and contact point between upside of object o_i and the circumscribe rectangle ($x_{H,i}$, $y_{H,i}$). From these parameters, the height of cluster is geometrically calculated by Equation 2.12 from Figure 2.17.

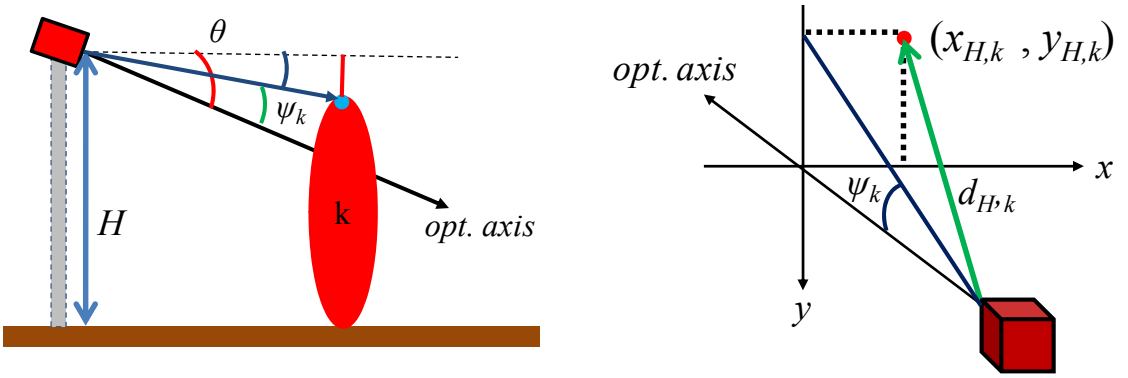

(a) side view (b) front view

Figure 2.17. Height calculation method from distance information and camera insulation parameters.

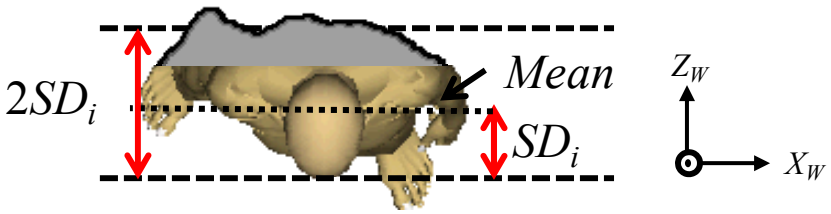

Figure 2.18. Examples thickness of a cluster.

$$h_i = H - \sqrt{{d_{H,i}}^2 - {x_{H,i}}^2}\,\sin(\theta - \psi_i) \quad \text{[m]} \tag{2.12}$$

Here, Ψ_i is calculated by Equation 2.13.

$$\psi_i = \arcsin\left(\frac{y_{H,i}}{\sqrt{{d_{H,i}}^2 - {x_{H,i}}^2}}\right) \quad \text{[rad]} \tag{2.13}$$

The height of objects is the primary factor to estimate a moving object. The height of adults is taller than that of children. Moreover, the height of human depends on the person.

The thickness is defined as breadth from back to front of body trunk. The thickness of cluster th_i is calculated from 3D position data P_{SRC}. To calculate the thickness, we determine the standard division (SD_i) of Z_W for any extracted object o_i. As shown in Figure 2.18, the thickness of cluster is defined as $SD_i \times 2$. If the object is human, the thickness is also ranged from 150 mm to 800 mm.

The aspect ratio ar_i and occupancy oc_i of object o_i are obtained from the circumscribe rectangle and mask image mi_i. Figure 2.19 shows a definition of aspect ratio and occupancy of an object. Equation 2.14 calculates the aspect ratio from the height and width of the circumscribe rectangle.

$$ar_i = \frac{W(cr_i)}{H(cr_i)} \quad \text{[n.u]} \tag{2.14}$$

The area $S(mi_i)$ of the mask image mi_i is calculated for the occupancy. Then, the occupancy is calculated by Equation 2.15.

$$oc_i = \frac{S(mi_i)}{W(cr_i) \times H(cr_i)} \quad \text{[n.u]} \tag{2.15}$$

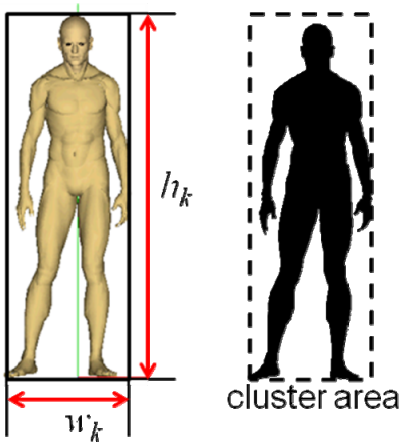

Figure 2.19. Definition of aspect ratio and occupancy of a cluster.

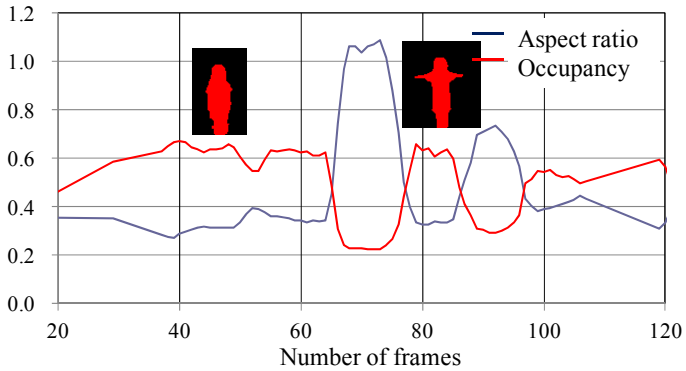

Figure 2.20. Example of transaction of aspect ratio and occupancy.

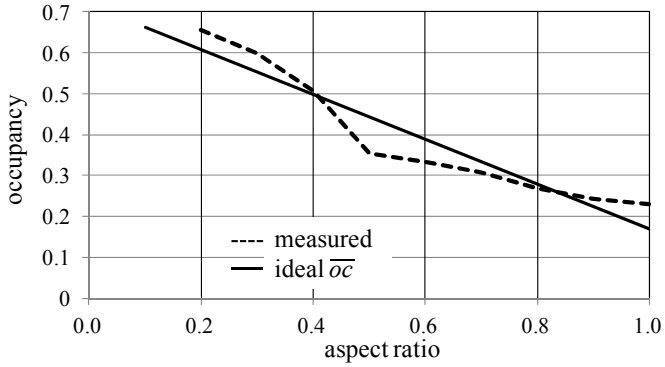

Figure 2.21. Relationship of aspect ratio and occupancy.

By using these features, the system classifies objects. In the human body, the aspect ratio is vertically long, and occupancy is not too large. Figure 2.20 and Figure 2.21 shows an example of relationship between aspect ratio and occupancy of a subject who is swinging down one's arms. There is an inverse correlation between aspect ratio and occupancy. By least-squares method, we obtained a model of ideal occupancy $\overline{oc_i}$ to aspect ratio shown by Equation 2.15.

$$\overline{oc_i} = -0.563 \times ar + 0.763 \quad [\text{n.u}] \tag{2.16}$$

The system compares calculated occupancy oc_i with the ideal occupancy $\overline{oc_i}$ to classify the object o_i to human or not.

2.4.2 Object Classification based on Fuzzy Inference

The system classifies moving object based on fuzzy inference. In this method, we classify the object to adult, child, toddler and other object. Human category is divided into adult, child and toddler, and they are classified from standard body height. In this paper, we use standard body height in Japan. The system can be optimized to country or family by these height parameters. Toddlers are intended more than primary school children whose standard body height is around 0.8 m. Similarly, children are intended for primary school children whose standard body height is around 1.2 m, and standard height of adults is around 1.6 m. The animals and other baggage are distinguished by the other features.

To classify these humans and objects, we use body height h_i, thickness th_i and occupancy oc_i. We consider the height of human is around the standard body height (Knowledge 1). We consider the thickness of human is around rational certain value (Knowledge 2). The occupancy of human is obtained similar value with the ideal occupancy calculated by Equation 2.15 (Knowledge 3). From these knowledge, the following fuzzy if-then rules are derived.

Rule 3 : IF the height h_i of the object o_i is *TALL*, THEN a fuzzy degree of adults $\mu_{Tall}(o_i)$ is high.

Rule 4 : IF the height h_i of the object o_i is *MIDDLE*, THEN a fuzzy degree of children $\mu_{Mid}(o_i)$ is high.

Rule 5 : IF the height h_i of the object o_i is *SHORT*, THEN a fuzzy degree of toddlers $\mu_{Sshort}(o_i)$ is high.

Rule 6 : IF the thickness th_i of the object o_i is *AROUND* rational certain value of human, THEN a fuzzy degree of human $\mu_{Thick}(o_i)$ is high.

Rule 7 : IF the occupancy oc_i of the object o_i is *CLOSE* to ideal occupancy $\overline{oc_i}$, THEN a fuzzy degree of human $\mu_{OC}(o_i)$ is high.

Here, the fuzzy membership functions, *TALL*, *MIDDLE*, *SHORT*, *AROUND* and *CLOSE* are defined by Figure 2.22. In the membership function *TALL*, *MIDDLE* and *SHORT* are optimized for Japanese average height. In the function *AROUND*, min_{th} and max_{th} are the thresholds that are determined based on average value of human. These fuzzy degrees $\mu_{Tall}(o_i)$, $\mu_{Mid}(o_i)$, $\mu_{Sshort}(o_i)$, $\mu_{Thick}(o_i)$ and $\mu_{OC}(o_i)$ are calculated by following equations.

$$\mu_{Tall}(o_i) = \min\left(TALL, S_{h_i}(h)\right) \text{ [degree]} \tag{2.17}$$

$$\mu_{Mid}(o_i) = \min\left(MIDDLE, S_{h_i}(h)\right) \text{ [degree]} \tag{2.18}$$

$$\mu_{Short}(o_i) = \min\left(SHORT, S_{h_i}(h)\right) \text{ [degree]} \tag{2.19}$$

$$\mu_{Thick}(o_i) = \min\left(AROUND, S_{th_i}(th)\right) \text{ [degree]} \tag{2.20}$$

$$\mu_{OC}(o_i) = \min\left(CLOSE, S_{oc_i}(oc)\right) \text{ [degree]} \tag{2.21}$$

From these fuzzy degrees, the system calculates a fuzzy degree of human $\mu_{Human}(o_i)$ by Equation 2.22.

$$\mu_{Human}(o_i) = w_1 \times \mu_{Thick}(o_i) + w_2 \times \mu_{OC}(o_i) \text{ [degree]} \tag{2.22}$$

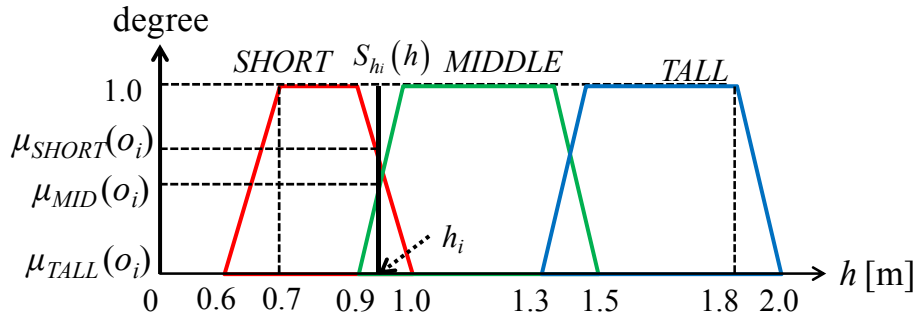

(a) fuzzy membership function for height of cluster

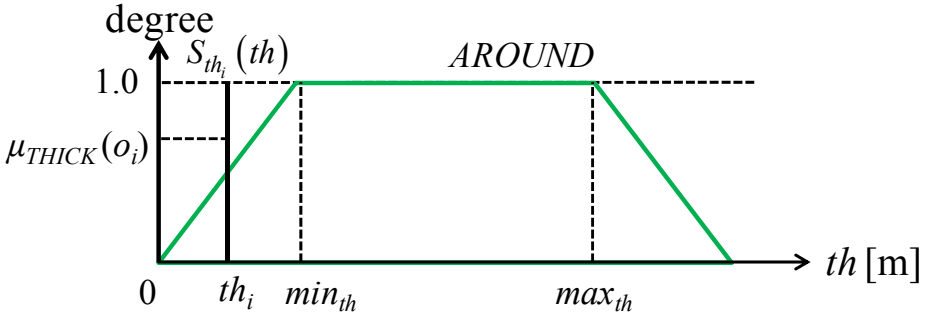

(b) fuzzy membership function for thickness of cluster

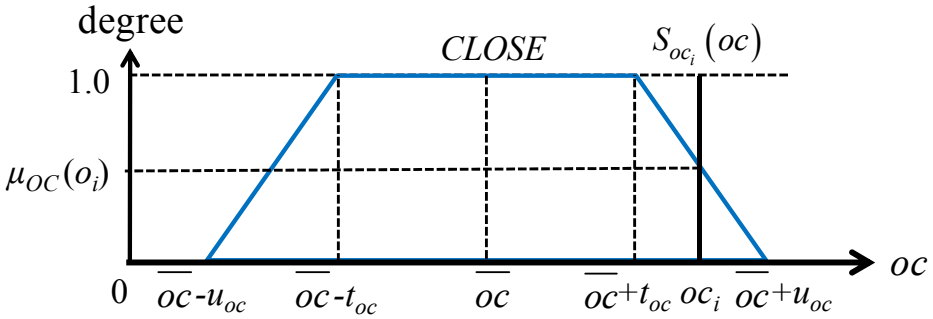

(a) fuzzy membership function for occupancy of cluster

Figure 2.22. Fuzzy membership functions for object classification system.

Here, w_1 and w_2 are weighting parameter, and $w_1 + w_2 = 1.0$. The system classifies human to adults, children and toddlers by using the height of the object. The fuzzy degrees of adult $\mu_A(o_i)$, children $\mu_C(o_i)$ and toddlers $\mu_T(o_i)$ are calculated by following equations.

$$\mu_A(o_i) = \mu_{Tall}(o_i) \times \mu_{Human}(o_i) \quad \text{[degree]} \tag{2.23}$$

$$\mu_C(o_i) = \mu_{Mid}(o_i) \times \mu_{Human}(o_i) \quad \text{[degree]} \tag{2.24}$$

$$\mu_T(o_i) = \mu_{Short}(o_i) \times \mu_{Human}(o_i) \quad \text{[degree]} \tag{2.25}$$

Furthermore, the fuzzy degree $\mu_O(o_i)$ is complement to the fuzzy degree of human categories. It is calculated by Equation 2.27.

$$\mu_O(o_i) = 1 - \left(\mu_A(o_i) + \mu_C(o_i) + \mu_T(o_i)\right) \quad \text{[degree]} \tag{2.26}$$

By using these fuzzy degrees, the system estimates the target object o_i as a class with the highest fuzzy degree. For example, if $\mu_A(o_i) = 0.0$, $\mu_C(o_i) = 0.63$, $\mu_T(o_i) = 0.31$ and $\mu_O(o_i) = 0.06$, the system estimates the object o_i as children.

Table 2.2 Information of volunteers.

Subject ID	Age [years]	Height [m]	Truth class
#A	4	0.98	Toddler
#B	5	1.11	Child
#C	7	1.13	Child
#D	9	1.31	Child
#E	21	1.55	Adult
#F	23	1.60	Adult
#G	22	1.72	Adult

Table 2.3 Experimental results for single target.

	Truth		SR-4000		D-IMager	
	height [m]	Class	$h(o)$ [m]	SD [m]	$h(o)$ [m]	SD [m]
#A	0.98	Toddler	0.932	0.102	0.804	0.078
#B	1.11	Child	1.068	0.098	1.081	0.032
#C	1.13	Child	1.247	0.047	1.293	0.030
#D	1.31	Child	1.246	0.067	1.303	0.028
#E	1.55	Adult	1.543	0.008	1.520	0.028
#F	1.60	Adult	1.650	0.008	1.637	0.010
#G	1.72	Adult	1.786	0.034	1.783	0.015

2.5 Experimental Results

In our experiments, installation parameters of Infrared TOF cameras were set as H = 1.6 m and θ = 10 degree. The parameters of fuzzy membership functions were experimentally determined as below: t_{th} = 10 cm, u_{th} = 60 cm, t_{OC} = 0.2 and u_{OC} = 0.6. In this paper, we tested our method for single target and multiple targets by using two types of cameras: SR-4000 and D-IMager. We performed our method by classification rate (CR) defined as Equation 2.27.

$$CR = \frac{\text{Correctly classified frames}}{\text{Number of detected frames}} \times 100 \ [\%] \tag{2.27}$$

Here, correctly classified frames are counted up when the method classifies the object to truth class.

In first experiment, we tested our method for single target. We employed seven volunteers as shown in Table 2.2. Each volunteer stood upright in front 4 m of the camera, and classified by our proposed method for about 20 sec / 15 fps. We compared classification accuracy between SR-4000 and D-IMager. Table 2.3 and Figure 2.23 show height estimation results of SR-4000 and D-IMager. The method estimated height of volunteer with 0.051 m mean absolute error in SR-4000 and 0.054 m mean absolute error in D-IMager. As the result, the proposed method was able to estimate the height in both SR-4000 and D-IMager with low estimation error. Table 2.4 and Table 2.5 show obtained fuzzy degrees and classification rates for single targets by SR-4000 and D-IMager, respectively. The mean classification rate of SR-4000 was 99.0%, and the rate of D-IMager was 98.1%. The proposed classification method equally classified these volunteers in both SR-4000 and D-IMager. Therefore, in after experiments, we tested our method by only SR-4000.

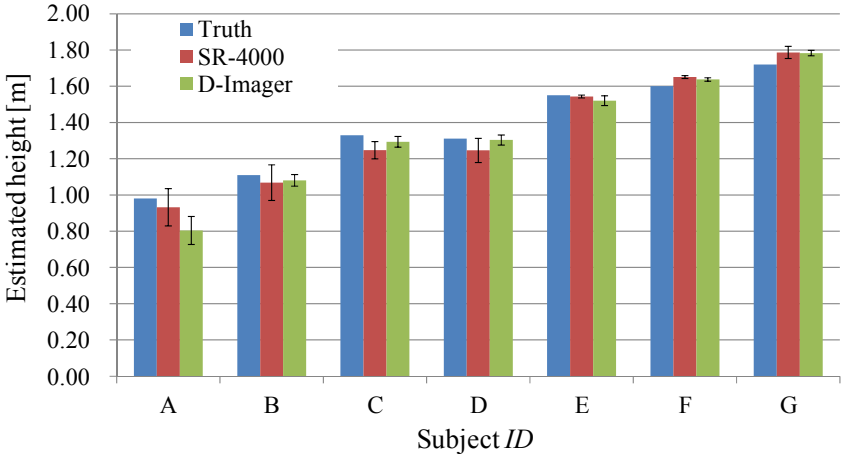

Figure 2.23. Height estimation results for singe target.

Table 2.4 Obtained fuzzy degree and classification results of SR-4000.

	Truth class	Mean fuzzy degree [degree]				CR [%]
		$\mu_A(o)$	$\mu_C(o)$	$\mu_T(o)$	$\mu_O(o)$	
#A	Toddler	0.017	0.261	0.510	0.211	97.2
#B	Child	0.031	0.813	0.039	0.117	97.1
#C	Child	0.003	0.774	0.004	0.220	98.8
#D	Child	0.004	0.817	0.000	0.170	99.6
#E	Adult	0.811	0.000	0.000	0.189	100
#F	Adult	0.990	0.000	0.000	0.010	100
#G	Adult	0.958	0.000	0.000	0.042	100

Table 2.5 Obtained fuzzy degree and classification results of D-IMager.

	Truth class	Mean fuzzy degree [degree]				CR [%]
		$\mu_A(o)$	$\mu_C(o)$	$\mu_T(o)$	$\mu_O(o)$	
#A	Toddler	0.000	0.019	0.886	0.095	96.2
#B	Child	0.000	0.960	0.004	0.035	98.1
#C	Child	0.276	0.678	0.000	0.045	93.0
#D	Child	0.370	0.612	0.000	0.018	99.2
#E	Adult	0.863	0.000	0.000	0.151	100
#F	Adult	0.990	0.000	0.000	0.010	100
#G	Adult	0.962	0.000	0.000	0.380	100

In second experiment, we measured multiple targets. Table 2.6 shows experimental situations and volunteer information. First, we measured an adult, a child and a box. Second, we measured two children and a box. The experiment has been done by SR-4000, because we confirmed the both camera has similar results for first experiment. Table 2.7 and Table 2.8 show estimation results of Case 1 and Case2, respectively. The classification rate was 84.9 ± 16.3% (mean ± standard deviation). Figure 2.24 and Figure 2.25 shows classification results. In this figure, colored area shows each cluster, and labels shows classification results. In the label, the notations '*A*', '*C*', '*T*' and '*O*' denote adults, children, toddler and object, respectively. In the Figure 2.25, a child subject sometimes vanished and connected with an adult subject by detection error, and in 76th and 91th frame, the subject false classified to toddler.

Table 2.6 Experimental situation.

Experiment	Subject	Age [years]	Height [m]
Case 1	Child	5	1.11
	Adult	34	1.55
	Box (object)	-	0.60
Case 2	Child	5	1.11
	Child	7	1.13
	Box (object)	-	0.60

Table 2.7 Obtained fuzzy degree and classification results of D-IMager.

	Subject	Height	Mean fuzzy degree [degree]				CR [%]
			$\mu_A(o)$	$\mu_C(o)$	$\mu_T(o)$	$\mu_O(o)$	
Case 1	Child	1.11	0.000	0.457	0.391	0.151	78.0
	Adult	1.55	0.934	0.000	0.000	0.066	85.7
	Box (object)	0.60	0.000	0.000	0.000	1.000	100
Case 2	Child	1.33	0.130	0.636	0.036	0.202	91.8
	Child	1.11	0.032	0.559	0.302	0.108	50.0
	Box (object)	0.60	0.004	0.021	0.006	0.968	100

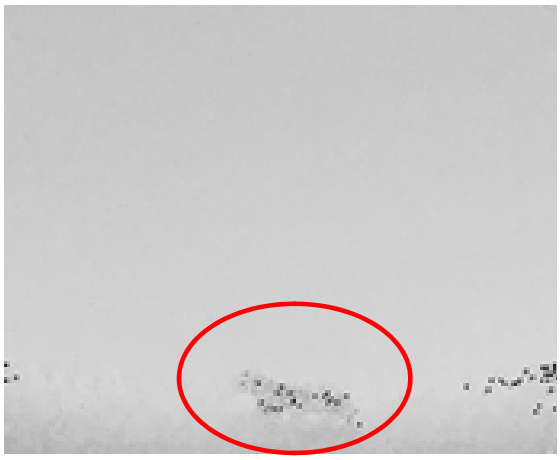

Figure 2.26. Acquired distance distribution data of dog.

In addition, we tested the proposed method for two dogs as the animal by SR-4000. The animal is hard to measure by the TOF camera, because the animal pelage is big noise source of the TOF camera as shown in Figure 2.26. We employed a white dog and a black dog. The white dog (about 40 cm) is bigger than black dog (about 20cm). Figure 2.27 shows classification results for a white dog. In the case, we classified the dog with 100% classification rate. Figure 2.28 shows classification results for a black dog. In the case, we classified the dog with 100% classification rate. Moreover, we took distance distribution data form a white dog with a child (1.25 m), and classified them. Figure 2.29 shows classification results of these targets. As shown in this figure, the system obtained 100 % classification rate for them. From these result, we considered the method detected and estimated animals.

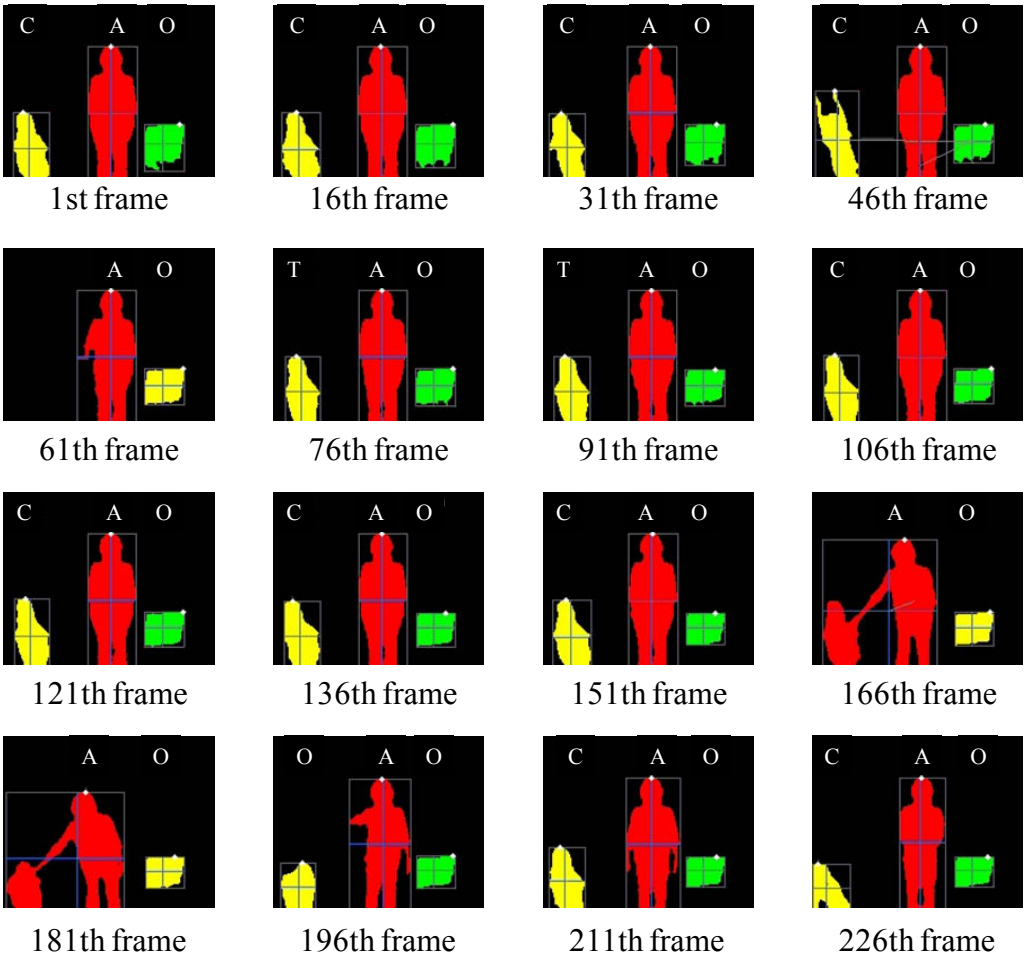

Figure 2.24. Classification result of Case 1.

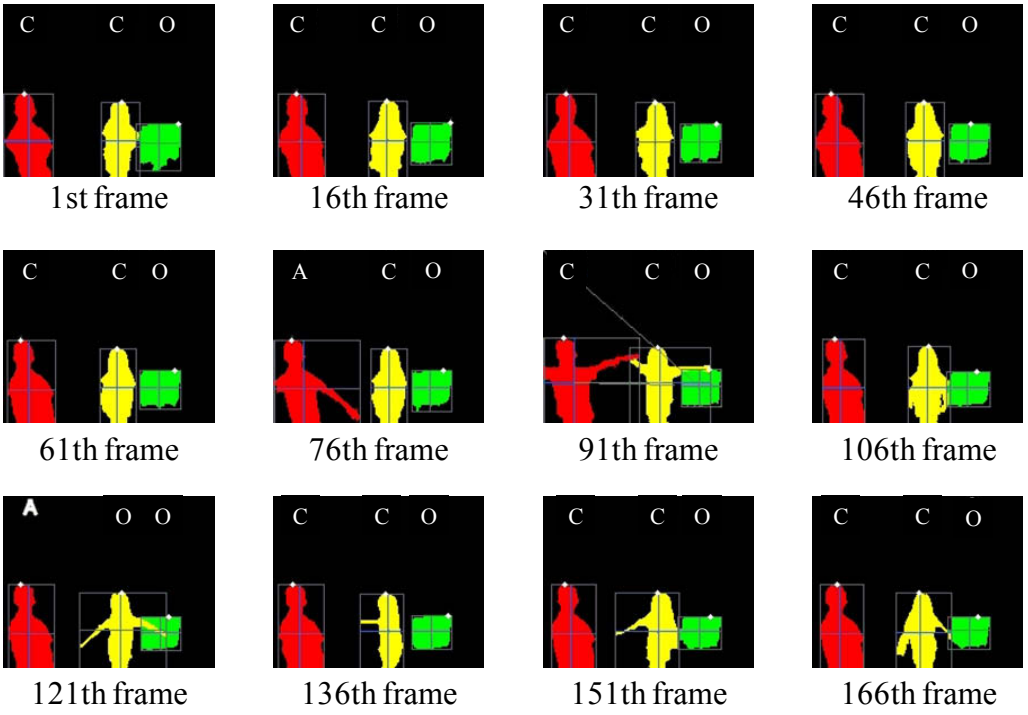

Figure 2.25. Classification result of Case 2.

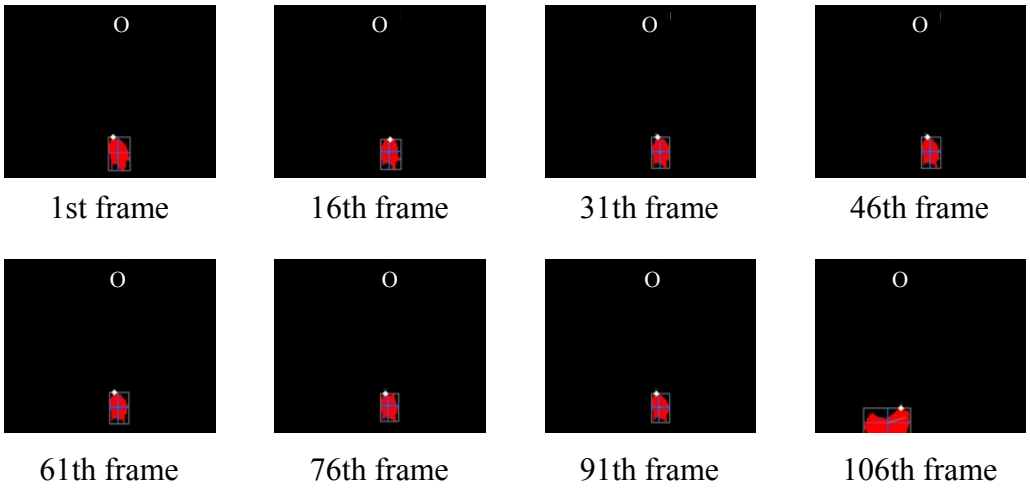

Figure 2.27. Classification result of white dog.

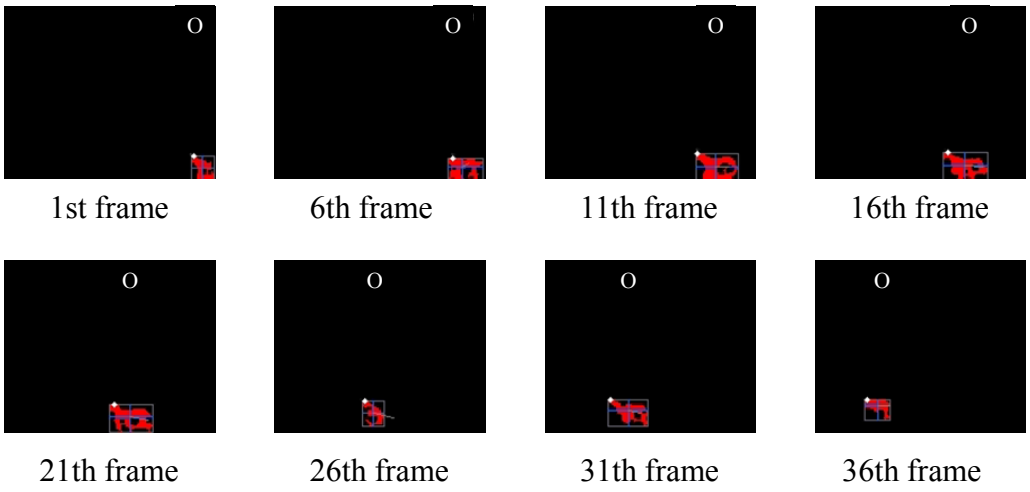

Figure 2.28. Classification result of black dog.

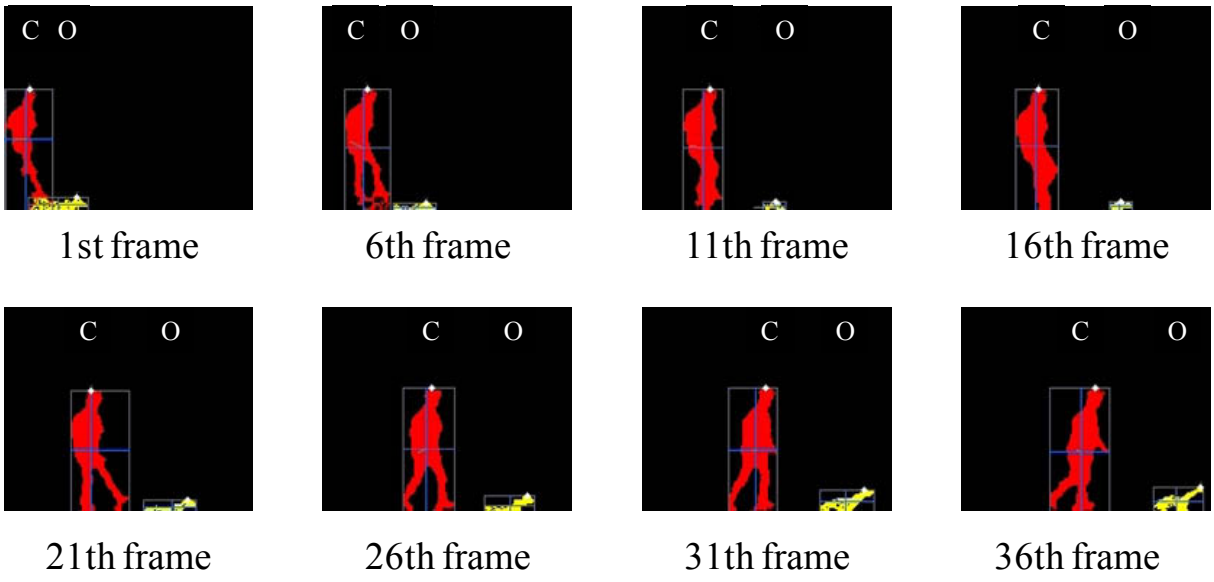

Figure 2.29. Classification result of white dog with a child.

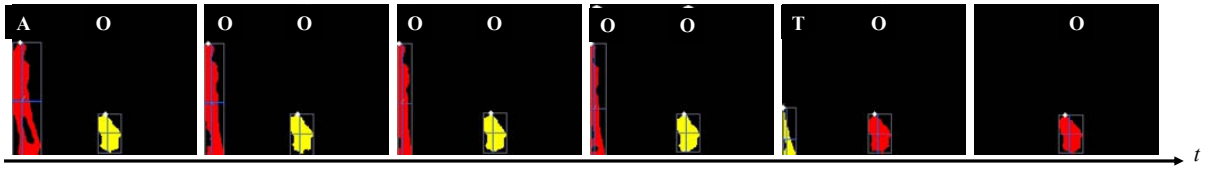

Figure 2.30. Example of false classifications by border of measurement area.

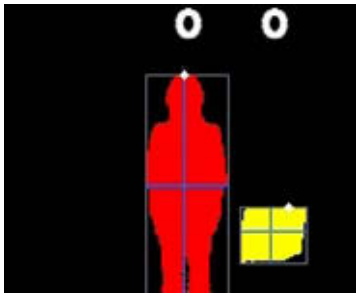

Figure 2.31. Example of false classification by legs existed outside of measurement area.

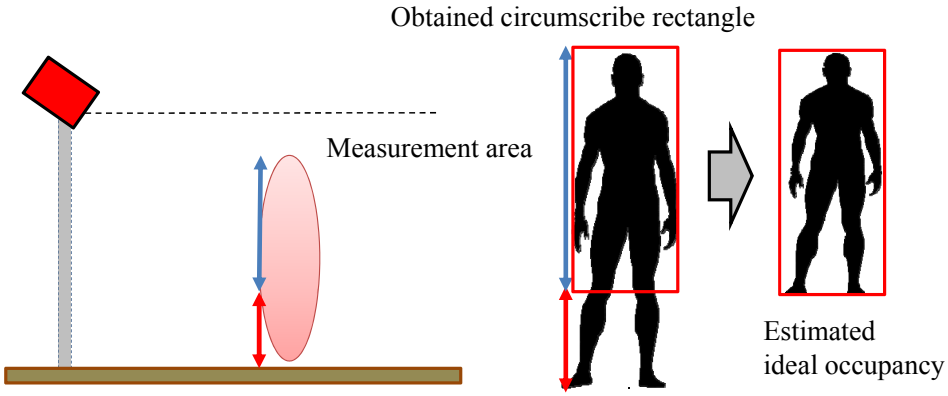

Figure 2.32. Occupancy and aspect ratio of legs existed outside of measurement area.

2.6 Discussions

In the experiment for multiple targets, the method failed to estimate an adult subject. We discuss the reason that the proposed method classified her to incorrect class. When we measured the distance distribution data, she did multiple frames in and frame out as shown in Figure 2.30. Moreover, because she stood on the screen edge, the sensor could not measure her whole body. In addition as shown in Figure 2.31, our method failed to classify an adult subject as object. In this case, legs of subject existed outside of measurement area. In this case, the occupancy was not matched with ideal occupancy that calculated from aspect ratio as shown in Figure 2.32.

In the experiments, we set the parameters of membership functions *TALL*, *MIDDLE* and *SHORT* by Japanese average height. In Table 2.4, the fuzzy degree of toddler $\mu_T(o)$ of the subject #A (toddler, 0.98 m) is lower value than fuzzy degrees of true class of other subjects. His estimated height was 0.932 m, and it was taller than average height of toddlers (0.800 m) in Japan. For the reason, we consider that his fuzzy degree became lower. When we set these membership functions fit to him and his family, we can improve the estimation accuracy. In the same way, the proposed method can be optimized any country or family by setting the parameter of membership functions for them.

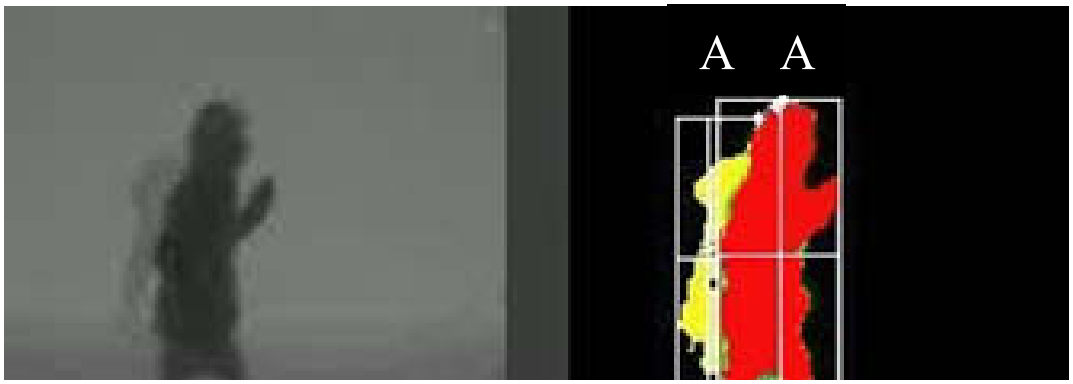

(a) raw image (b) classification result

Figure 2.33. Example of classification result for occluded scene.

Figure 2.33 shows a classification result of two adults. From this result, we can see the system classified the occluded person. We consider this is an advantage to use TOF camera. However, because, our method classifies object based on the height, if the top of object is occluded, our method may fail.

2.7 Conclusion

In this chapter, we proposed a moving object estimation method by infrared TOF camera. The camera measured distance distribution data. Our method detected and clustered the moving objects by fuzzy aided *k*-means clustering. The method estimated the objects by fuzzy inferences of height, thickness, aspect ratio and occupancy. In the experiment, we tested our method by using two kind infrared TOF cameras. The SR-4000 measures distance distribution with higher resolution than the D-IMager that measures the distribution with wider range. However, the proposed method equally classified these volunteers in the both. Thus, our proposed algorithm is high availability to camera. Moreover, we employed two dogs which are strongly noise source for a TOF camera. The proposed method estimated both dogs with 100% classification rate. This method is useful to moving object estimation in daytime and night time. It is applicable to home security system to classify the subjects to family member or not. It remains as future studies to investigate the applicability of security system in large institute, i.e. classification of larger number of people.

3 Foot Age Estimation Method from Sole Pressure Distributions

This chapter proposes a fuzzy logic based foot-age estimation method form sole pressure distribution change while walking. The method estimates foot-age by classifying the acquired sole pressure to young age, middle age and elderly groups. Moreover, by using the estimated foot-age, the method diagnoses walking abilities, and advises to improve the abilities. Section 3.1 introduces the foot age estimation system. Section 3.2 shows overall procedures of the system. Section 3.3 describes our sensor system and data acquisition method. Section 3.4 shows gait features extraction method. Section 3.5 explains foot age estimation method. Section 3.6 describes experimental results. Section 3.7 discusses the system. Section 3.8 concludes this chapter.

3.1 Introduction

Walking is the most natural movement, and we perform it mundanely. The walking way called gait pattern is individually different, and the difference is caused by age, gender, body weight, physical condition, habit of a person and so on. Hence, we are able to find individual and health information of the person by analyzing the gait. On the other hand, the quantification of athletic abilities is useful for various fields. For example, we are able to schedule an exercise for individual, and we can quantify the degree of effect of rehabilitations. Moreover, quantified athletic ability is useful to health care and risk managements. Today, the athletic ability is quantitatively evaluated by physical fitness test. However, the physical fitness test imposes a big burden on subject. Additionally, the test requires long time for the evaluation. Thus, we need an evaluation method with few physical burden and short evaluation time. We consider that the athletic ability can be evaluated by the gait analysis. The evaluation system based on the gait has few physical and physiological burdens, because walking is a natural movement. The gait motion capture systems, several wearable sensors, pressure sensors and the other sensors were known to acquire gait pattern and evaluated it [13]-[17]. Fukayama *et al*. [17] estimated age of walker by optical camera. The gait features such as step length, cadence, gait speed, standard deviation of height and so on were extracted from silhouette movie. This study classified people to child (6-12 years old), adult (13-64 years old) and elderly people (65-80 years old) by *k*-nearest neighbor (*k*-NN) method with 74.3% in classification accuracy. However, the method did not diagnose their athletic abilities. Moreover, because this method used height of walker as gait feature, camera installation parameters such as camera height, angle, positional relation between camera and walkway and so on are fixed. In the same reason, disadvantages of motion capture systems include systems need special room and they are not suitable for portable system. The wearable sensors such as acceleration sensor and electrical angle meter acquires gait pattern anywhere. However, the acquisition data can be different from sensor insulation parameter such as angle and position. Therefore, these wearable sensors require spatial knowledge about the sensor and anatomy [13]. In this study, we focus on pressure sensors. Pressure sensors acquire pressure distribution between the sensor and sole of walker as the gait pattern [18]-[22]. In this paper, we call the pressure as “sole pressure”. The sole pressure distribution is affected

by the posture and weight shift of walker. We easily calculate several gait features from dynamic change in sole pressures by simple image processing. Sole pressures during walking are measured by insole-type pressure sensors [18], [19] or mat-type pressure sensors [20]-[22]. Hessert *et al*. [18] researched difference between young (30±5.2 years old) and elderly (68.7±4.8 years old) people. In this research, insole-type pressure sensor measured sole pressure distribution, and maximum and mean pressures on anatomical region of subjects were calculated to compare young and elderly. This study found the differences were confined to calcaneus and hallux regions and to medial side of foot. Yonekawa *et al*. [19] proposed a fatigue alerting shoes which detects fatigue of walking people. In this study, pressure sensing tips were attached to both right and left shoes on heel and toe side. These pressure sensors measured sole pressure change, and then system extract maximum pressure, time of feet on the ground and ratio of current pressure and before fatigued pressure values to evaluate a fatigue. From these features, the method calculated fatigue scale same as opinions of subjects. As shown in these, insole-type pressure sensors are suitable to measure sole pressures for a person. However, because the sensor is calibrated for target person, it is inconvenience in diagnosis for many people in hospital or medical welfare. On the other hand, mat-type pressure sensors are able to use without any calibration to target person. Moreover, we are easily able to install and carry the sensor. We think mat-type pressure sensor is good device to diagnose walking abilities of people. By using mat-type pressure sensor, Sudo *et al.* [21] measured temporal-change of total sole pressure, maximum sole pressure and center-of-sole pressure, and they found differences from gender and age. Yamato *et al.* [22] developed large area pressure sensor, and they visualized gait features by image and time chart. Then, these features are compared between healthy subject and hemiplegia patient by Lader chart. Shimada *et al*. [20] evaluated gait ability in elderly people by gait speed and frequency of temporal-change of ground contact area. In it, Lader chart is used for visualization and evaluation. These studies achieved to visualize each gait feature for assistance a diagnosis by medical doctor. However they did not evaluate walking abilities quantitatively. Thus, we need to develop a quantitative index for evaluate walking abilities.

In the proposal method, to achieve quantitatively evaluation, we propose a novel age related index called foot-age as the quantitative index for automated diagnosis system. Here, age related indexes are well known as bone-age, skin-age and body-age. The foot-age shows a degree of the aging of gait condition. In general, we diagnose our body by comparing these age related indexes with our true age. This study models the foot-age by using several gait features extracted from sole pressure distribution. The goal of this study is to develop an evaluation and diagnosis system based on foot-age estimation. The system diagnoses a bad habit and weak muscle of the subject from sole pressure distribution. In addition, the system can advise the subject to exercise the muscle and correct the habit.

In this Chapter, we introduce a foot-age estimation system based on fuzzy logic [23]-[25]. The fuzzy logic is one of soft computing techniques, and it explicitly converts human knowledge and senses to rules for computation. In our experiment, we employed 93 male and 132 female volunteers, and took their sole pressures. We tested the proposed system by leave-one-out cross-validation method. In the result, the proposed method successfully estimated

their foot-ages and advices an appropriate exercise for volunteers being higher foot-age than the same age group.

3.2 Overall processing flow of our system

Our diagnosis system consists of four processing such as acquisition, gait features extraction, foot-age estimation and diagnosis as shown in Figure 3.1. In acquisition process, mat-type load distribution sensor acquires sole pressure distribution while walking. In gait feature extraction, step length, step center of sole pressure (CSP) width, distance of single support and time of double support are extracted from the acquisition data. In foot-age estimation, system estimate foot-age as an index of gait ability by fuzzy MIN-MAX center of gravity method. In diagnosis process, the system compares estimated age and true age of the person. When the foot-age older than true age, our system provides advises the person to exercise. In estimation and diagnosis process, we used learning datasets for fuzzy membership determination and comparison, respectively. The learning data set consists of collected sole pressure data of volunteers with their true age and gender.

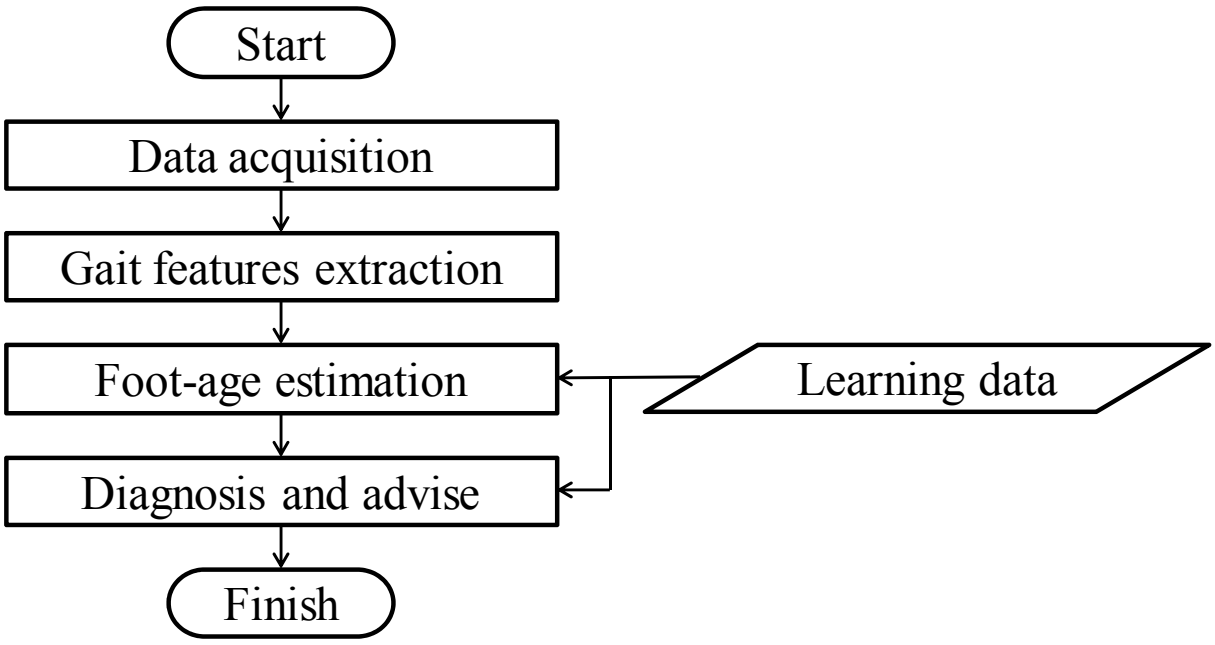

Figure 3.1. Procedure of diagnosis system based on foot-age.

Table 3.1 Specification of mat-type load distribution sensor.

Sensor type	Mat
Sensor size (width × length)	50 × 200 cm
Size of effective area (width × length)	33 × 176 cm
Pressure sensor array size (width × length)	64 × 256 channels
Sensor interval (width × length)	5 × 7 mm
Output	8bit (0 ~ 256)
Sampling Interval	100 msec

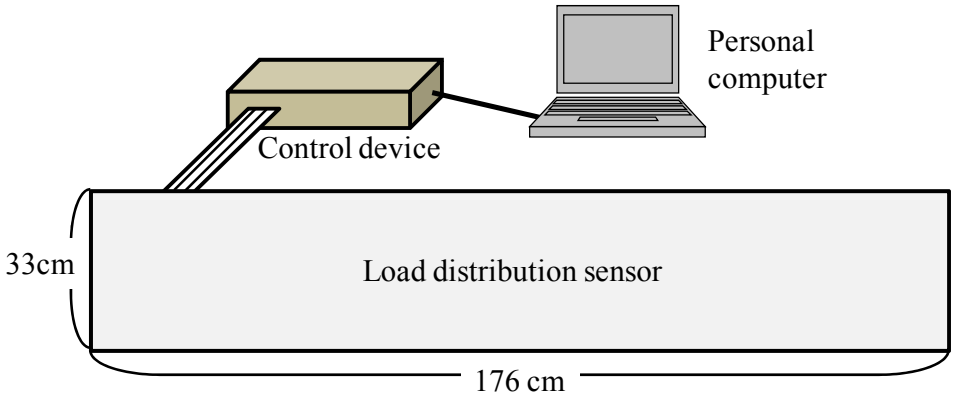

Figure 3.2. Data acquisition system; the system consists of load distribution sensor, control device and personal computer.

3.3 Load Distribution Sensor

In this section, we explain our data acquisition system. Table 3.1 shows specification of our data acquisition system. The system consists of a mat-type load distribution sensor (Arrow Industry Co., Ltd. AS-64X256-7PM) a control device (Arrow Industry Co., Ltd. AS-64X256) and a personal computer. Figure 3.2 illustrates the data acquisition system, and Figure 3.3 shows appearance of the load distribution sensor. Figure 3.4 explains internal constitution of the load distribution sensor. The sensor has 256 vertical electrode sheets and 64 transverse electrode sheets. In intersection of the vertical and transverse electrode sheets, a resistive element is sandwiched. Every intersection of these sheets are sensing points, thus, the load distribution sensor has 64 × 256 sensing points. When we put the pressure to the sensing points, the resistive elements decrease electric resistance value. The control device converts the electric resistances of the sensing points into 8-bit digital signal, and provides the data for all pressure values to the personal computer. Figure 3.5 shows the relationship of pressure value and 8-bit digital signal. The sampling interval is 100 msec. The sampling interval of our system is longer than that of the other pressure sensors. However, we consider that it is enough to measure gait pattern. In this sensor, sampling interval is in a relation of the trade-off with sampling area. We think our method based on long sampling interval is able to use a large area pressure sensor. Figure 3.6 shows the load distribution data of one sampling time. In this paper, high pressure points are shown by black, especially high pressure points are done by red and low pressure points are done by white. The gray level is ranged from 0 to 255. This sensor acquires sole pressure distribution during two or three steps.

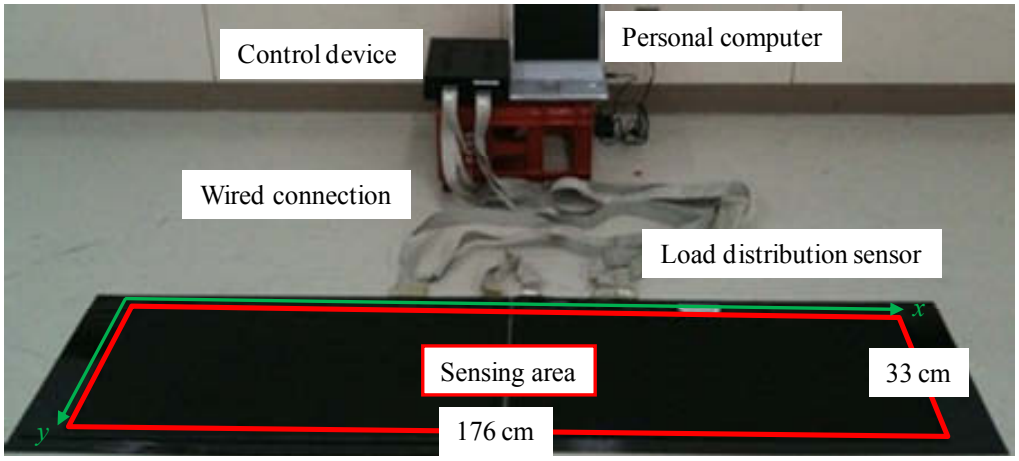

Figure 3.3. Appearance of the load distribution sensor.

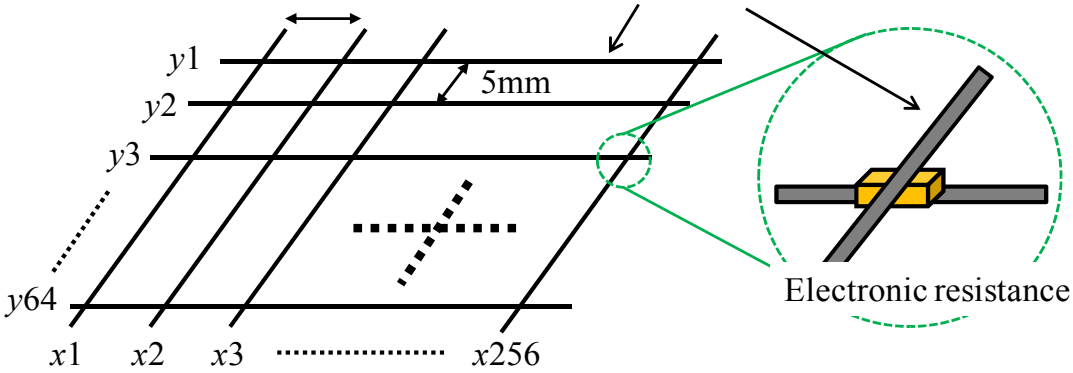

Figure 3.4. Internal constitution of the load distribution sensor.

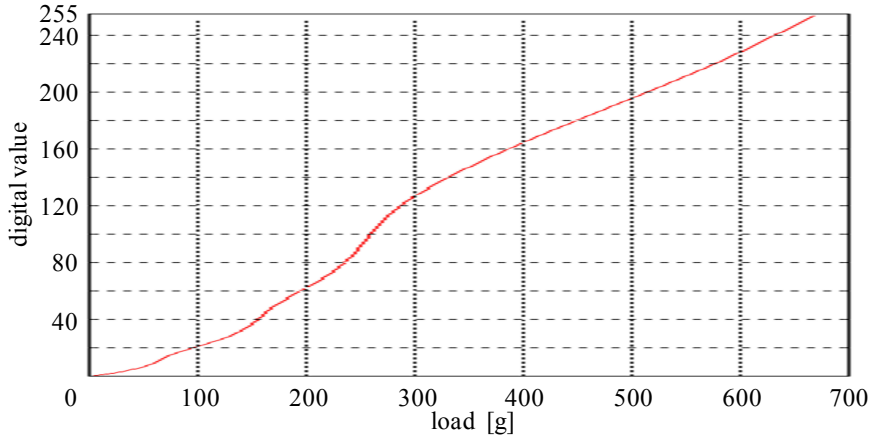

Figure 3.5. Relationship of pressure value and 8-bit digital signal of our mat-type load distribution sensor.

Figure 3.6. Example of load distribution data of one sampling time.

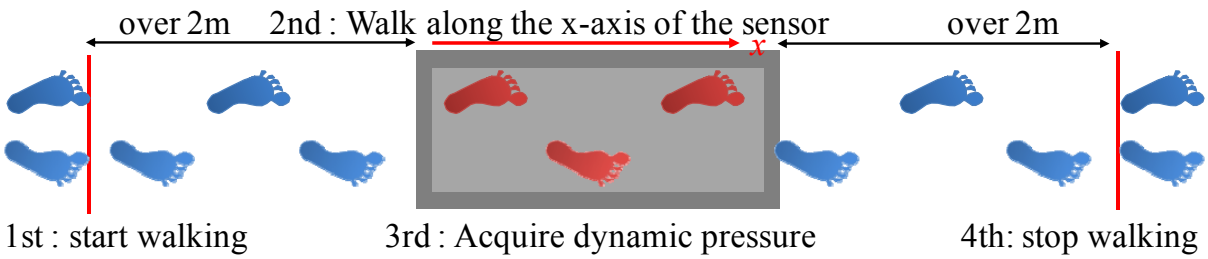

Figure 3.7. Data acquisition protocol to acquire sole pressure distribution.

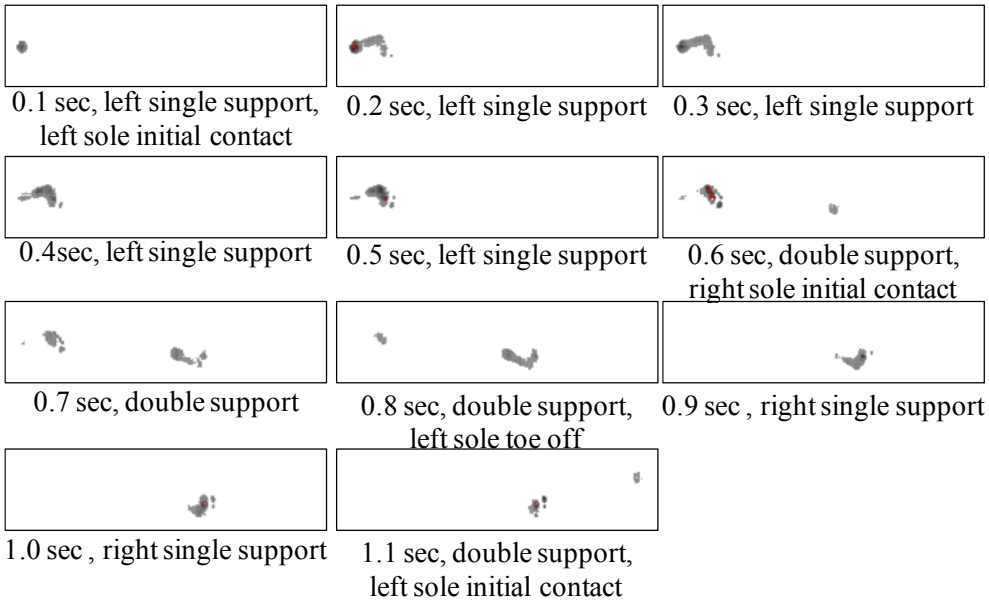

Figure 3.8. An example of the sole pressure distribution while one gait cycle.

In data acquisition process, we ask subjects to walk on the load distribution sensor as shown in Figure 3.7, and acquire sole pressure distribution change during walking. They walk along the *x*-axis of the sensor by bare foot or socks. A person starts walking from 2 m away the sensor. Figure 3.8 shows examples of the sole pressure distribution change while one gait cycle. In this figure, the initial contact (*IC*), the toe off (*TO*), the single support and the double support are periods of gait cycle. Here, the gait cycle is used to describe the complex activity of walking. Figure 3.9 shows an example of gait cycle. The gait cycle begins when one foot contacts the ground and ends when that foot contacts the ground again. Thus, each cycle begins at initial contact (heel strike) with a stance phase and proceeds through a swing phase until the cycle ends with the limb's next initial contact. Stance phase accounts for approximately 60 percent, and swing phase for approximately 40 percent, of a single gait cycle [26], [27]. The initial contact means a moment when a heel contacts the ground, and toe off means a moment when a toe leaves the ground. The single support period and double support period means a period when person supports a body with single leg and double legs, respectively.

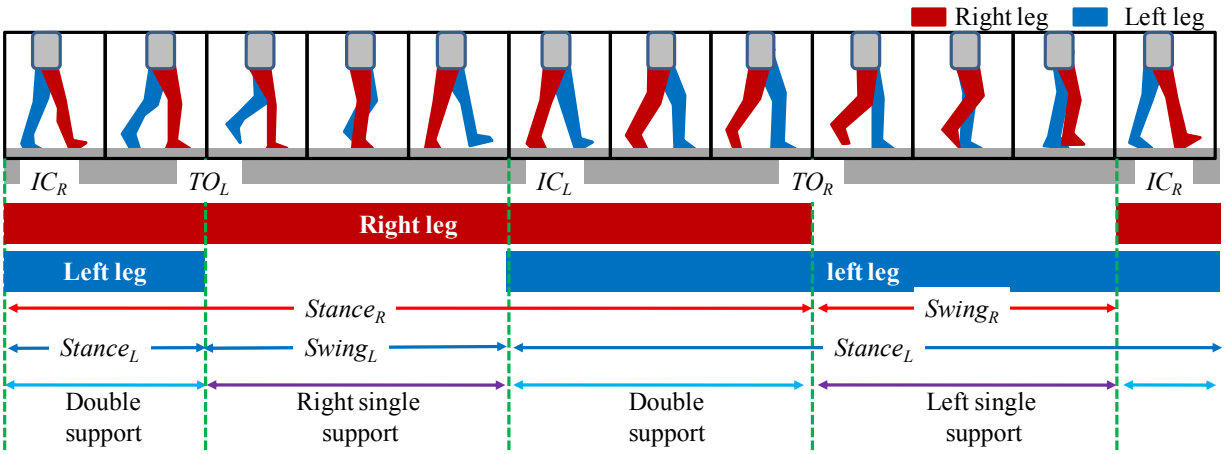

Figure 3.9. Explanation of gait cycle.

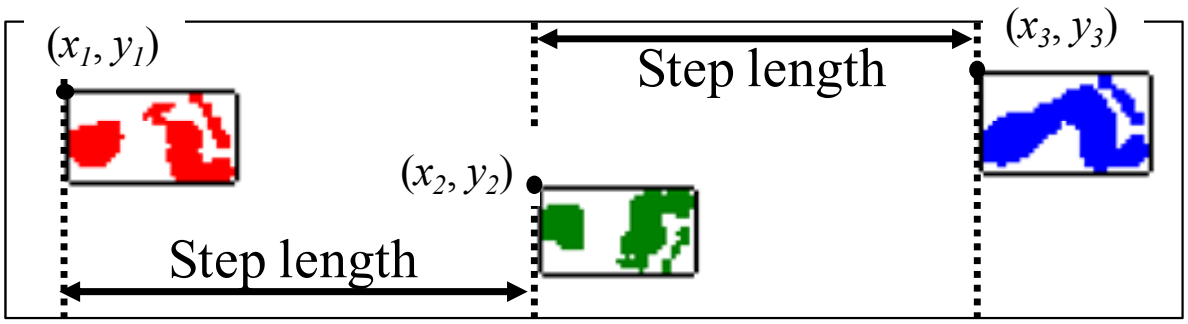

Figure 3.10. An example of foot shape image and definition of step length.

3.4 Gait Feature Extraction

This section introduces and evaluates four gait features $f_X(G)$ for gait data G of a given person. The notation X denotes index of the gait features ($X = L$, W, D and T). These features are calculated from acquired sole pressure data. We employ 93 male and 132 female volunteers to evaluate these gait features. In this study, we employ four measure gait features such as step length, width of right and left sole, time of double support and trajectory of center of sole pressure (CSP). These features are selected from learning data set and opinions of medical doctor.

First feature is step length $f_L(G)$ as shown in Figure 3.10. In this figure, the black rectangles are circumscribed quadrangle of each footprint. To calculate step length, we get a coordinate value at origin of the black rectangle, (x_i, y_i). Here, the notation i denotes an index of steps ($i = 1, 2, ..., N$). The step length is defined by x-coordinate value between the heels of two consecutive footprints. Because an acquisition data includes several steps, the system calculates the mean step length $f_L(G)$ by Equation 3.1.

$$f_L(G) = \frac{1}{N-1}\left(\sum_{i=1}^{N-1}(x_{i+1} - x_i)\right) \quad \text{[pixels]} \tag{3.1}$$

Step length is related to leg muscles of walker. Long step length means high athletic ability and short step length means low athletic ability.

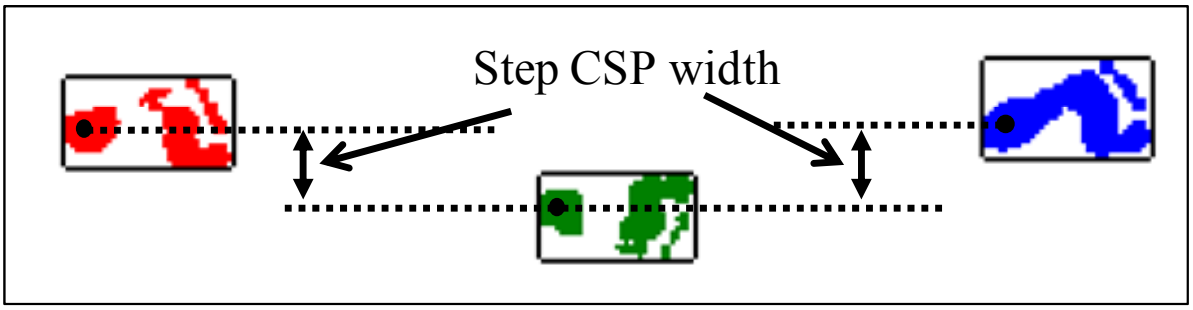

Figure 3.11. An example of foot shape image and definition of step CSP width.

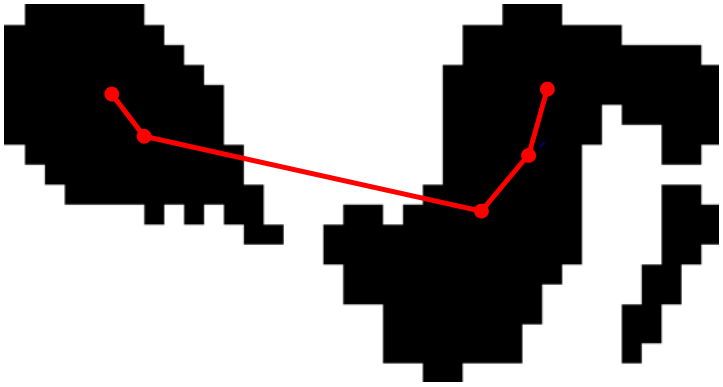

Figure 3.12. An example of right footprint and CSP trajectory.

Second feature is step CSP width $f_W(G)$ as shown in Figure 3.11. We calculate the coordinate value of CSP by Equation 3.2.

$$CFP = \left(\overline{x_i}(t), \overline{y_i}(t)\right) = \left(\frac{\sum_{x=x_i}^{x_i+l_i} \sum_{y=y_i}^{y_i+w_i} \left(x \times m(x,y,t)\right)}{\sum_{x=x_i}^{x_i+l_i} \sum_{y=y_i}^{y_i+w_i} \left(m(x,y,t)\right)}, \frac{\sum_{x=x_i}^{x_i+l_i} \sum_{y=y_i}^{y_i+w_i} \left(y \times m(x,y,t)\right)}{\sum_{x=x_i}^{x_i+l_i} \sum_{y=y_i}^{y_i+w_i} \left(m(x,y,t)\right)} \right) \quad (3.2)$$

Here, $m(x, y, t)$ denotes pressure value at point (x, y) on time t ($0 \leq x \leq 255$, $0 \leq y \leq 63$). The notations l_i and w_i denote a length and a width of the circumscribed rectangle, respectively. The step CSP width is defined by y-coordinate value between the CSP of two consecutive sole pressures at the initial contact. The mean step CSP width $f_W(G)$ is calculated by Equation 3.3.

$$f_W(G) = \frac{1}{N-1}\left(\sum_{i=1}^{N-1} \left| \overline{y}(IC_i) - \overline{y}(IC_{i+1}) \right| \right) \quad \text{[pixels]} \quad (3.3)$$

Step CSP width related to balance ability of walker. We consider extremely long CSP width means that the risk of the fall is big. This feature has low correlation between ages of subjects. However, this feature is useful to discover worse balance ability. Thus, we employ step CSP width for foot-age estimation.

Third feature is distance of single support period $f_D(G)$ as shown in Figure 3.12. We define the feature as the length of CSPs trajectory while single support period. This feature shows a foot gripping force. To calculate the features, the CSPs of single support period are determined. Next, the system calculates the length of CSPs trajectory LT_i by Equation 3.4.

$$LT_i = \sum_{t=t_a}^{t_b-1} \left| CSP(t-1) - CSP(t) \right| \text{ [pixels]} \tag{3.4}$$

CSPs trajectory is related to way of weight movement. When this feature is long, weight of walker is moved from heel to toe via the outside of arch. It is good weight movement. When our weight movement is worse, the weight is directly moves heel to toe, and the trajectory is short. Here, in this step, the beginning of single support period is denoted by t_a, and the ending is done by t_b. Moreover, the system calculates mean value of LT for foot-age estimation, and employs foot-age estimation.

Fourth feature is time of double support period $f_T(G)$. The feature is measured by the number of frames with both right and left sole pressures. The acquisition system measures this feature at interval 100 msec. We calculate the mean value of the feature of every step. Time of double support is related to gait speed. Because, our sensor is too short to calculate gait speed correctly, we employ time of double support instead to gait speed. Moreover, this feature shows ability to stand on single leg.

Figures 3.13 to 3.16 show features evaluation results for 93 male and 132 female volunteers. Table 3.2 shows correlation coefficients and R^2 value between these features and their true ages. From these result, we can see the step length and the distance of single support had negative correlation for true ages. The time of double support of elderly people were longer than middle and young people.

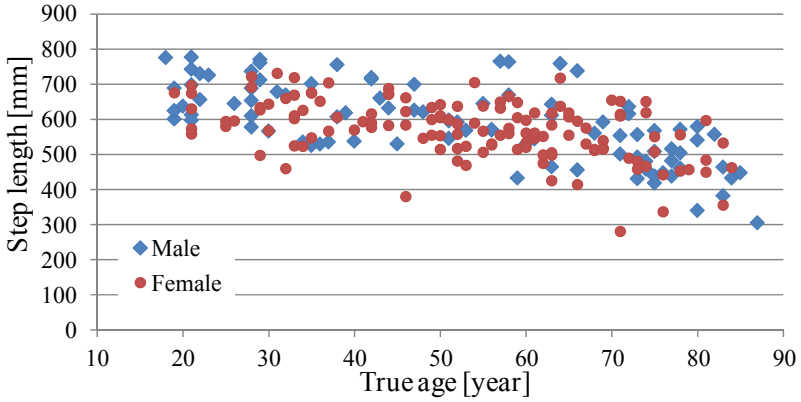

Figure 3.13. Feature evaluation result of step length.

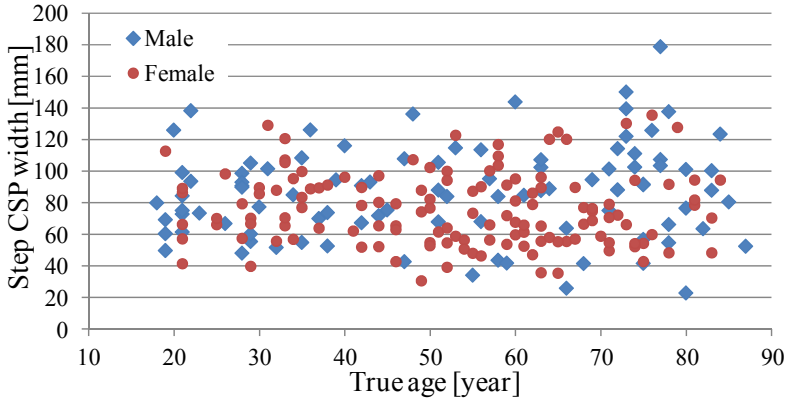

Figure 3.14. Feature evaluation result of step CSP width.

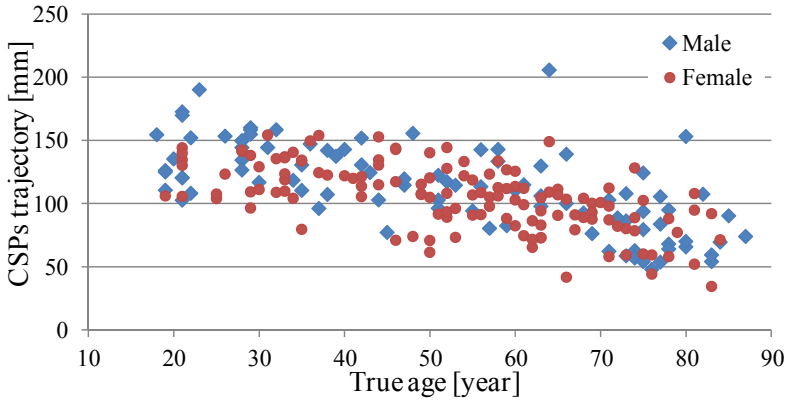

Figure 3.15. Feature evaluation result of CSP trajectory.

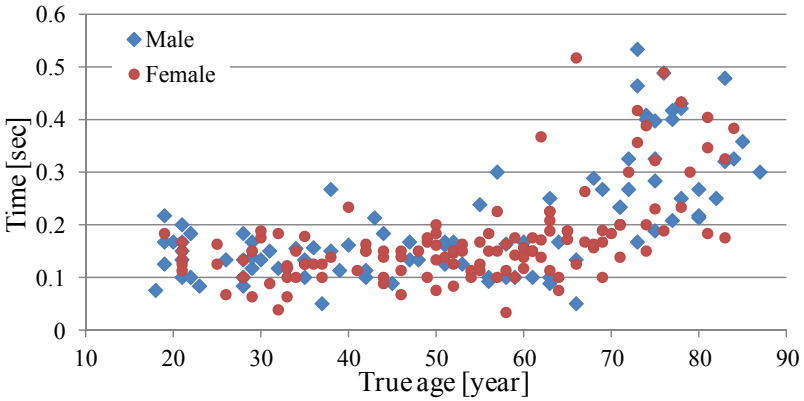

Figure 3.16. Feature evaluation result of time of double support.

Table 3.2 Numerical results of gait feature evaluation.

Gait Features	Male subjects		Female subjects	
	Correlation coefficient	R^2	Correlation coefficient	R^2
Length	-0.67	0.447	-0.49	0.237
CSP width	0.13	0.018	-0.05	0.003
CSP trajectory	-0.67	0.449	-0.61	0.371
Double support	0.65	0.419	0.54	0.294

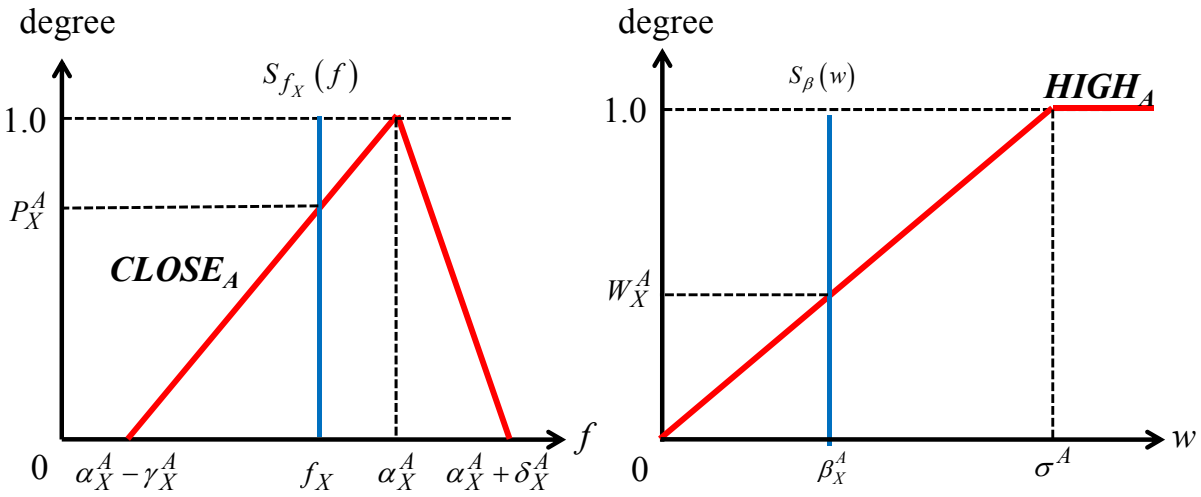

(a) CLOSE (b) HIGH

Figure 3.17. Fuzzy membership functions for foot-age estimation.

3.5 Foot Age Estimation by Fuzzy Logic

The system estimates foot-age based on fuzzy logic. To estimate foot-age, our system determines fuzzy degrees for young age $\mu_Y(G)$ middle age $\mu_M(G)$ and elderly group $\mu_E(G)$ from these gait features for the data G. Then, the foot-age of the walking person is estimated by fuzzy MIN-MAX center of gravity method.

We explain how to calculate fuzzy degrees $\mu_A(G)$ for each age group, where A denotes an index of the age group (A = *Young age group*, *Middle age group* and *Elderly group*). We employ following fuzzy if-then rules for foot-age estimation.

Rule 1 : IF gait feature value $f_X(G)$ is $CLOSE_A$ to the baseline value α_X^A of an age group, THEN the fuzzy degree of the feature $P_X^A(G)$ is high.

Rule 2 : IF classification score β_X^A of a gait feature $f_X(G)$ in learning process is $HIGH_A$, THEN the fuzzy degree of the feature $W_X^A(\beta_X^A)$ is high.

The fuzzy membership functions $CLOSE_A$ and $HIGH_A$ are defined by Figure 3.17. The parameters of these fuzzy membership functions are statistically determined by using learning data. Here, we describe learning process to determine the parameters α_X^A, β_X^A, γ_X^A, δ_X^A and σ^A in Figure 3.17 for each gait feature X and age group A. In this learning process, young, middle and elderly groups have N_Y, N_M and N_E learning sole pressure data, respectively. The learning process consists of seven steps as below.

1. We calculate a mean $\overline{f_X^A}$ and a standard deviation SD_X^A of learning data of target age group.
2. We initialize $\alpha_X^A \leftarrow \overline{f_X^A}$, $\gamma_X^A \leftarrow SD_X^A$ and $\delta_X^A \leftarrow SD_X^A$.
3. Classification score β_X^A of these parameters is calculated by a difference value between an average fuzzy degree of the interest age group and that of the other age groups. For example, the classification score β_X^A of the young group is calculated by Equation 3.5.

$$\beta_X^Y = \frac{\sum_{j=0}^{N_Y} P_X^Y\left(G_j^Y\right)}{N_Y} - \frac{\sum_{j=0}^{N_M+N_E} P_X^Y\left(G_j^A\right)}{N_M+N_E} \text{ [degree]} \tag{3.5}$$

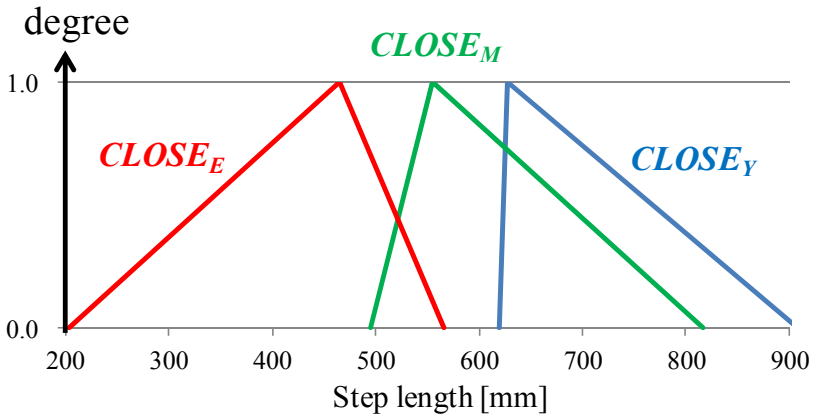

Figure 3.18 Example of learned fuzzy membership function for each age group.

Here, the notation G_j^A denotes a learning data of target age group A. The notation j denotes index of the learning data. The fuzzy degree of a feature is calculated by Equation 3.6 with related to parameters α_X^A, γ_X^A and δ_X^A.

$$P_X^A(G) = \min\left(CLOSE, S_{f_X}(f)\right) \text{ [degree]} \tag{3.6}$$

Here, the notation $S_{f_X}(f)$ denotes a fuzzy singleton function.

4. We repeat the calculation of classification score for all domains of as following equations.

$$\overline{f_X^A} - SD_X^A \le \alpha_X^A \le \overline{f_X^A} + SD_X^A \tag{3.7}$$

$$0 \le \gamma_X^A \le 4SD_X^A \tag{3.8}$$

$$0 \le \delta_X^A \le 4SD_X^A \tag{3.9}$$

We obtain the classification score from all domains. We employ parameters α_X^A, γ_X^A and δ_X^A with the highest β_X^A among all domains for the f_X of interest age group A.

5. We repeat the determination process for all X and A. Figure 3.18 shows examples of the obtained fuzzy membership functions $CLOSE_A$ of step length.
6. We calculate parameter σ^A of the fuzzy membership function *HIGH* by Equation 3.10.

$$\sigma^A = \beta_L^A + \beta_W^A + \beta_D^A + \beta_T^A \text{ [degree]} \tag{3.10}$$

The fuzzy degree $W_X^A\left(\beta_X^A\right)$ is defined by Equation 3.11.

$$W_X^A\left(\beta_X^A\right) = \min\left(HIGH_A, S_{\beta_X^A}(w)\right) \text{ [degree]} \tag{3.11}$$

7. We calculate the fuzzy degree of acquisition data for young, young age group $\mu_Y(G)$ middle age group $\mu_M(G)$ and elderly group $\mu_E(G)$ by Equation 3.12.

$$\begin{aligned}\mu_A(G) = &\left(P_L^A(G) \times W_L^A\left(\beta_L^A\right)\right) + \left(P_W^A(G) \times W_W^A\left(\beta_W^A\right)\right) \\ &+ \left(P_D^A(G) \times W_D^A\left(\beta_D^A\right)\right) + \left(P_T^A(G) \times W_T^A\left(\beta_T^A\right)\right)\end{aligned} \text{ [degree]} \tag{3.12}$$

In this study, we estimate foot-age by fuzzy MIN-MAX center of gravity method [25]. Figure 3.19 shows fuzzy membership functions *YOUNG*, *MID* and *ELD*. The parameters of these fuzzy membership functions are determined by minimization of estimation error for learning data. The foot-age is calculated by following process.

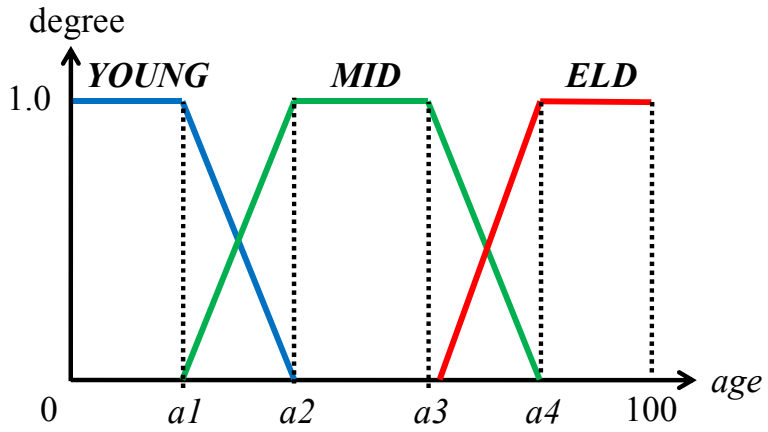

Figure 3.19 Fuzzy membership functions for three age groups.

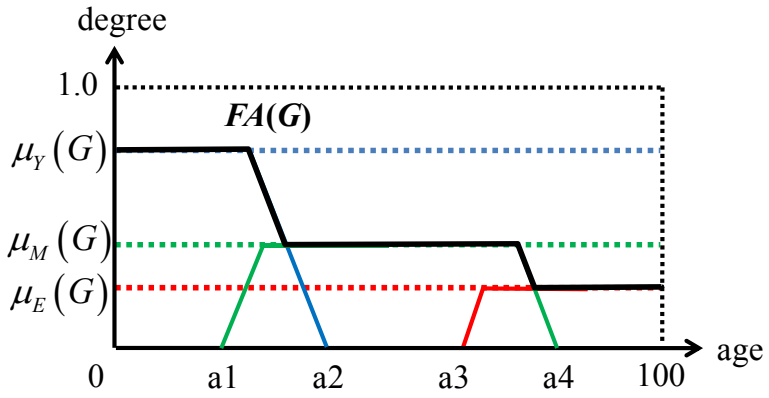

Figure 3.20 Example of fuzzy membership function *FA*(*G*).

1. The system calculates fuzzy degree for young age group $\mu_Y(G)$ middle age group $\mu_M(G)$ and elderly group $\mu_E(G)$.
2. The system calculates a fuzzy membership function $FA(G)$ by performing minimum and maximum operation for fuzzy degrees and functions by Equation 3.13.

$$FA(G) = \max\left\{\min\left(\mu_Y(G), YOUNG\right), \min\left(\mu_M(G), MID\right), \min\left(\mu_E(G), ELD\right)\right\} \quad (3.13)$$

   Figure 3.20 shows an example of the membership function $FA(G)$.
3. We estimate a foot-age of walking person as the center-of-gravity $g_{FA}(G)$ of the fuzzy membership function $FA(G)$ is defined by Equation 3.14.

$$g_{FA}(G) = \frac{\sum_{a=1}^{100}\left\{\min\left(FA(G), S_a(age)\right)\times a\right\}}{\sum_{a=1}^{100}\min\left(FA(G), S_a(age)\right)} \quad (3.14)$$

In a practical health care system, we diagnose walking people by using their estimated foot-age and extracted gait features. The diagnosis system compares the estimated foot-age with true age of the walking person. When the foot age estimated appears to be younger than the true age of the person, no advice would be made, otherwise the system will provide advises the subject to exercise. Next, we find features being for from mean value of his/her age group. Furthermore, the system advises the person to exercise a corresponding muscle.

Table 3.3 shows an example of advice written by a medical doctor. The medical expert also makes several examples of advice to the specific persons.

Table 3.3 Example of advices by a medical doctor.

Gait features	Advice
Length	Your muscles of the legs are not enough. And a range of motion of ankle/hip joint is limited. You should do squat exercise to build up the leg muscles. Moreover, you should stretch to train these joints.
CSP width	The long step CSP width means that the risk of the fall is big. To prevent a fall, you should exercise a leg muscles and the balance ability. For building up the leg muscles, you act the squat exercise and “dynamic flamingo therapy (unipedal standing therapy)”. This therapy consists of one minute standing with the right foot and the left foot. You should act the therapy three sets in a day. For your safety, you had better act the therapy in the side of handrail or the desk.
CSP trajectory	The CSP trajectory of younger people is longer. The short distance of single support means that your weight movement is not enough. You should walk with being conscious of weight movement.
Double support	The long double support shows low ability to stand on single leg. To improve the ability, you should train muscle of the legs and balance ability. You should do squat exercise to build up the leg muscles. In addition, “dynamic flamingo therapy” is also effective to train the muscles and balance ability

3.6 Experimental Results

In our experiment, we employed 93 male and 132 female volunteers as shown in Table 3.4. Here, we divide them to young age group (18-34 years old), middle age group (35-64 years old) and elderly age group (65-90 years old). These age groups are decided based on marketing field. All volunteers walked on the sensor without any rehearsal. We took their sole pressure data three times by the load distribution sensor. We considering fluctuation of gait, we used mean gait features of the three sole pressures to foot-age estimation. We estimated their foot-ages by our proposed method (Fuzzy model) and multiple linear regression analysis (MRA). Fuzzy model is one of nonlinear model. MRA is one of multivariate statistics method, and linear prediction model. Here, our MRA model is defined by Equation 3.15.

$$Footage(G) = A_L f_L(G) + A_W f_W(G) + A_D f_D(G) + A_T f_T(G) + A_0 \tag{3.15}$$

Here, the parameters A_L, A_W, A_D and A_T are partial regression coefficients, and A_0 denotes constant term. These parameters were statistically determined by using learning data. We tested these methods by leave-one-out cross-validation method. To evaluate accuracy of our algorithm, we need their actual gait condition. However, we cannot take it. Then we evaluated estimated foot-ages by mean absolute error (*MAE*) between their true ages. Because foot-age is one of age-related indexes, we consider that there are linear relationship between the estimated foot-age and their true age. Then, we showed the correlation coefficient between estimated foot-age and true-age as a reference of model accuracy. Then, the correlation coefficient was employed for evaluation of estimation models.

As the results, Figure 3.21 and Table 3.5 show results of foot-age estimation and numerical evaluation, respectively. The proposed method obtained 9.2 and 9.8 years old in *MAE* for male subjects and female subjects, respectively. The proposed method based on fuzzy logic obtained better *MAE* than MRA model. We consider this reason that relationship between gait features and ages were nonlinear. Expressly, the time of double support was strongly nonlinear. The estimation accuracy of female volunteers is worse than these of male volunteers.

Table 3.4 Volunteer information.

Age	≤29	30-39	40-49	50-59	60-69	70-79	80-89	Total
Male	22	11	9	12	10	20	9	93
Female	14	19	17	29	29	18	6	132
Total	36	30	26	41	39	38	15	225

Table 3.5 Numerical results of foot-age estimation.

Method	Male subjects		Female subjects	
	MAE [year]	Correlation coefficient	*MAE* [year]	Correlation coefficient
Fuzzy	9.2	0.85	9.8	0.68
MRA	11.6	0.72	10.5	0.60

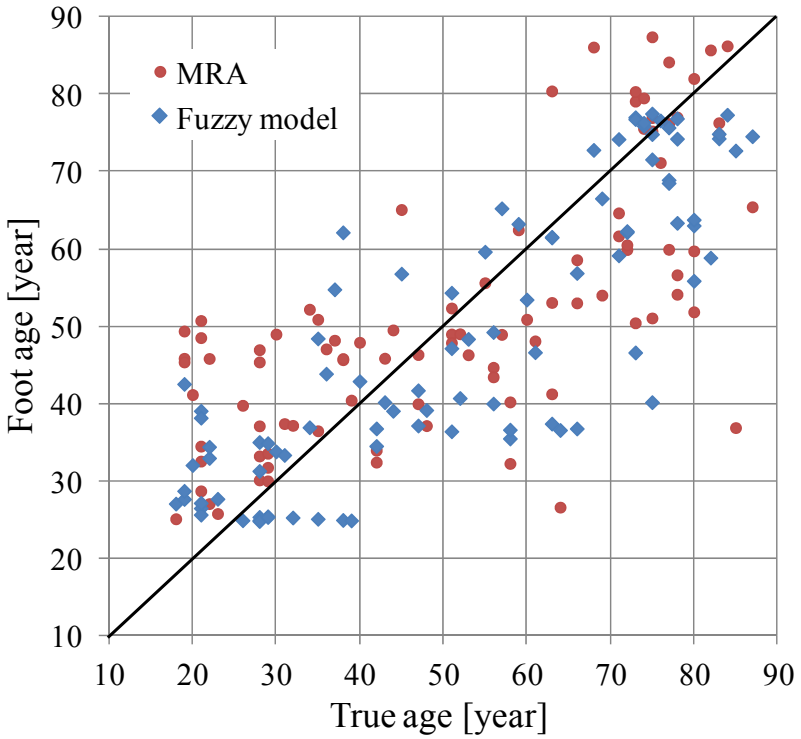

(a) Male subjects

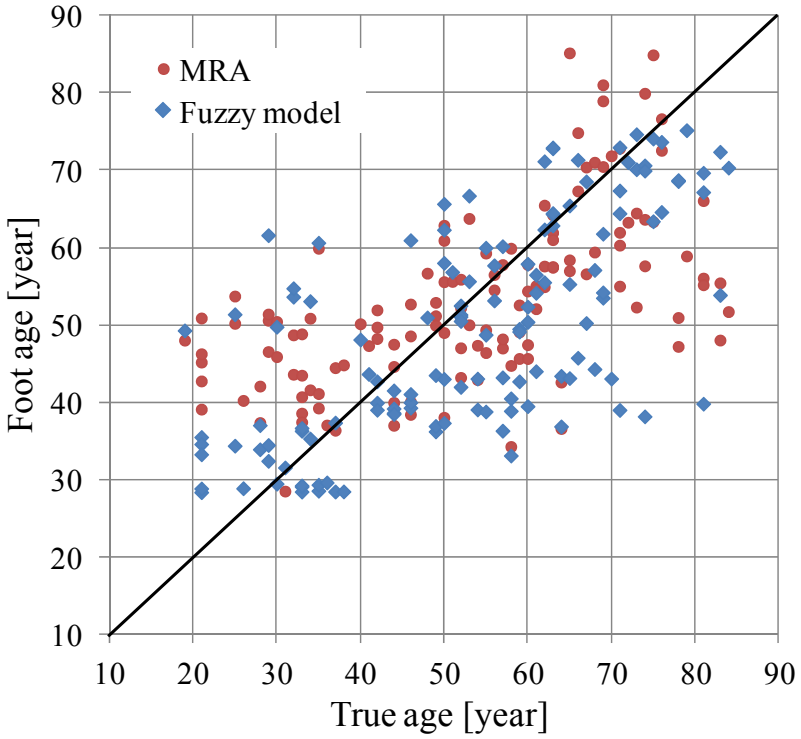

(a) Female subjects

Figure 3.21 Foot-age estimation results of the proposed method and MRA method for 93 male and 132 female subjects.

Table 3.6 Example of gait features of a male subject.

Gait feature	His value	Mean ± SD of 40-50 years old subjects
Length [mm]	529.4	650.6±60.8
CSP width [mm]	75.4	90.6±30.0
CSP trajectory [mm]	77.1	130.0±18.5
Double support [sec]	0.09	0.15±0.04

3.7 Discussions

From Figure 3.21(b), we can see that foot-ages of young volunteers were estimated similar values of foot-ages of middle ages volunteers. In our collected sole pressures, female middle age volunteer were worked in a factory, and they walked more than normal people. Thus, we think their athletic abilities were similar to young people, and our method estimated their foot-age as similar values. In learning process to determine fuzzy membership function, we used these data as the learning data. We consider that they might be noise for foot-age estimation. To improve our model, we might collect sole pressure data from other middle age people.

In clinical practice, the system is used as follows. For example, Table 3.6 shows gait features of a 45 years old male subject and Mean ± SD of subjects registered by our database. His estimated foot-age is 56.6 years old. The foot-age is much older than his true age. Our system advises the subject according to Table 3.3. His step length is shorter than that of similar age registered people. Therefore, the system advises him to build up the leg muscles. Moreover, because his distance of double support is shorter than that of similar age registered people, the system advises him to walk with being conscious of weight movement.

3.8 Conclusion

This paper proposed the foot-age estimation system as a human healthcare system. In this paper, we attempt to find the relation between obtained gait pattern and their true age. Although walking abilities in the same age are different from person to person, the whole data of the corresponding age is considered as their walking ability. Therefore, the data mining of the difference is one of our research goals. Figures 3.13 to 3.16 showed that the extracted features depended on the age. Our system was considered as a success to estimate foot-age from dynamics of sole pressure distribution while walking. Foot-age was calculated by fuzzy MIN-MAX center of gravity method. In our experiment, we employed 225 volunteers. Fuzzy logic based model estimated foot-age with the lower error than MRA. Thus, fuzzy model excellently express their foot-ages. By using estimated foot age and extracted gait features, we achieved to develop a quantitative evaluation and diagnosis system for walking ability. As shown in Table 3.3, the diagnosis system advises for walker by comparing extracted features and features of his/her age groups.

4 Gait Level Estimation Method from Sole Pressure Distributions

This chapter proposes a gait level estimation method for evaluating walking abilities of patients who undergoing rehabilitation. The method estimates gait level index which is one of quantization index to evaluate walking abilities by classifying acquired sole pressure data to patients or commons. Section 4.1 introduces the gait level estimation system. Section 4.2 describes our data acquisition protocol. Section 4.3 shows gait features extraction method. Section 4.4 shows a fuzzy aided gait level index estimation method. Section 4.5 describes experimental results. Section 4.6 discusses about the estimation system. Section 4.7 concludes this chapter.

4.1 Introduction

Reentry, the super-aging society is progressing quickly in developed countries. In Japanese investigation on 2012 [28], the ratio of elderly people was 23.3%, and the ratio is the highest in the world. If the tendency continues, those aged 65 years old or more will account for 30% of the population within 10 years. Due to this tendency, medical and healthcare services for elderly people are especially needed. One of the medical services, rehabilitations is provided in hospital and medical welfare. Patients are admitted into hospitals and medical facilities for various reasons, for example, injury, traffic accident, falling and illness. Some of them cannot move alone because of impairment, for example, pain, paralysis and muscle weakness, and rest to be required on treatment and so on. Thus, patients have different causes and conditions. One of the main causes is cerebrovascular disease such as cerebral apoplexy. In this case, leg of the patients is affected by paralysis or painful to move. They need to train way of walking of low-impact for diseased parts or alleviation of pain [29]-[31]. Locomotor apparatus disease such as by the bone fracture caused by fall is other main cause for rehabilitation. A muscle of their leg weakens by hospitalization [32], [33]. They need to train their muscle by walking exercises or strength-training machine such as walking machine. Moreover, because degrees of disorder are different in individuals, patients receive personalized rehabilitation program. As it stands, rehabilitation is performed according to gait level of patients. Doctors and physical therapists have to decide the gait level by evaluating their autonomy walk of patients, and they plan rehabilitation program based on the evaluation. These decisions of gait level are determined based on their experiences in many cases and subjectivity. However, these are different in individuals [34]. Moreover, some staffs in medical welfare without any therapists have difficulties in deciding gait level. There are dangerous situations with miss directions. Thus, any quantitative index to estimate gait level is needed. As previous studies, we could get to know that gait level have relations of body functions such as balance ability [35], gait speed [36]-[38]. In either study, relations are verified between gait level and just one of body functions. Then these relations do not always be clearly demonstrated. Thus, we propose a gait level estimation system with combining several factors.

In this study, to evaluate the autonomy walk, the gait level index is estimated from a gait data. The gait data is acquired as the dynamic foot pressure distribution by a mat type load distribution sensor. The sensor is used for study of gait analysis such as biometrics security from gait data and system of estimating gait level of independence. To estimate the gait level index, we compare the gait features extracted from the gait data between commons and patients. The method extracts maximum gait speed, time of double support period, gait balance and total time of stance phase as gait features. Form differences of gait features between commons and patients, eight fuzzy if-then rules are derived. The gait level index is estimated by fuzzy MIN-MAX center of gravity method. In our experiment, we employed ten patients and ninety commons, and took their gait data. We tested our method by leave-one-out cross validation method, and compared the results with results of two method using support vector machines. The proposed method obtained higher classification rate.

4.2 Data Acquisition

In this section, we explain about our data acquisition method. To acquire sole pressure distribution, we use mat-type load distribution sensor (Arrow Industry Co., Ltd. AS-64X256-7PM) explained by Chapter 3.2. Because the sensor is compact and potable sensor, we can use it for rehabilitation room or a passageway in hospital, retirement home and other medical welfares. In this system, we acquire sole pressure distribution by same way of foot age estimation system. First, subject starts walking from over 2 m away from the load distribution sensor without their shoes. Second, subject walks along x-axis of the sensor. Here, we instruct subjects to walk as fast as possible to obtain maximum gait speed. Third, the sensor acquires foot pressure distribution data with 100 msec intervals. Finally, the subject stops walking over 2m behind the sensor. Figure 4.1 shows examples of overlapped foot pressure distribution change of two elderly persons and two patients. From these figures, we can see that step length of patient are shorter than the healthy elderly persons, and patients walk like drunkenly. Figure 4.2 illustrates about gait cycle. In this figure, red zone shows right leg contacts on the ground, and blue zone shows left leg contacts on the ground. The notation $Stance_R$ and $Stance_L$ denote stance phase of right leg and left leg, respectively. $Swing_R$ and $Swing_L$ denote swing phase of right leg and left leg, respectively. Here, stance phase means a period when the leg contacts the ground. On the other hand, swing phase means a period when the leg leaves the ground. The initial contact (IC_R, IC_L) and toe off (TO_R, TO_L) of right and left leg mean moments when the leg contacts and leaves the ground, respectively. Single support period and double support period means a period when person supports a body with single leg and double legs, respectively.

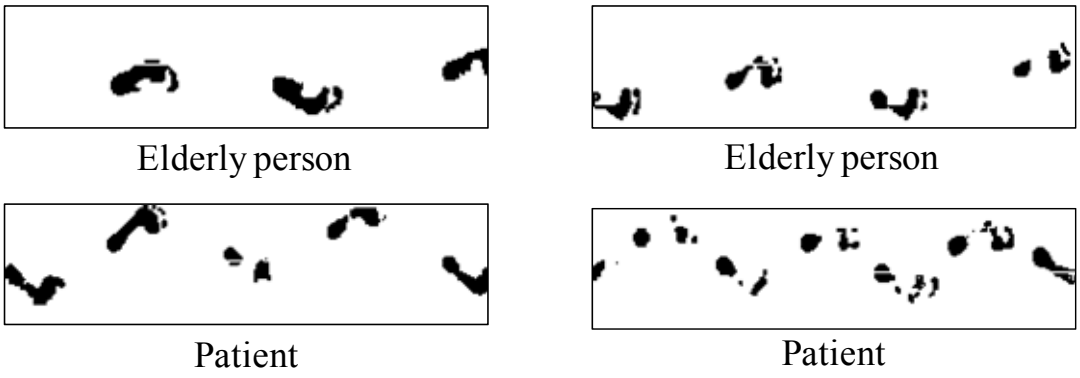

Figure 4.1 Examples of overlapped foot pressure distribution change of two elderly persons and two patients.

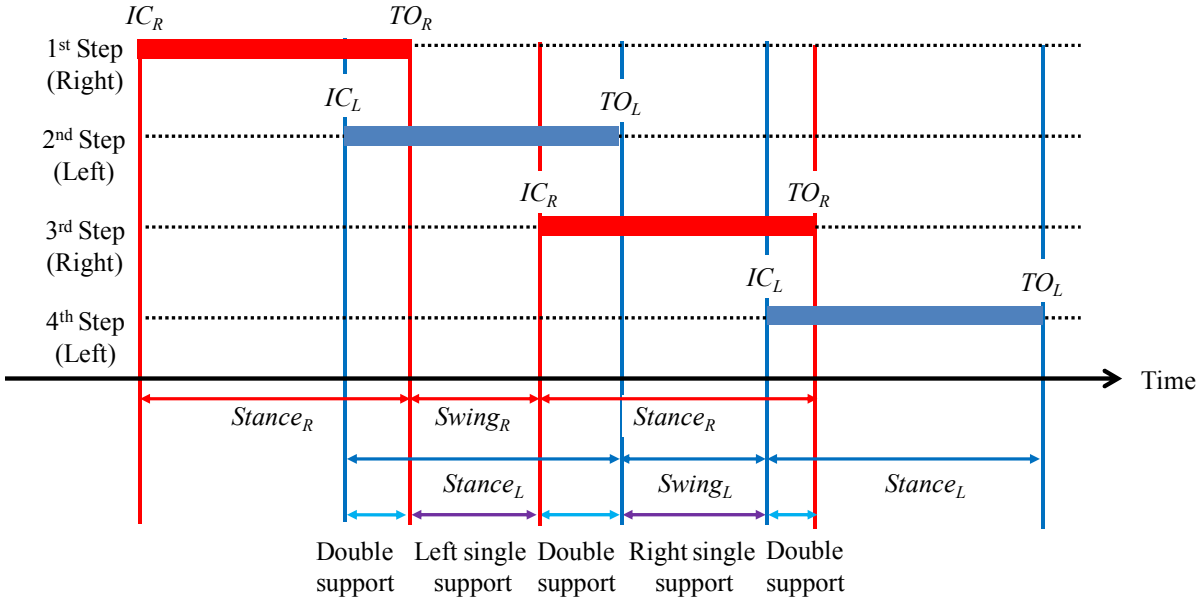

Figure 4.2 A correspondence of sole pressure and gait cycle.

4.3 Gait Feature Extraction

For estimating gait condition, we extract four gait features. In our method, maximum gait speed $v(G)$, time of double support $T_{DS}(G)$, total time of stance phase $T_{totalST}(G)$ and gait balance $B(G)$ are extracted from acquired gait data G. In our study, we believe our sensor can acquire over four steps, because elderly people and patients have short step length. Figure 4.3 illustrates footprints of the gait data G. The footprint is an overlapped and clustered image made from binalized foot pressure distribution. From the footprint, we calculate stride $ST(G)$ of the subject. The stride is calculated by x-coordinate value between a heel of 2nd step and that of 4th step. Figure 4.4 shows an example of time-series data of the gait data G. In the figure, blue line describes periods that left leg are on the ground, and red line describes periods that right leg are on the ground. $t_{IC,i}(G)$ means time of the initial contact of ith step, and $t_{TO,i}(G)$ means time of the toe off of ith step. Then time of gait cycle $T_{GC}(G)$ is defined with Equation 4.1

$$T_{GC}(G) = t_{IC,4}(G) - t_{IC,2}(G) \quad \text{[sec]} \tag{4.1}$$

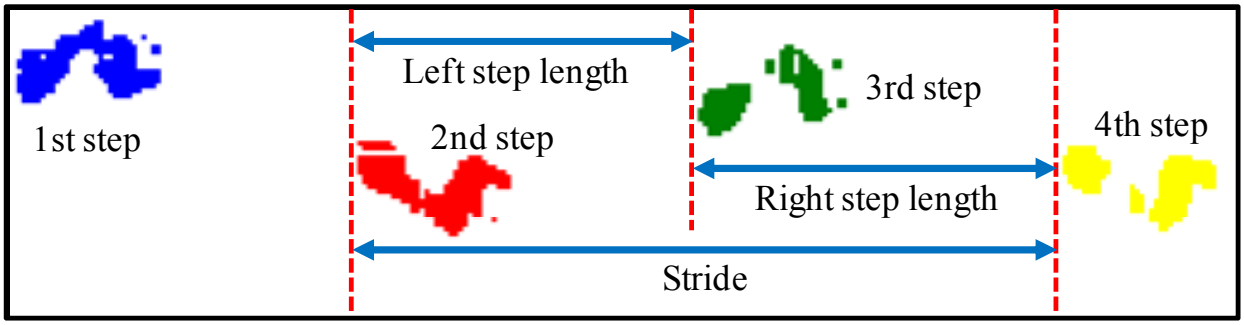

Figure 4.3 An example of footprints and gait features.

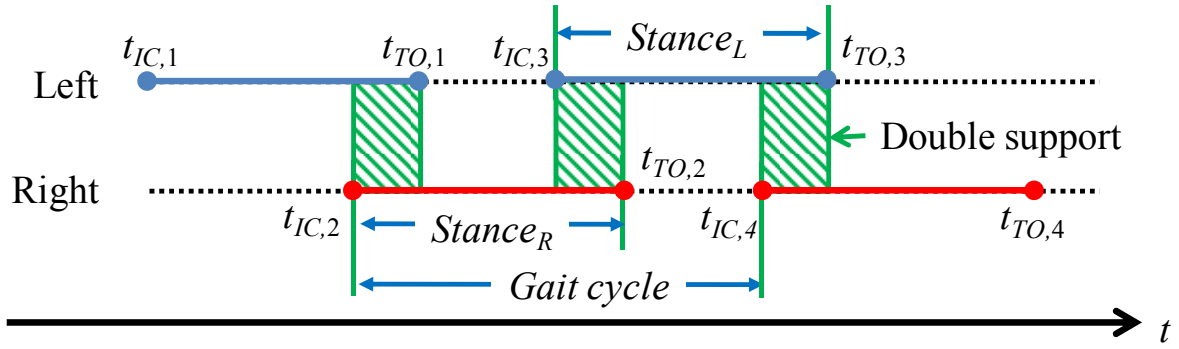

Figure 4.4 An example of time-series data of the gait data.

Firstly, we calculate maximum gait speed $v(G)$ from the stride $ST(G)$ and the time of gait cycle $T_{GC}(G)$. The method calculates the maximum gait speed $v(G)$ by Equation 4.2.

$$v(G) = \frac{ST(G)}{T_{GC}(G)} \quad \text{[cm/sec]} \tag{4.2}$$

Maximum gait speed is one of general assessment methods on gait and reflects the gait ability more properly than comfortable walking speed. Commons who does not have any disturbance in gait can walk fast. If the gait speed is fast, then it shows the subject might be commons like. On the other hand, when the subject walks slowly, we consider that the subject is patients like.

Secondly, we extract time of double support $T_{DS}(G)$. It shows how long does sobject take to take next step. Patients who have weaken muscle in their leg or some worrys about their legs cant take next step fastly. Then we can use this feature as one of the index for extraction. Taking long double support shows subjects gait might be patients like. The time of double support appeare in green zone of Figure 4.4. In our method, we calculate mean time of double support by Equation 4.3.

$$T_{DS}(G) = \frac{1}{3}\sum_{i=1}^{3}\left\{t_{TO,i}(G) - t_{IC,i-1}(G)\right\} \quad \text{[sec]} \tag{4.3}$$

Thirdly, we extract gait balance $B(G)$. Gait balance means how deferent between right leg and left leg. The balance is defined as the ratio of stance phase of right leg $T_{ST,R}(G)$ to that of left leg $T_{ST,L}(G)$. Here, the stance phase is defined as Equation 4.4.

$$T_{ST}(G) = t_{TO}(G) - t_{IC}(G) \quad \text{[sec]} \tag{4.4}$$

Generally, commons have small imbalance for laterality of their habit. However, if a subject has an impairment of one side of leg, for example, paralysis due to stroke and muscle

weakness due to femoral neck fracture, stance of healthy side of leg is especially longer than the unhealthy side. Thus, we think patients have poor gait balance. The gait balance $B(G)$ of the gait data G is defined as Equation 4.5.

$$B(G) = \begin{cases} \dfrac{T_{ST,R}(G)}{T_{ST,L}(G)} & if\ T_{ST,R}(G) < T_{ST,L}(G) \\ 2 - \dfrac{T_{ST,R}(G)}{T_{ST,L}(G)} & otherwise \end{cases} \quad [\text{n.u}] \tag{4.5}$$

On the gait cycle, time of stance phase is always larger than 0. Therefore, the gait balance $B(G)$ is within from 0 to 2. When time of stances of both leg are same value, the gait balance is 1. Then, if calculated gait balance is near by 1, we consider gait condition of the subject is might be healthy. If not, gait condition of the subject is might be unhealthy. Some unhealthy people care about their gait balance. They have a good gait balance. However, their stance phases are longer than commons. Thus, we employ total time of stance phase for gait condition estimation. The total time of stance phase $T_{totalST}(G)$ is defined as Equation 4.6.

$$T_{totalST}(G) = T_{ST,R}(G) + T_{ST,L}(G) \quad [\text{sec}] \tag{4.6}$$

Long score of calculated total time of stance phase shows taking long time for each step.

4.4 Gait Level Index Estimation by Fuzzy Logic

Our method estimates gait condition based on fuzzy inference. We consider following knowledge for gait features of commons and patients.

Knowledge 1 : The maximum gait speed of commons is faster than that of patients.
Knowledge 2 : Commons can take next step quickly. However some patient cannot.
Knowledge 3 : Commons walk with same stance between right and left. However patients cannot walk with same stance between right and left.
Knowledge 2 : Patients walk with too much care about their gait balance then they take long stance of each step.

From these knowledge, we derive eight fuzzy if-then rules as shown in Table 4.1. For example Rule 1 is represented as "IF maximum gait speed $v(G)$ is *Slow* and time of double support $T_{DS}(G)$ is *Long* and gait balance is *Bad*, THEN gait level of the walker is *Unhealthy*. Here, *Slow*, *Fast*, *Short*, *Long*, *Balance*, *Imbalance*, *Unhealthy*, *Worse*, *Better* and *Healthy* are fuzzy linguistic values. Here, The linguistic values *Unhealthy*, *Worse*, *Better* and *Healthy* are defined by Figure 4.5. And, *Slow*, *Fast*, *Short* and *Long* are defined by Figure 4.6. The *Bad* and *Good* are calculated from membership functions *Balance* and *Stance* as shown in Figure 4.7. The *Balance* depends on gait balance, and *Stance* depends on time of total stance. From these fuzzy membership functions, following fuzzy degrees are calculated.

$$\mu_B(G) = \min\left(Balance, S_{B(G)}(B)\right) \text{ [degree]} \tag{4.7}$$

$$\mu_{ST}(G) = \min\left(Stance, S_{T_{ST}(G)}(T)\right) \text{ [degree]} \tag{4.8}$$

Table 4.1 Fuzzy if-then rules for gait condition evaluation .

Rule	Input			Output
	Speed, $v(G)$	DS, $T_{DS}(G)$	Gait balance	Gait level
Rule 1	*Slow*	*Long*	*Bad*	*Unhealthy*
Rule 2	*Fast*	*Long*	*Bad*	*Worse*
Rule 3	*Slow*	*Short*	*Bad*	*Worse*
Rule 4	*Slow*	*Long*	*Good*	*Worse*
Rule 5	*Fast*	*Short*	*Bad*	*Better*
Rule 6	*Fast*	*Long*	*Good*	*Better*
Rule 7	*Slow*	*Short*	*Good*	*Better*
Rule 8	*Fast*	*Short*	*Good*	*Healthy*

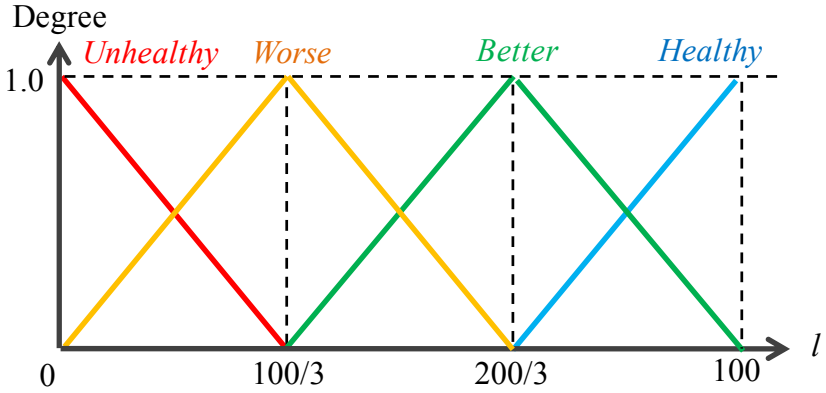

Figure 4.5 Fuzzy membership functions for gait level.

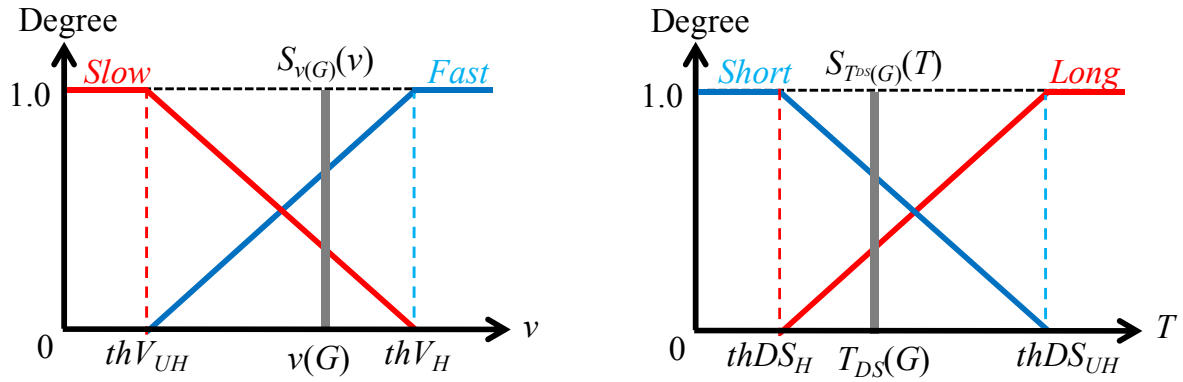

(a) maximum gait speed (b) time of double support

Figure 4.6 Fuzzy membership functions for gait speed and double support.

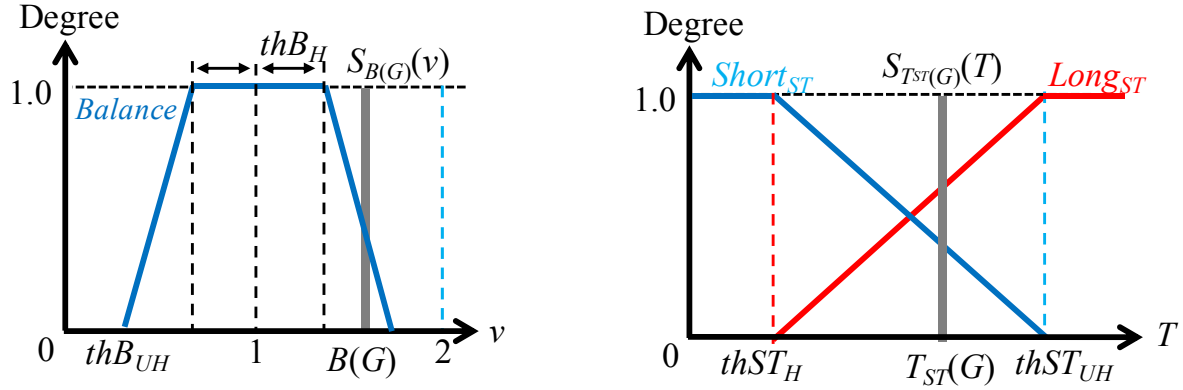

(a) Gait balance (b) total time of stance

Figure 4.7 Fuzzy membership functions for gait balance.

Here, the notation $S_\alpha(\beta)$ denotes a fuzzy singleton function. The linguistic values *Good* and *Bad* are calculated by Equation 4.9 and Equation 4.10, respectively. These equations are based on the knowledge 3 and 4.

$$Good = \begin{cases} \mu_B(G) & if\ \mu_B(G) < 0.2 \\ 1-\mu_{ST}(G) & otherwise \end{cases} \quad \text{[degree]} \tag{4.9}$$

$$Bad = \begin{cases} 1-\mu_B(G) & if\ \mu_B(G) < 0.2 \\ \mu_{ST}(G) & otherwise \end{cases} \quad \text{[degree]} \tag{4.10}$$

In this method, a gait level index (*GLI*) is estimating as an index of the gait condition by fuzzy MIN-MAX center of gravity method [39]. Figure 4.8 explains the process of the fuzzy MIN-MAX center of gravity method. Firstly, we get a minimum value from each input fuzzy linguistic values. Then, we perform a minimum operation to the value and corresponding fuzzy membership function. Figure 4.8(b) shows example of the minimum operation for Rule2. We perform the operation for every rule, and eight fuzzy membership functions are obtained. Secondly, we performed maximum operation for these fuzzy membership functions. By this operation, a fuzzy membership function GL_G for the acquired gait data G is obtained. Figure 4.8(c) shows the example of the operation and obtained membership function. Finally, the *GLI* is calculated as a center of gravity of the fuzzy membership function GL_G by Equation 4.11.

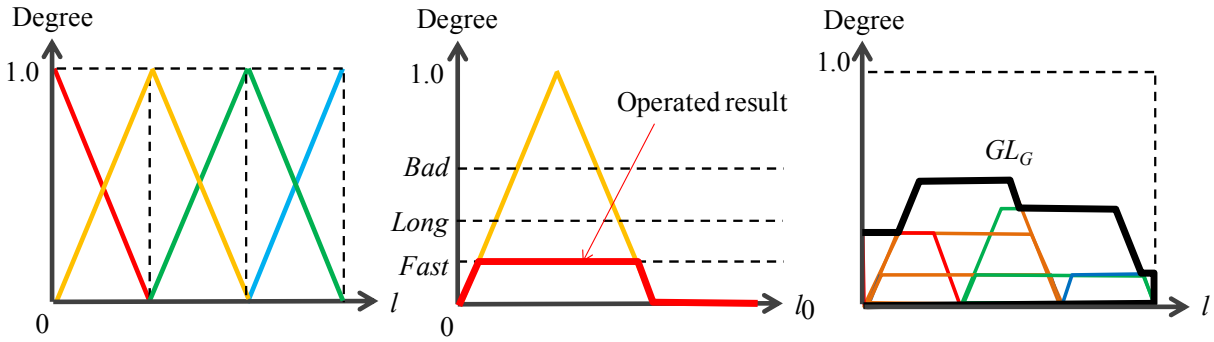

(a) gait condition (b) minimum operation (c) maximum operation

Figure 4.8 Procedure of GLI calculation.

$$GLI(G) = \frac{\sum \{GL_G(l) \times l\}}{\sum GL_G(l)} \tag{4.11}$$

Here, the notation l denotes level value of gait condition.

In our proposed method, fuzzy membership functions *Fast*, *Short*, *Balance* and *Stance* are individually decided by learning gait data of N patients and M commons as following process.

1. Initialize parameters of the function.
2. Calculate fuzzy degree of commons for all subjects.
3. Classify these data to Commons and Patients by the calculated fuzzy degree. Here, when the fuzzy degree lager than 0.5, we classify the data to Commons. Otherwise, the data is classified to Patients.
4. Calculate an entropy H by Equation 4.12.

$$H = -\log_{10}\left(\frac{FN}{TP+TN} + \frac{FP}{TN+FN}\right) \tag{4.12}$$

   Here, the notation TP and TN denote number of true classified commons and patients, respectively. The FN and TN denote number of false classified commons and patients, respectively.
5. Update parameters, and repeat calculating the entropy.
6. Decide the function with the highest entropy.
7. The fuzzy membership function *Slow* and *Long* are decided as a complement set of the *Fast* and *Short*, respectively.

4.5 Experimental Results

In our experiment, we took gait data from one hundred volunteers consisted of ten patients and ninety commons. Ten patients underwent rehabilitation in Ishikawa hospital in Japan. In acquisition, therapists were abreast of the patient if it is indicated. The patients are selected by following four qualifications.

1. Patients in recovery phase rehabilitation ward in Ishikawa Hospital.
2. Patients whose physical therapist has more than three year's experiences at rehabilitation department.
3. Patients whose gait level is "independence", "supervision" and "assistance"
4. Patients being able to understand instructions in measuring gait.

The gait conditions or abilities of patients are different individuals as shown in Table 4.2. In this table, gait shows the way of walking on the sensor. The independent gait means the subject walked without any equipment and supports. The cane walk means the subject walked with cane. Moreover, supports such as assistance, supervision and independent show how much therapists take care about subjects at the acquisition. The assistance means therapist did some support to walk on the sensor. The supervision means therapist supervised with keeping abreast of the patient just in case. The independent means therapist did not be abreast of the patient. These evaluations were evaluated by their physical therapists. Ninety commons did not need any supports. We evaluated our method by leave-one-out cross validation method. However, we do not have any true value of gait conditions of patients. Therefore, we evaluate with sensitivity, specificity and accuracy of classification. In the classification, if obtained *GLI* is above 50, it is classified as Commons. Else, it is classified as Patients. Here, the sensitivity, specificity and accuracy are defined by following equations.

$$Sensitivity = \frac{TP}{TP + FN} \tag{4.13}$$

$$Specificity = \frac{TN}{TN + FP} \tag{4.14}$$

$$Accuracy = \frac{TN + TP}{TP + FN + TN + FP} \tag{4.15}$$

Table 4.2 Information of patients.

Patient ID	Age [years]	Gait	Supports
#1	85	Independent gait	Independent
#2	77	Cane walk	Supervision
#3	70	Cane walk	Supervision
#4	52	Cane walk	Independent
#5	83	Independent gait	Independent
#6	83	Cane walk	Assistance
#7	72	Cane walk	Supervision
#8	84	Cane walk	Supervision
#9	62	Independent gait	Independent
#10	82	Cane walk	Independent

Figure 4.9 show extracted gait features for all subjects. Figure 4.10 shows estimated *GLI* of patients. And, Figure 4.11 shows GLI estimation result for all subjects. In the Figure 4.10, patients are sorted with their *GLI*. From this figure, patients #1 and #9 who walked with independently obtained higher *GLI* than the others, and they were classified to Commons. Moreover, the cane walked and supervision patients and assisted walk patient were obtained lower *GLI*. Table 4.3 and Figure 4.12 show classification results. Eight of ten patients and eighty-six of ninety commons are successfully classified. The mean value of estimated *GLI* was 33.2 in patients and 83.0 in commons. In this experiment, the sensitivity was 0.96, specificity was 0.80 and accuracy was 0.94.

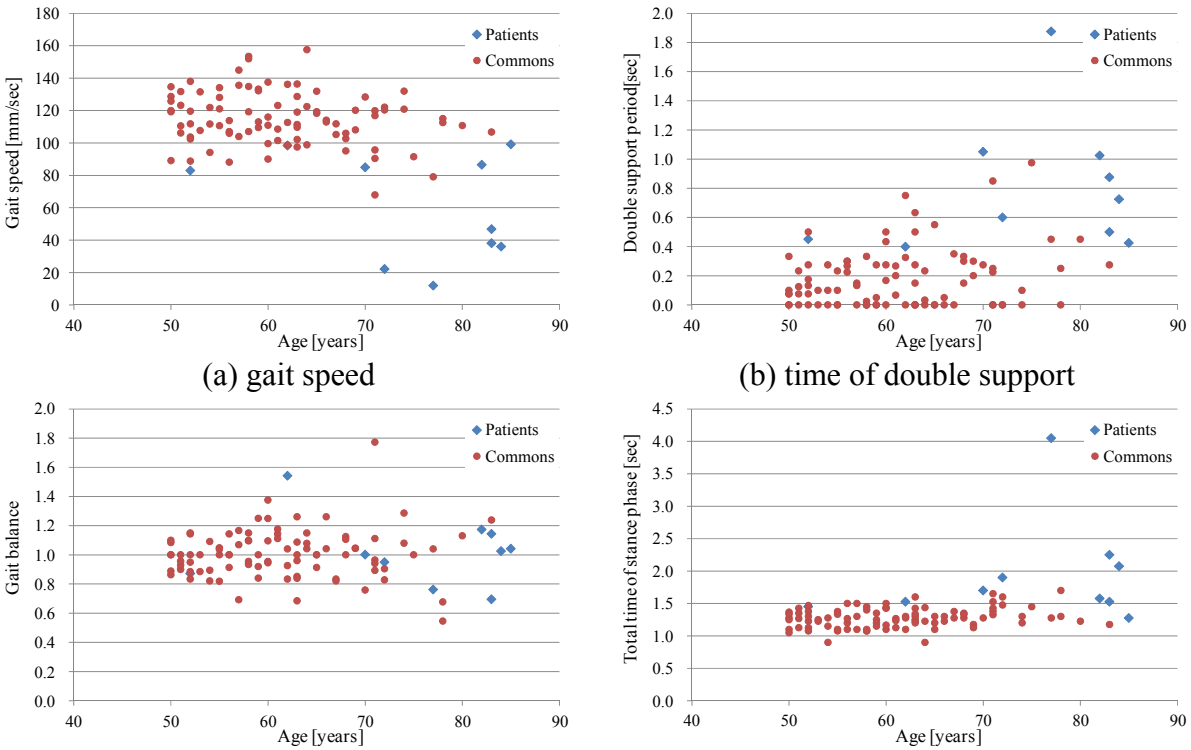

Figure 4.9 Gait features extraction results for 10 patients and 90 commons

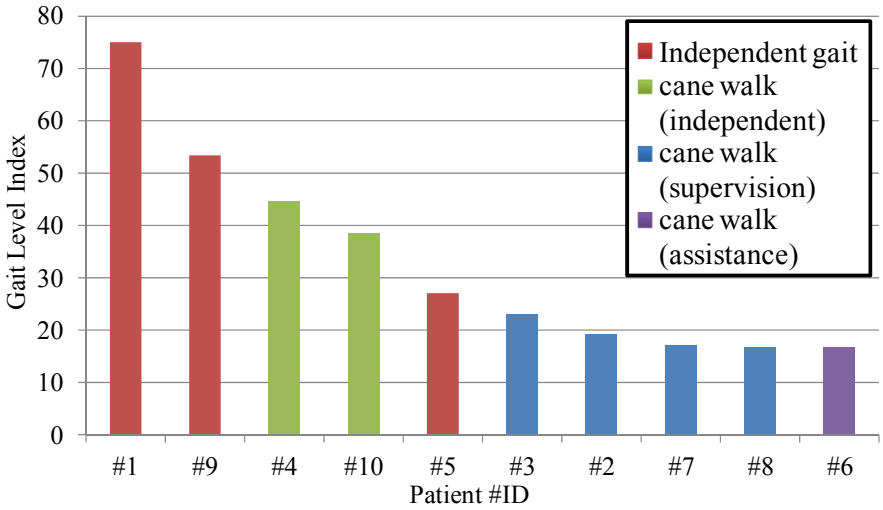

Figure 4.10 Gait level index estimation results for patients.

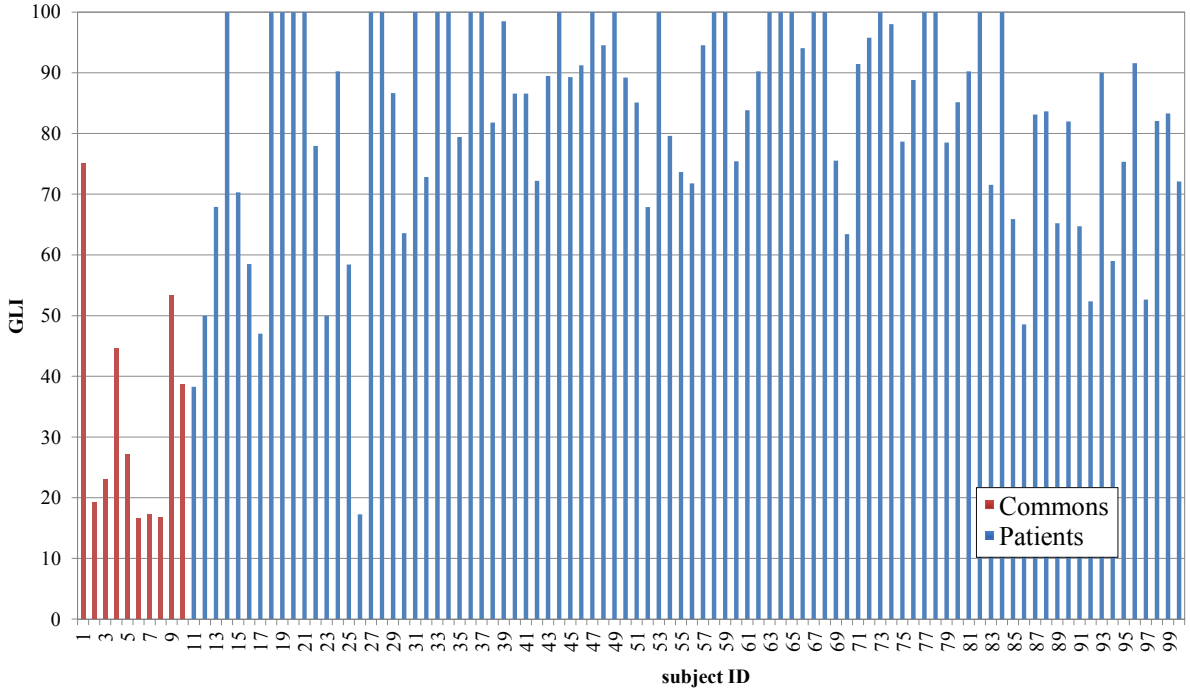

Figure 4.11 Gait level index estimation results for all subject.

Table 4.3 Classification results by GLI.

Subjects	Number of subject [persons]	Number of True classified [persons]	Estimated GLI	
			Mean	SD
Patients	10	8 (TN)	33.2	19.6
Commons	90	86 (TP)	83.0	17.6

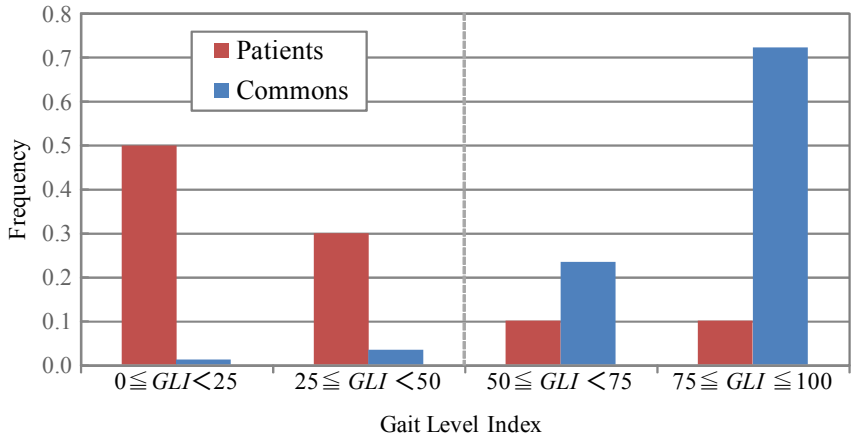

Figure 4.12 Classification results of 10 patients and 90 commons.

For evaluation of classification results, we compared our method with support vector machine (SVM) with spline kernel [40], [41]. We employed extracted features based SVM and principal component analysis (PCA) [42], [43] based SVM. The extracted based SVM classified the volunteers by using same features of our proposed method. PCA based SVM classified volunteers by using feature which extracted by PCA. Here, we input fourteen features as shown in Table 4.4 consist of gait features and age of the subjects to PCA. In PCA, inputted data are standardized to be dispersion is 1 and mean is 1 before extraction. Then, the

standardized data is analyzed. Table 4.5 shows the contributing ratio and cumulative contribution ratio of each principal component. From considering about cumulative contribution ratio, we decided to employ four principal components, 1st, 2nd, 3rd and 4th. Then, we classified into commons and patients by SVM. Table 4.6 shows comparison results. From this table, we can see that our proposed method obtained the highest accuracy and better sensitivity and specificity. Thus, the proposed method is better than the other method.

Table 4.4 Gait features fro PCA.

Subject age	Stride
Right step length	Left step length
Cadence	Maximum gait speed
Time of gait cycle	Time of double support period
Time of right single support period	Time of left single support period
Time of right stance phase	Time of right stance phase
Total time of stance phase	Gait balance

Table 4.5 Cumulative contribution ratio of each Principal component.

Principal component	Contributing ratio [%]	Cumulative contribution ratio [%]
#1	48.9	48.9
#2	12.6	61.4
#3	10.6	72.0
#4	8.6	80.7
#5	6.0	86.6
#6	4.7	91.3
#7	2.9	94.3
#8	2.5	96.7
#9	1.5	98.2
#10	1.2	99.4
#11	0.5	99.9
#12	0.1	100
#13	0.0	100
#14	0.0	100

Table 4.6 Comparison result of classification by *GLI*.

Method		Sensitivity	Specificity	Accuracy
Proposed method		0.96	0.80	0.94
Extracted feature based SVM		0.99	0.50	0.94
PCA based SVM	1st	0.66	1.00	0.69
	1st, 2nd	0.72	1.00	0.75
	1st, 2nd, 3rd	0.72	1.00	0.75
	1st, 2nd, 3rd, 4th	0.67	1.00	0.70

4.6 Discussions

In discussion, we focus on the estimated *GLI* of a patients and a common volunteer *GLI*. From Figure 4.14, patient #1 scored the highest *GLI* that was 75.0 and whose gait mean is independent walk. However, this score is much higher than any other patients. Her *GLI* shows that she did not have big problem about her gait. Actually, she was undergoing rehabilitation for pain relief or controlling her own pain not for her gait. Thus, we consider that the obtained *GLI* described the gait condition. Next, we discuss about a common volunteer whose estimated low *GLI*. Her estimated *GLI* was 17.3 that showed she had some problem in her gait. About this common, the physical therapist said that extracted gait features that including we did not employed in our proposed method shows she was likely undergoing rehabilitation. Thus she might be too nervous to walk on the sensor or actually she has some problem in her gait. Thus, this estimation system found gait defective from commons as well.

4.7 Conclusion

This chapter proposed the gait condition estimation method based on fuzzy inference. In our proposed method, we acquired gait data by the mat type load distribution sensor. From four knowledge about human gait, we employed four gait features such as maximum gait speed, time of double support, gait balance and total time of stance phase. Finally we calculated gait level index by fuzzy MIN-MAX center of gravity method. The results show that our proposed method successfully estimated the *GLI*. For evaluation, we classified one hundred gait data into Common or Patient by estimated *GLI*. In classification results, our proposed method classified gait data with higher accuracy than PCA based SVM and extracted feature based SVM. From these results, our proposed method estimated *GLI* almost successfully and found gait defective from patients and commons. In this way, our proposed method was justified as the estimation system of gait condition.

By using this system, it could be used in medical welfare and support diacritic of doctors. Thus, we will build up the system of this method in the future. Toward these futures, we have to continue to research and improve the system for calculating the index more specifically and successfully with acquired gait data from more patients.

5 Biometric Personal Authentication Based on Gait Features

This chapter proposes fuzzy aided biometric personal authentication system by using both of right and left sole pressure distribution. The method classifies acquired sole pressure data to individual from characteristics of gait pattern. Section 5.1 introduces the walking based biometric authentication system. Section 5.2 shows data acquisition protocol and sole coordinate system. Section 5.3 describes gait features for authentication system. Section 5.4 shows fuzzy logic based personal authentication method. Section 5.5 describes experimental results. Section 5.6 discusses about the biometric personal authentication system. Section 5.7 concludes this chapter.

5.1 Introduction

Information technologies and network based services, such as healthcare, commercial and social services become indispensable parts of our lives. Reliable authentication of users is needed for secure access to these services to avoid compromising our privacy. Passwords and PINs are still the major authentication methods for network services. However, we have to remember a lot of passwords or PINs for several services. Moreover, the information might be stolen by shoulder surfing, keystroke logging and so on. Biometrics is an emerging technology to authenticate a person based on physical or behavioral features. While techniques using physical features such as fingerprint [44], [48] and iris can achieve high recognition accuracy, behavioral features such as signature [49], speech [50] and walking [51] - [56] are more user-friendly.

We focus on a biometric method based on sole pressure and dynamics in walking. Because walking is the most natural daily motion, biometrics systems that use walking do not require any training for authentication. This method can be conveniently used to authenticate people while passing through a door or passageway. It is available to an application where a person entering a room and walking toward a device or a computer can be authenticated and immediately logged in the room. Walking patterns can be captured with cameras [51], [52], acceleration sensors [53] and pressure sensors [54]-[60]. The pressure sensor measures a walking as a dynamic change of pressures. Several studies [54]-[58] have been introduced on this topic. Addlesee *et al.* [56], Orr *et al*. [57] and Yamakawa *et al*. [58] focus on sole pressure change. These methods use some features such as peak pressure value, time to peak pressure and form of pressure change curve. They authenticate the walking person by employing only one foot. Qian *et al*. [55] has used step lengths, 3D trajectories of center of pressure and angles between right and left soles. They measure over three steps for authentication by the use of large pressure sensor (3.7 m × 4.5 m). However, these methods did not use shape information of the sole. Jung *et al*. [54] use footprint and center-of-pressure trajectory for authentication. They employ both of right and left sole pressures, but their pressure sensor is too small to measure both foot (40 cm × 80 cm). Furthermore, authentication accuracies of these methods are not enough to use them for security field.

In this study, we propose a kind of integration approach [59]-[61] to improve authentication performance of biometrics based on walking. Integration approaches improve

authentication accuracy by combining multi-methods, multi-features or multi-sampling. This study combines the authentication score of right and left sole pressure data. These right and left sole pressures are measured by middle size load distribution sensor, and it is designed to accommodate two steps of an average walker. The load distribution sensor is a kind of the pressure sensors arranged on a two-dimensional pattern. This arrangement of sensors enables us to acquire dynamic change of sole pressure distribution. To authenticate person, gait features are extracted from the sole pressure distribution. The gait features consist both of sole pressure change and footprint. As the authentication score, the system calculates fuzzy degrees of each sole pressure for registered person. The fuzzy degree means a degree of similarity of acquired sole pressure and registered data set for a person. Here, fuzzy membership functions are statistically determined in learning process. The system combines the fuzzy degree of right and left sole by a combination operator, and uses it for authentication. In the experiment, we employed six combination operators and evaluated these authentication performances. We show the experimental results of 90 volunteers of each combination operator. Then, we describe an optimal operator for combining left and right sole pressures.

5.2 Preliminaries

This personal authentication system acquires sole pressure distribution as the walking pattern. The sole pressure distribution is acquired by mat-type load distribution sensor (Arrow Industry Co., Ltd. AS-64X256-7PM) explained by Chapter 3.2. The effective area of the load distribution sensor is 33 cm × 178 cm. It is enough to acquire sole pressure distribution of a pair of right and left foot while walking. In the experiments, subjects were asked to walk normally on the load distribution sensor platform. The protocol is such that the subject must first halt right before the sensing area, and then walks through and past the sensor, typically involving two or three steps. We consider the walking sense as the x-axis of the sensor. The system acquires the sole pressure distribution during these steps and stores data in a computer as biometric evidence. One limitation of the experiment is that the subjects must walk with bare feet or with socks.

From the acquired sole pressure data, the system separates a right sole pressure data and a left sole pressure data. The separated right sole and left sole pressure data is shown in Figure 5.1. We define sole coordinate system as shown in Figure 5.2. We consider a registered person set $Y = \{y_1, y_2, ..., y_r, ..., y_n\}$. Here, the notation n denotes the number of registered person. We take the sole pressure distribution data N times from each registered person, and use these pressure data in learning process of our system. The notation X^S denotes a pressure distribution change data when a person "y_s" is walking. A pressure data X^S has a right sole pressure data X_R^S and a left sole pressure data X_L^S.

Figure 5.3 shows procedure of the authentication system. The system calculates authentication scores from right sole X_R^S and left sole X_L^S, independently. Then these scores are combined to authenticate a person.

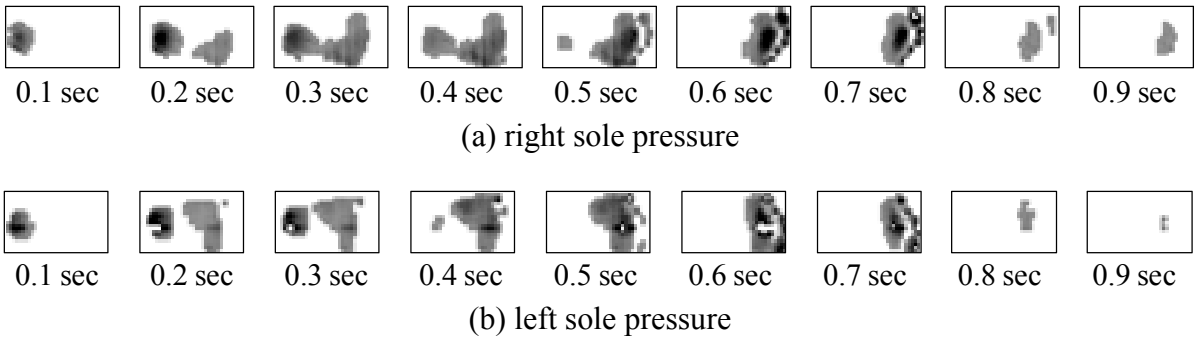

Figure 5.1 Examples of separated right sole and left sole pressure data.

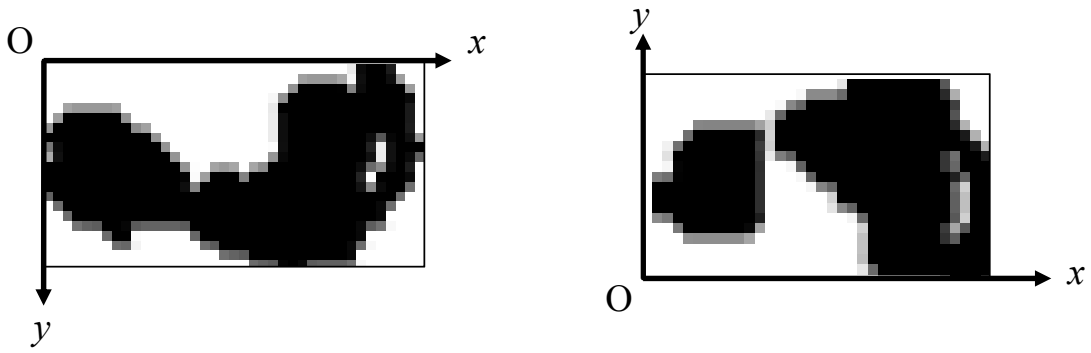

Figure 5.2 Examples of separated right sole and left sole pressure data.

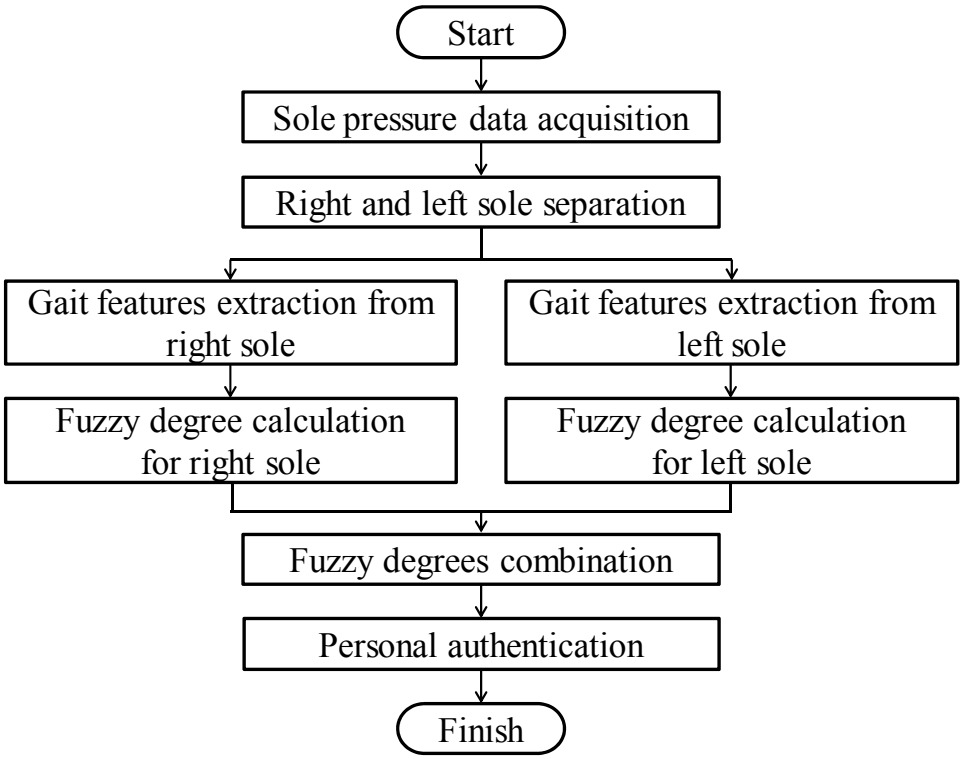

Figure 5.3 Procedure of personal authentication system.

Table 5.1 Gait features of a sole pressure data.

sole pressure data X_k^S	
Notation	Feature
$f_1(X_k^S)$	The length of footprint
$f_2(X_k^S)$	The width of footprint
$f_3(X_k^S)$	The area of footprint
$f_4(X_k^S)$	The angle of footprint
$f_5(X_k^S)$	The area of inner side of heel
$f_6(X_k^S), f_7(X_k^S)$	The area of arch on footprint
$f_8(X_k^S)$	The area of a big toe on footprint
$f_9(X_k^S)$	The area of outer side of heel on footprint
$f_{10}(X_k^S), f_{11}(X_k^S)$	The area of arch on footprint
$f_{12}(X_k^S)$	The area of toes on footprint
$f_{13}(X_k^S) \sim f_{21}(X_k^S)$	The normalized CSPs on footprint
$f_{22}(X_k^S) \sim f_{30}(X_k^S)$	The normalized HSPs on footprint
$f_{31}(X_k^S) \sim f_{39}(X_k^S)$	The normalized areas on footprint

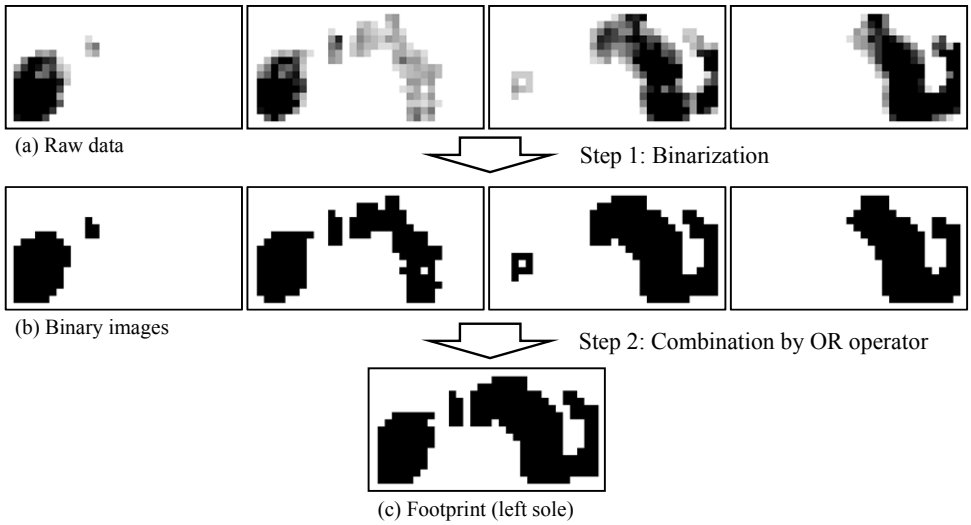

Figure 5.4 Procedure of the footprint production.

5.3 Gait Feature Extraction

For authentication, our system extracts thirty nine gait features from each sole pressure data X_k^S, where the notation k denotes the index of the right foot ($k = R$) or the left foot ($k = L$). Twelve features are based on a footprint, and twenty seven features based on weight shift while walking. The notation $f_i(X_k^S)$ denotes a gait feature with respect to a sole pressure data X_k^S where i denotes the index of each feature. Table 5.1 shows the notation indexes with respect to a sole pressure data X_k^S.

The system extracts twelve features $f_i(X_k^S)$ from every footprint made from a sole pressure data X_k^S. A footprint is one of overlapped pressure distribution of the sole, and it is obtained by maximum of binary images of pressure distribution for all frames. Figure 5.4 shows procedure of the footprint production. Binary images are calculated from every frame

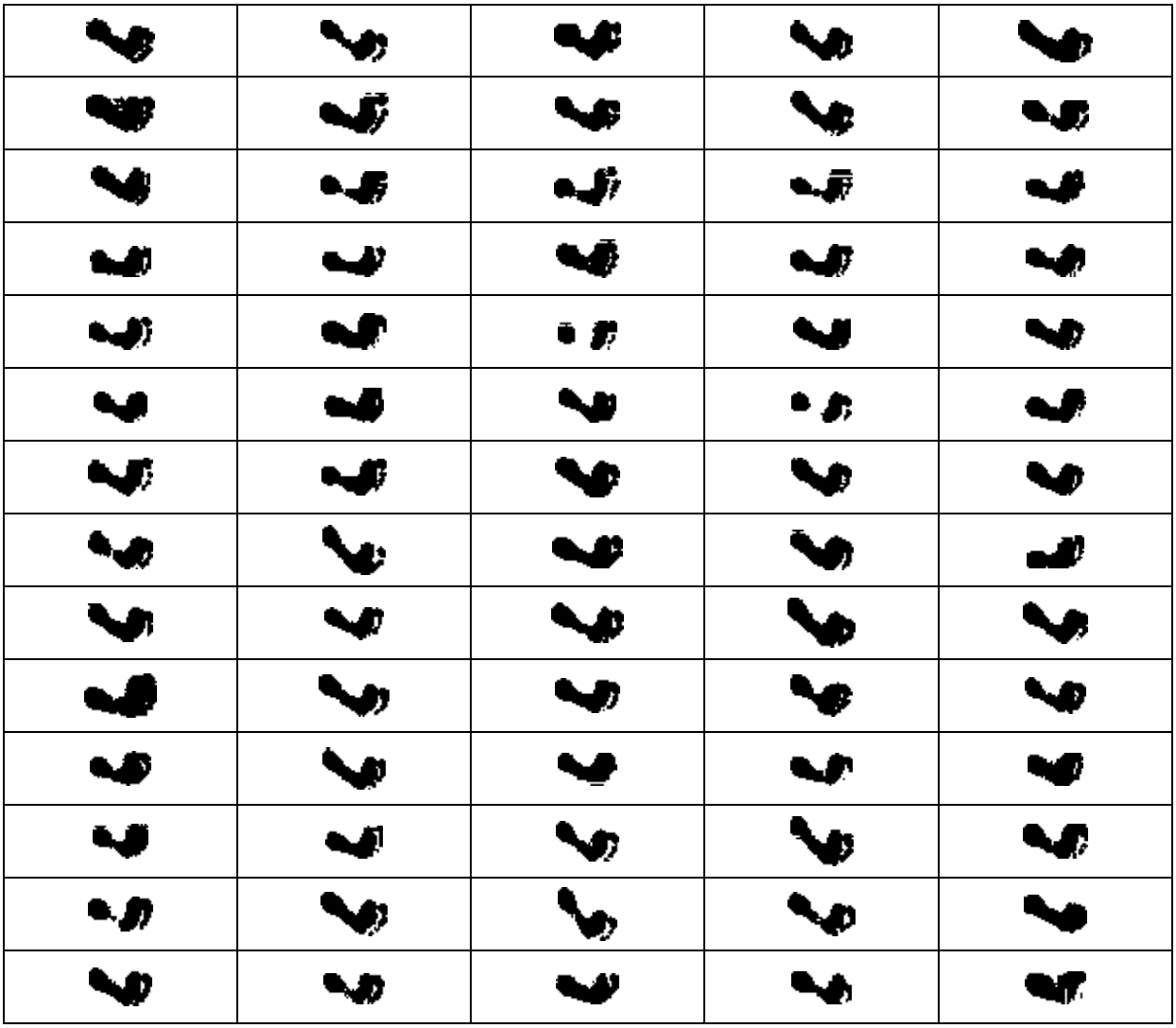

Figure 5.5 Examples of right footprints of 70 subjects.

of the sole pressure data. Black pixels have pressure values and white pixels do not have pressure value. Figure 5.5 shows examples of right footprints. As shown in this figure, footprints are different among persons. From this footprint, we extract the length of footprint $f_1(X_k^S)$, the width of footprint $f_2(X_k^S)$, the area of footprint $f_3(X_k^S)$, the angel between the direction of footprint and x-axis of load distribution sensor $f_4(X_k^S)$ and the distribution of footprint $f_5(X_k^S)$,..., $f_{12}(X_k^S)$ as features. It is shown in Figure 5.6. In this figure, white colored area shows non-sole area and black colored areas show the footprint. The area of footprint $f_3(X_k^S)$ is calculated by the number of sole pixels in the footprint. The area of footprint shows a sole size of the walking person. The red straight line is obtained least square method for footprint. We calculate the angle $f_4(X_k^S)$ between the red line and x-axis of the sensor. This feature means an angle between a foot and walking direction because the data acquisition protocol sets the x-axis as a direction of walking. The green rectangle is the circumscribed rectangle. We use the length of long side of the this green circumscribed rectangle as the length of footprint $f_1(X_k^S)$ and use the length of short side as the width of footprint $f_2(X_k^S)$ as the features. Since there are differences in the length and width of foot

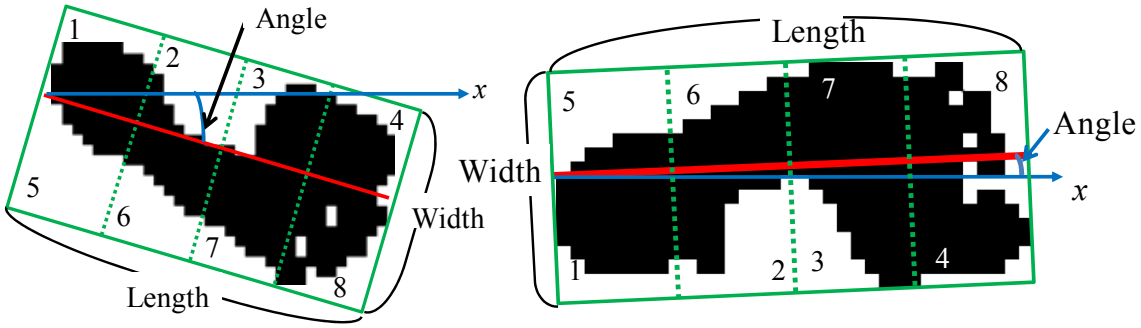

(a) Right sole (b) Left sole

Figure 5.6 Example of footprint and these features.

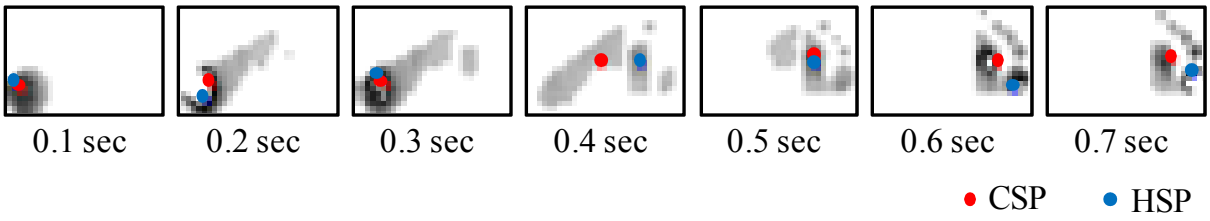

Figure 5.7 Example of CSP and HSP of each frame.

between individuals, we employ these features for authentication. The green dotted lines are quarter of the green circumscribed rectangle. Then, we obtain eight small areas surrounded by the red straight line, the green circumscribed rectangle and the green dotted lines. The distribution of footprint $f_5(X_k^S)$,..., $f_{12}(X_k^S)$ are calculated by number of sole pixels in each small areas. For example, when the walking person has a flat foot, the area of arch on footprint $f_6(X_k^S)$ and $f_7(X_k^S)$ are bigger than that of normal foot. Moreover, several footprints lack the area of toes $f_{12}(X_k^S)$, when the walker puts his/her weight on only a big toe. As seen from the above, the area of footprint $f_3(X_k^S)$ shows a size of footprint, whereas the distribution of footprint $f_5(X_k^S)$,..., $f_{12}(X_k^S)$ express foot shape and posture of walk.

The system extracts twenty seven features from every frame of a sole pressure data X_k^S. We calculate the center of sole pressure (CSP), the highest sole pressure point (HSP) and the area of footprint from each frame. The area is calculated by the number of sole pixels from each frame. Figure 5.7 shows examples of CSPs and HSPs of each frame. Generally, the area changes with a period of gait cycle, and the changes express weight shift of the walker. The CSPs and HSPs show significant locations of sole pressure at the time. Generally, these trajectories are drawn lines from heel to toe. The CSPs trajectory is famous feature of gait analysis, and it is related to center-of-gravity while walking. On the other hand, the HSP shows a point that is applied to the highest power by the walker on the time. Figure 5.8 shows two different right sole pressure data. Thus these two data vary in the number of frames, thus the gait periods of two sole pressures are different. To solve this problem, we normalize these features to nine frames sole data. We suppose that the dynamic changes of each feature are similar in one step. Therefore, the system approximates these features by a polygonal line, and the nine features are interpolated by liner interpolation. The interpolated nine CSPs $f_{13}(X_k^S)$,..., $f_{21}(X_k^S)$ and nine HSPs $f_{22}(X_k^S)$,..., $f_{30}(X_k^S)$ are extracted from these trajectory, as shown in Figure 5.9. The interpolated nine areas $f_{31}(X_k^S)$,..., $f_{39}(X_k^S)$ are extracted from the polygonal lines as shown in Figure 5.10.

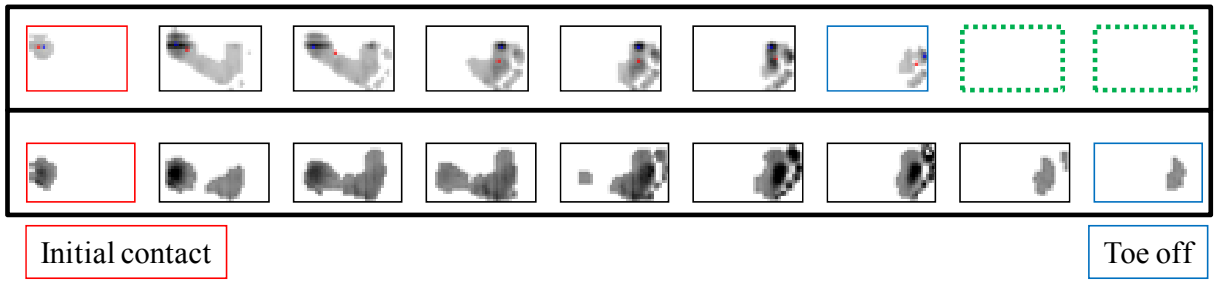

Figure 5.8 Two sole data that the number of frames is different.

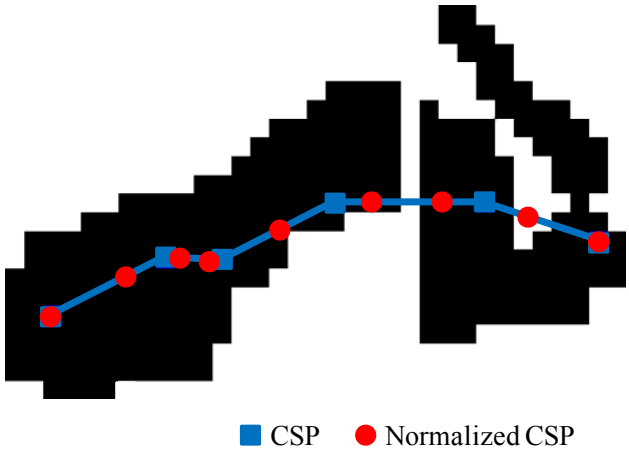

Figure 5.9 An example of CSPs trajectory and nine normalized CSPs.

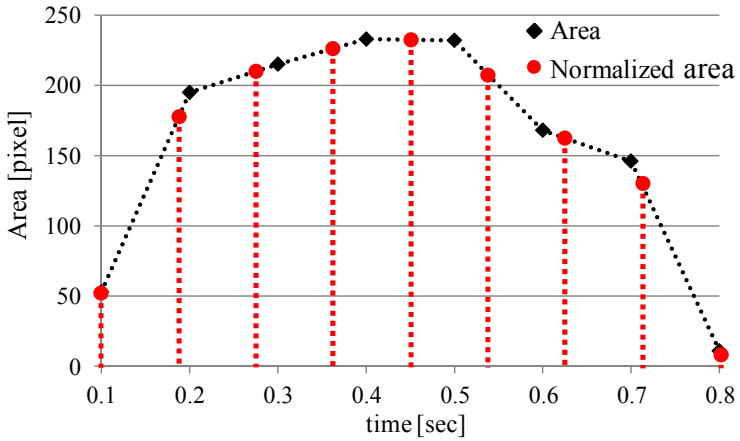

Figure 5.10 Example of nine normalize areas..

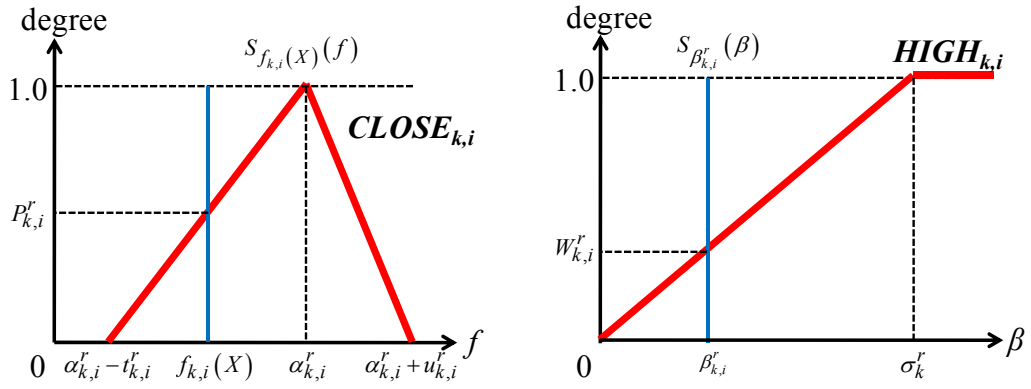

(a) Rule1 (*CLOSE*) (b) Rule2 (*HIGH*)

Figure 5.11 Fuzzy membership functions for personal authentication.

5.4 Personal Authentication by Fuzzy Logic

In this section, we explain a calculation method of two fuzzy degrees $\mu^r_R\left(X^S_R\right)$ and $\mu^r_L\left(X^S_L\right)$ for a registered person y_r. The fuzzy degrees $\mu^r_R\left(X^S_R\right)$ and $\mu^r_L\left(X^S_L\right)$ are calculated from each sole pressure data X^S_R and X^S_L, respectively. We employ these fuzzy degrees for authentication score of each foot. We consider the following as knowledge about gait features for biometrics security.

Knowledge 1 : Features of same person are similar.

Knowledge 2 : Feature with higher classification performance in learning pressure is more primary for personal authentication more than other features.

From these knowledge, the following fuzzy IF-THEN rules are derived.

Rule 1 : IF feature $f_i(X^S_k)$ is $CLOSE_{k,i}$ to a baseline value $\alpha^S_{k,i}$ of a registered person y_r, THEN the degree of similarity $P^r_{k,i}\left(X^S_k\right)$ of the feature is high.

Rule 2 : IF classification score $\beta^S_{k,i}$ of learning sole pressure data is $HIGH_{k,i}$, THEN the degree of contribution $W^r_{k,i}\left(\beta^r_{k,i}\right)$ for the authentication of the feature is high.

The fuzzy membership functions $CLOSE_{k,i}$ and $HIGH_{k,i}$ are defined in Figure 5.11. These functions have parameters $\alpha^r_{k,i}$, $\beta^r_{k,i}$, $t^r_{k,i}$, $u^r_{k,i}$ and σ^S_k. Here, the notations $t^r_{k,i}$ and denotes width of the membership function $CLOSE_{k,i}$. The notation σ^S_k is a sum of the classification score $\beta^r_{k,i}$ of all features. These parameters are determined by learning process. The determination method of these parameters for any k and i is as follows. Consider one test data and N learning data for a person, and determine the parameters by the learning data of all registered persons for the test data. First, the system calculates the mean $Mean^r_{k,i}$ and a standard deviation $SD^r_{k,i}$ of N learning data for k and i of y_r. Second, we initialize $\alpha^r_{k,i} \leftarrow Mean^r_{k,i}$, $t^r_{k,i} \leftarrow SD^r_{k,i}$ and $u^r_{k,i} \leftarrow SD^r_{k,i}$. By this initialization, the membership function $CLOSE_{k,i}$ is formed as shown in Figure 5.12(a), and classification score $\beta^r_{k,i}$ is calculated by Equation 5.1.

$$\beta^r_{k,i} = \frac{\sum_{j=1}^{N} P^r_{k,i}\left(L^{r,j}_k\right)}{N} - \frac{\sum_{t=1}^{n-1}\sum_{j=1}^{N} P^r_{k,i}\left(L^{t,j}_k\right)}{N\times(n-1)} \quad \text{[degree]} \tag{5.1}$$

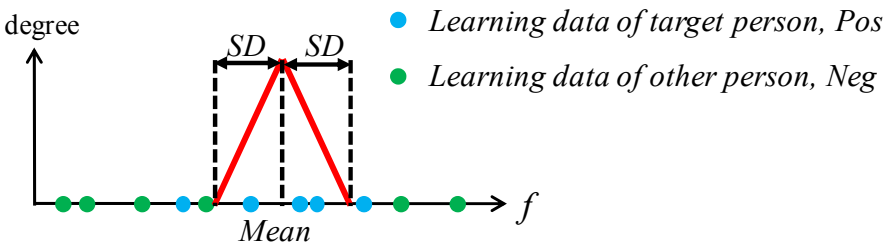

(a) Example of initialized fuzzy membership function *CLOSE*

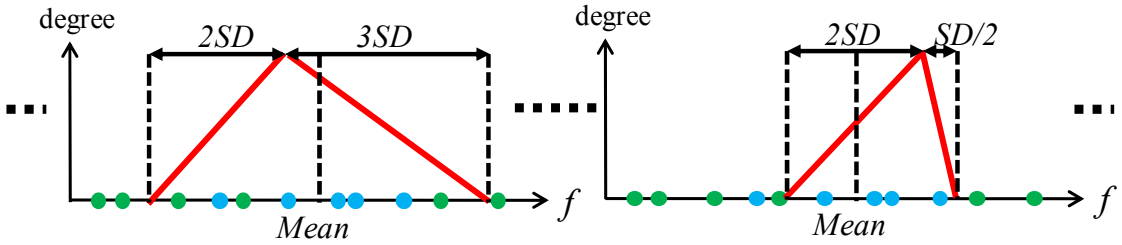

(b) Example of deformed fuzzy membership function *CLOSE*

Figure 5.12 Examples of fuzzy membership functions deformation.

Here, the notation $L_k^{r,j}$ and $L_k^{t,j}$ denote learning data of the target person y_r and those of other registered persons y_t, respectively. The notation j denotes an index of learning data. The notation N denotes the number of training samples of a registered person, and the notation n does the number of registered person. The fuzzy degree of similarity $P_{R,i}^r\left(X_k^S\right)$ of the feature is calculated by Equation 5.2.

$$P_{k,i}^r\left(X_k\right) = \min\left(CLOSE, S_{f_i(X_k)}(f)\right) \quad \text{[degree]} \tag{5.2}$$

Here, the notation $S_\alpha(\beta)$ denotes a fuzzy singleton function. The Equation 5.1 means the difference between the average degree of similarity $P_{R,i}^r\left(X_k^t\right)$ for other person and the average $P_{R,i}^r\left(X_k^r\right)$ for the target person y_r. We employ this value as the classification score. Third, the system repeats the calculation of Equation 5.1 for all domains of $Mean_{k,i}^r$ - $SD_{k,i}^r \le \alpha_{k,i}^r \le Mean_{k,i}^r + SD_{k,i}^r$, $0 \le t_{k,i}^r \le 4\,SD_{k,i}^r$ and $0 \le u_{k,i}^r \le SD_{k,i}^r$ at the interval of $SD_{k,i}^r$ / 10. Figure 5.12(b) shows examples of the deformed membership function $CLOSE_{k,i}$. We obtain the classification score $\beta_{k,i}^r$ from all domains. The system employs these parameters $\alpha_{k,i}^r$, $t_{k,i}^r$, and $u_{k,i}^r$ with the highest $\beta_{k,i}^r$ among all domains for a feature $f_i(X_k^S)$ of person y_r. The determination process are repeated for all k and i of y_r. The parameter σ_k^S of membership function $HIGH_{k,i}$ is calculated by sum of classification score $\beta_{k,i}^r$ of a person y_r. It is calculated by Equation 5.3.

$$\sigma_k^r = \sum_{i=1}^{39} \beta_{k,i}^r \quad \text{[degree]} \tag{5.3}$$

The fuzzy degree for a feature $Q_{k,i}^r\left(X_k^S\right)$ is defined by Equation 5.4. We calculate the degree $Q_{k,i}^r\left(X_k^S\right)$ for all k and i of pressure data X_k^S.

$$Q_{k,i}^r\left(X_k^S\right) = P_{k,i}^r\left(X_k^S\right) \times W_{k,i}^r\left(\beta_{k,i}^r\right) \quad \text{[degree]} \tag{5.4}$$

Here the fuzzy degree of contribution $W_{k,i}^r\left(\beta_{k,i}^r\right)$ means the effectiveness of $f_i(X_k^S)$ for person y_r, and it is defined by Equation 5.5.

$$W_{k,i}^r\left(\beta_{k,i}^r\right) = \min\left(HIGH_{k,i}, S_{\beta_{k,i}^r}(w)\right) \quad \text{[degree]} \tag{5.5}$$

Table 5.2 Example of authentication process.

Sole pressure	Fuzzy degree				
	$\mu^1_{Sole}(X^S)$	$\mu^2_{Sole}(X^S)$	$\mu^3_{Sole}(X^S)$	$\mu^4_{Sole}(X^S)$	$\mu^5_{Sole}(X^S)$
X^S	0.1	0.8	0.6	0.4	0.3

Finally, the system calculates a fuzzy degree $\mu^r_k(X^S_k)$ of a sole pressure data X^S_k for all y_r by Equation 5.6. Here, the fuzzy degree of a sole pressure $\mu^r_k(X^S_k)$ means an authentication score for the registered person calculated from one sole pressure data

$$\mu^r_k(X^S_k) = \sum_{i=1}^{39} Q^r_{k,i}(X^S_k) \quad \text{[degree]} \tag{5.5}$$

In order to authenticate person, we calculate a combined fuzzy degree $\mu^r_{Sole}(X^S)$. The combined fuzzy degree is calculated from fuzzy degrees of right sole $\mu^r_R(X^S_R)$ and left sole $\mu^r_L(X^S_L)$. In this method, we identify and verify person by the fuzzy degree $\mu^r_{Sole}(X^S)$. For personal identification (1:n collation), the system calculates the combined fuzzy degree $\mu^r_{Sole}(X^S)$ for every registered person y_s. We obtain the highest fuzzy degree among the registered persons. The system identifies the walking person y_s as a registered person y_r with the highest combined fuzzy degree. For personal verification (1:1 collation), the system calculate combined fuzzy degree of X^S for a target person y_r. If the combined fuzzy degree is higher than a threshed, the system verifies the walking person y_s as the target person y_r. For example, Table 5.2 shows an example of the fuzzy degrees for 5 registered persons. In this case, because fuzzy degree for registered person y_2 is the highest, the system identifies the walking person as the person y_2. On the verification, when the threshold is set as 0.5, person y_2 and y_3 are verified as the waling person.

In this paper, we employ mean (Equation 5.7), minimum (Equation 5.8), maximum (Equation 5.9), product, probabilistic sum (Equation 5.10) and weighted sum (Equation 5.11) as the combination operator.

$$\mu^r_{Sole}(X^S) = \frac{1}{2}\left\{\mu^r_R(X^S_R) + \mu^r_L(X^S_L)\right\} \quad \text{[degree]} \tag{5.7}$$

$$\mu^r_{Sole}(X^S) = \begin{cases} \mu^r_R(X^S_R) & \textit{if } \mu^r_R(X^S_R) < \mu^r_L(X^S_L) \\ \mu^r_L(X^S_L) & \textit{otherwise} \end{cases} \quad \text{[degree]} \tag{5.8}$$

$$\mu^r_{Sole}(X^S) = \begin{cases} \mu^r_R(X^S_R) & \textit{if } \mu^r_R(X^S_R) > \mu^r_L(X^S_L) \\ \mu^r_L(X^S_L) & \textit{otherwise} \end{cases} \quad \text{[degree]} \tag{5.9}$$

$$\mu^r_{Sole}(X^S) = \left\{\mu^r_R(X^S_R) + \mu^r_L(X^S_L)\right\} - \left\{\mu^r_R(X^S_R) \times \mu^r_L(X^S_L)\right\} \quad \text{[degree]} \tag{5.10}$$

$$\mu^r_{Sole}(X^S) = w \times \mu^r_R(X^S_R) + (1-w) \times \mu^r_L(X^S_L) \quad \text{[degree]} \tag{5.11}$$

Here, the notation w is the weighting parameter, and w is within [0, 1]. When w is 0, the combined fuzzy degree equals the fuzzy degree of the left sole pressure, and when w is 1.0, the combined fuzzy degree equals the fuzzy degree of the right sole pressure. In addition, when w is 0.5, the weighting sum operator means the mean operator.

5.5 Experimental Results

In this experiment, we employed 90 volunteers as shown in Table 5.3. For each volunteer, we took the sole pressure data six times. These sole pressure data are acquired with socks. We used five data for learning and used one data as test data. We evaluate the proposed method by six-hold cross validation method. False rejection rate (FRR), false acceptance rate (FAR) and equal error rate (EER) are employed for the performance test. FRR and FAR are defined by Equation 5.12 and Equation 5.13, respectively. FRR is concerned with the number of instance defined as an authorized individual being falsely rejected by an identification system. FAR is concerned with the number of instances defined as an unauthorized individual being falsely accepted by an identification system. The higher FRR decreases the user-friendliness and higher FAR increases the risk of intrusion.

$$FRR = \frac{\text{Number of false rejectans}}{\text{Number of authrized attempts}} \times 100 \quad [\%] \tag{5.12}$$

$$FAR = \frac{\text{Number of false acceptances}}{\text{Number of impostor attempts}} \times 100 \quad [\%] \tag{5.13}$$

The EER is the error rate that FRR equals to FAR in verification. The lower EER implies higher accurate and more reliable personal authentication.

We identified and verified the subjects by the proposed method. We compared the combined fuzzy degrees $\mu^r_{Sole}\left(X^S\right)$ with the fuzzy degree of right sole $\mu^r_R\left(X^S_R\right)$ and left sole $\mu^r_L\left(X^S_L\right)$. We compared authentication results of these combination operators with results of an authentication method based on Euclidean distance. In the authentication method based on Euclidean distance, firstly, the system normalizes every gait feature using the maximum and minimum value. Secondly, the system constructs template data for each registered person. The template data is made by mean value of learning data. Thirdly, the Euclidean distance D^r is calculated by Equation 5.14.

$$D^r = \sqrt{\sum_{i=1}^{39}\left\{tmp^r_{R,i} - f_i\left(X^S_R\right)\right\}^2 + \sum_{i=1}^{39}\left\{tmp^r_{L,i} - f_i\left(X^S_L\right)\right\}^2} \tag{5.14}$$

Here, tmp^r_k denotes the template data of the registered person y_r. The template data is made by mean value of the feature $f_i(L^r_k)$ of learning data L^r_k as shown in Equation 5.15.

$$tmp^r_{k,i} = \frac{1}{N}\sum_{j=1}^{N} f_i\left(L^r_{k,i}\right) \tag{5.15}$$

Here, the notation j denotes an index of learning data. The notation N denotes the number of training samples of a registered person. In identification, the system calculates the Euclidean distance D^r for every registered person, and the walking person is identified as a registered person with the shortest Euclidean distance. In verification, the system calculates the

Table 5.3 Volunteers information of personal authentication system.

Age [year]	20-29	30-39	40-49	50-59	60-69	70-79	80-89	Total
Male [person]	11	4	5	2	2	8	4	36
Female [person]	28	3	4	4	1	9	5	54
Total [person]	39	7	9	6	3	17	9	90

Euclidean distance D^r for target person, if the Euclidean distance shorter than a threshold, the system accepts the walking person.

We performed authentication for 20, 30, 40, 50 and 90 volunteers as shown in Table 5.4. Tables 5.5, 5.6 and 5.7 show a comparison of authentication results for each number of subjects. From these results, we can see that the weighted sum operator had lower FRR and FAR than the other operators. The probabilistic sum and the mean operators obtained lower EER than the others. The mean, probabilistic sum and weighting sum operators had similar FRR, FAR and EER. Figure 5.13 shows FRR and FAR of the mean operator for 20 and 90 subjects with the threshold [0, 1]. The authentication performance of any operator decreases with the increment of the number. Figure 5.14 shows the FRR and EER of with the weighting parameter [0, 1]. From this figure, we can see that the operator obtained the lowest FRR and EER when the weighting parameter almost 0.5. From this fact, we consider that the mean operator was an optimal operator for sole pressure based biometrics. Moreover, all combination operators achieved lower error rates than the results using only right or left sole pressure data.

Table 5.4 Data set for performance test of authentication system.

Number of subjects	Age [year]						
	20-29	30-39	40-49	50-59	60-69	70-79	80-89
20	10	1	1	3	1	3	1
30	17	1	2	3	1	5	1
40	18	3	5	3	2	8	1
50	20	3	5	3	3	10	6
90	39	7	9	6	3	17	9

Table 5.5 FRRs in identification of combination operators.

Data set	FRR [%]								
	Combination operator						μ_R^r	μ_L^r	Euclidian distance
	mean	min.	max.	product	prob.	weighting sum			
20	0.0	8.3	10.0	3.3	0.0	0.0 (w=0.49)	16.7	16.7	32.5
30	3.9	14.4	13.9	5.6	4.4	3.3 (w=0.51)	22.8	27.2	45.6
40	7.5	19.2	21.3	7.9	7.1	7.1 (w=0.49)	30.4	33.8	50.0
50	12.7	27.7	26.3	13.3	13.3	11.7 (w=0.52)	40.0	41.7	56.3
90	35.0	49.3	48.0	35.6	36.1	35.0 (w=0.50)	59.4	59.6	73.7

Table 5.6 FARs in identification of combination operators.

Data set	FAR [%]								
	Combination operator						μ_R^r	μ_L^r	Euclidian distance
	mean	min.	max.	product	prob.	weighting sum			
20	0.00	0.44	0.53	0.18	0.00	0.00 (w=0.49)	0.87	0.87	1.71
30	0.13	0.50	0.49	0.19	0.15	0.11 (w=0.51)	0.79	0.93	1.57
40	0.19	0.49	0.54	0.20	0.18	0.18 (w=0.49)	0.78	0.87	1.28
50	0.26	0.56	0.54	0.27	0.27	0.24 (w=0.52)	0.81	0.85	1.15
90	0.39	0.55	0.54	0.40	0.41	0.39 (w=0.50)	0.67	0.67	0.82

Table 5.7 EERs in verification of combination operators.

Data set	EER [%]								
	Combination operator						μ_R^r	μ_L^r	Euclidian distance
	mean	min.	max.	product	prob.	weighting sum			
20	3.27	5.57	4.12	3.33	2.52	2.52 (w=0.49)	8.09	7.37	17.5
30	3.33	6.65	4.44	3.33	3.29	3.33 (w=0.51)	9.58	8.44	19.4
40	4.17	7.12	5.01	4.57	3.76	4.15 (w=0.49)	9.69	9.35	21.8
50	5.25	8.65	6.36	5.66	5.09	5.11 (w=0.52)	10.60	11.92	23.3
90	8.78	11.33	10.30	9.03	8.90	8.78 (w=0.50)	13.49	14.97	29.2

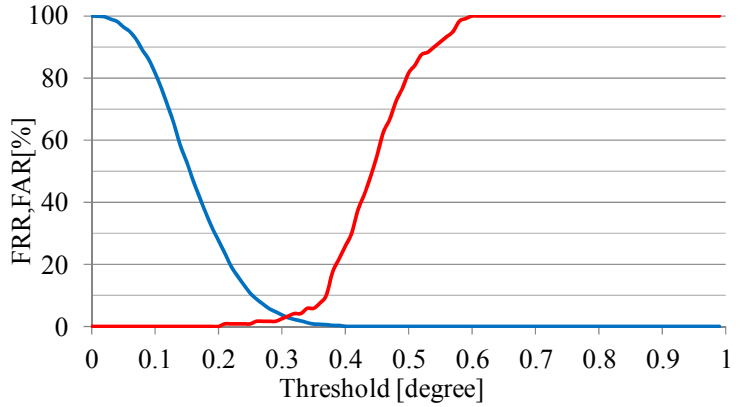

(a) 20 volunteers

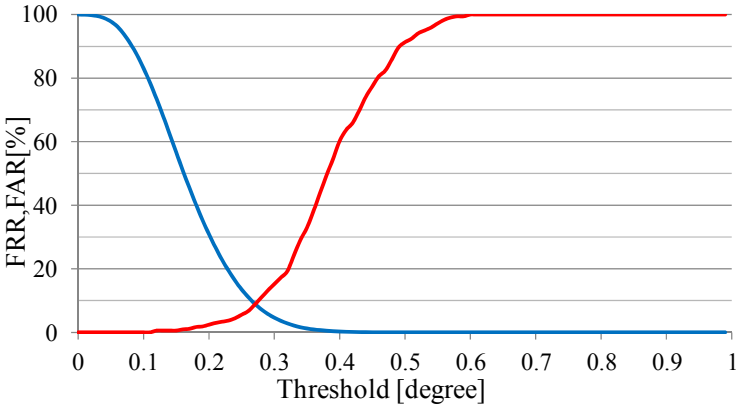

(b) 90 volunteers

Figure 5.13 Fuzzy membership functions for personal authentication.

We compared the proposed method with the biometrics based on walking. The proposed method achieved 12.7% FRR in 50 subjects. Considering past recognition systems by walking data, Ref. [62] achieved 85% recognition rate (15% FRR) in 10 subjects. The comparison method has authenticated person based on image matching between acquired footprints and template. Ref. [63] achieved 4.3% FAR and 65.1% FRR in 8 subjects. The method used center of pressures trajectory of one foot for authentication. The center of pressure is modeled by Hidden Markov Model. And Ref. [53] did 0.14% FAR and 1.36% FRR in 11 subjects. The method used both of footprint and center of pressure trajectory. The method calculated two authentication scores from footprint based on template matching and center of pressure based on Hidden Markov Model. Then a LM learning method weighed

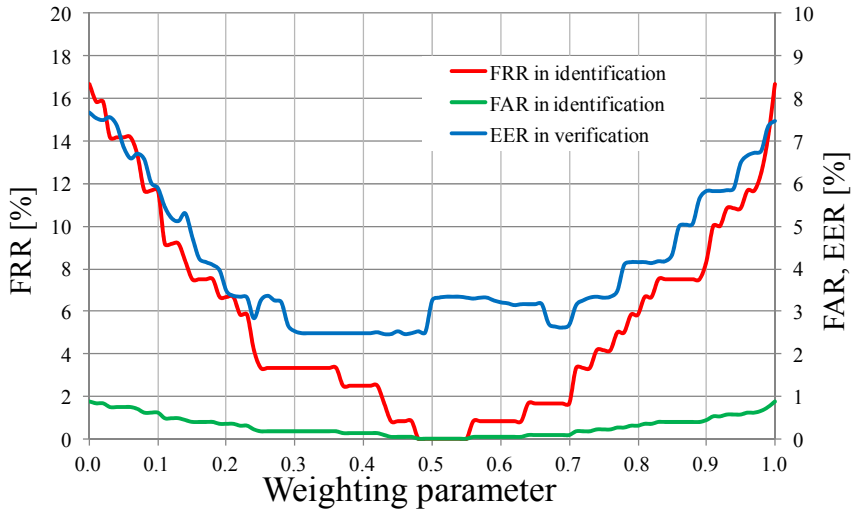

(a) 20 volunteers

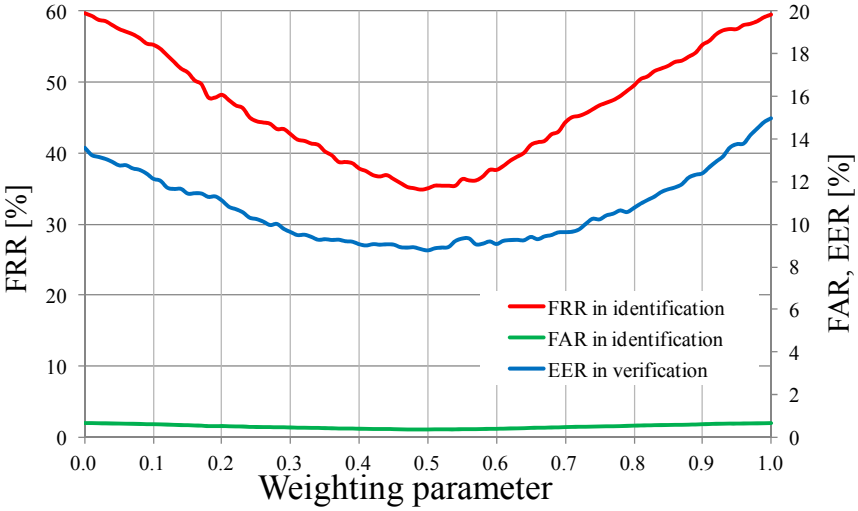

(b) 90 volunteers

Figure 5.14 Authentication performances on weighting sum operator.

each score, and the method calculated authentication score by weighted sum operation. Our method achieved the lowest FRR among these methods. Thus, our method aided by fuzzy logic would be a stepping stone future footprint biometric system.

Table 5.8 Volunteer information of performance test with slipper.

#	*Age* [*year*]	*Gender*	*Body height* [*cm*]	*Body weight* [*kg*]
1	24	Male	165	58
2	23	Male	172	63
3	22	Male	173	60
4	23	Male	170	81
5	24	Male	160	44
6	22	Male	171	62
7	22	Male	169	62
8	24	Male	175	62
9	23	Male	172	70
10	23	Male	162	48
11	23	Male	173	63

5.6 Discussions

From our experimental results, there was no great difference between the authentication performances by using right sole ($\mu_R^r\left(X_R^S\right)$) and left sole ($\mu_L^r\left(X_L^S\right)$). Furthermore, the best weighting parameter was obtained almost 0.5. However, the authentication performances were improved by using the combined fuzzy degree. From the fact, we consider that the personal authentication method based on the combined fuzzy degree can use for other biometrics authentication system to improve its performance.

In all operators, authentication performances were deteriorated with increasing the number of subjects. Our method totally employed seventy eight features from both sole pressures. However, the normalized CSPs were extracted from CSP trajectory, and the trajectory explains about a pattern of dynamics of weight shift. Thus, we treat the nine normalized CSPs as one feature. In the same way, we consider that the normalized HSPs and areas as one feature in each. Thus, thirty features were substantially used for authentication. By the limit of dimensionality, we consider that authentication performances were deteriorated on over thirty volunteers.

In the experiments, all volunteers waked with socks or bare feet. However, in the real situation, subject might be ware shoes. To test our method for shoes, we authenticate slippered person wearing slippers as a preliminary experiment for shoes. In this experiment, we employ 11 volunteers shown in Table 5.8. The system took sole pressure distribution with slippers as shown in Figure 5.15. In this figure, *Slippers 1* is thinner type slippers and the thickness is 0.6 cm. On the other hand, *Slippers 2* is thicker one and the thickness is 2.5 cm in heel area and 1.5cm in toe area. Figure 5.16 shows examples of the right footprints of bare foot, *Shipper 1*, and *Slipper 2*. We took the sole pressure data 18 times for a volunteer with bare foot (6 times), *Slipper 1* (6 times) and *Slipper 2* (6 times). We call these data set that *BARE*, *SL1* and *SL2*, respectively. We verified these volunteers by the proposed method with mean operator. First, we tested our proposed method by learning data of each data set. Table 5.9 shows the verification results of each learning data and test data, and Figure 5.17 shows FRR and FAR with threshold parameter change. The proposed method obtained low EER for

the test data of same type data as the learning data. However, we obtained high EER for the other test data. Second, we tested the proposed method by employing two or three type learning data for a volunteer. Table 5.10 shows the verification result of employing two or three type learning data for each volunteer. We obtained low EER when the learning data included the same type data. In addition, we obtained lower EER for the other test than that of employing one test dat. Table 5.11 shows the FAR of threshold parameter was 0.35. From these result, the proposed method was able to reject unauthorized individual being. From these results, we think that to verify walking person wearing shoes, the system needs to employ learning data of various situation.

(a) top view

(b)side view

Figure 5.15 Appearance of thinner type slippers (left) and thicker type slippers (right).

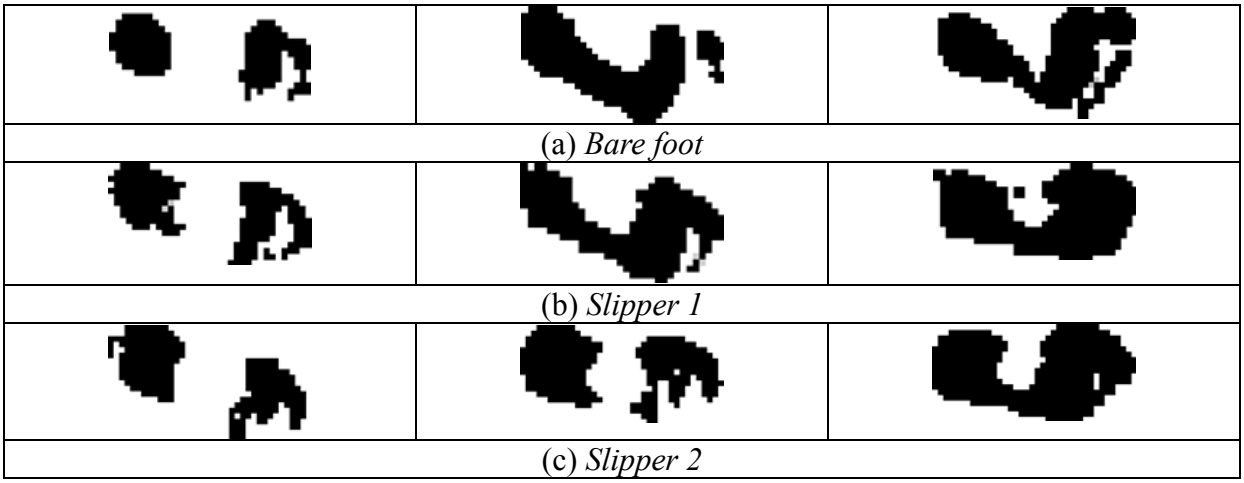

(a) *Bare foot*

(b) *Slipper 1*

(c) *Slipper 2*

Figure 5.16 Examples of footprint with bare foot, *Slipper* 1 and *Slipper* 2.

Table 5.9 Verification results by one learning data set.

Learning data	EER for each test data [%]			*Mean* ± *SD*
	BEAR	*SL1*	*SL2*	
BARE	1.29	23.79	26.7	17.24 ± 13.90
SL1	27.12	1.15	21.14	16.47 ± 13.60
SL2	25.68	12.65	0.15	12.82 ± 12.77

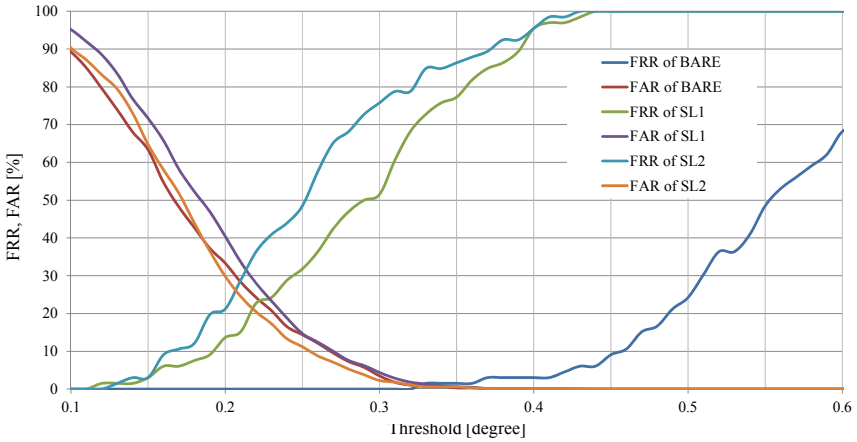

(b) FRR and FAR of learning data, *BARE*.

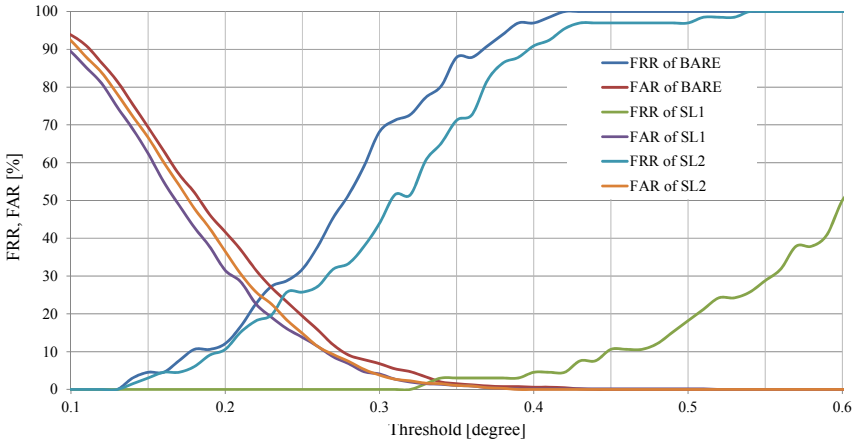

(b) FRR and FAR of learning data, SL1

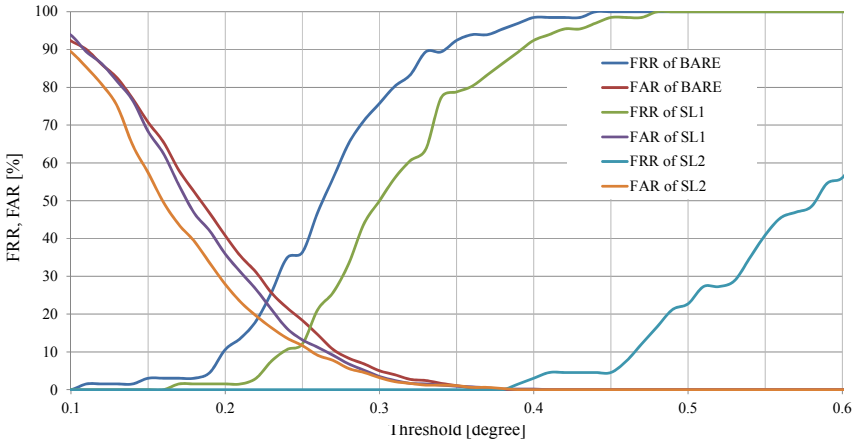

(b) FRR and FAR of learning data, SL2

Figure 5.17 Appearance of thinner type slippers (left) and thicker type slippers (right).

Table 5.10 Verification results by two or three learning data set.

Learning data	EER for each test data [%]			*Mean* ± *SD*
	BEAR	*SL1*	*SL2*	
BEAR and SL1	4.39	2.26	16.97	8.21 ± 7.61
BEAR and SL2	2.88	12.58	2.27	5.91 ± 5.78
SL1 and SL2	19.84	0.83	2.12	7.60 ± 10.62
BEAR, SL1 and SL2	6.44	3.33	2.87	4.22 ± 1.94

Table 5.11 False acceptance rate in parameter was 0.35.

Learning data	EER for each test data [%]			*Mean* ± *SD*
	BEAR	*SL1*	*SL2*	
BARE	0.12	0.00	0.15	0.09 ± 0.08
SL1	0.61	0.15	0.00	0.25 ± 0.32
SL2	0.00	0.15	0.00	0.05 ± 0.09
BEAR and SL1	1.97	1.06	1.06	1.36 ± 0.53
BEAR and SL2	1.21	1.36	0.91	1.16 ± 0.22
SL1 and SL2	2.42	0.91	0.91	1.41 ± 0.87
BEAR, SL1 and SL2	4.09	2.58	1.97	2.88 ± 1.09

5.7 Conclusion

We have proposed a biometric personal authentication system based on fuzzy logic. We employed right and left sole pressure distributions duaring walking. A mat-type load distribution sensor acquired the sole pressure data. In authentication, the biometrics system extracted thirty nine features from each sole pressure data, and it described fuzzy if-then rules with statistically determined fuzzy membership functions in learning process for each feature. A fuzzy degree of both sole pressure data was calculated by combination operators. It was evaluated in the personal authentication. In identification, the system calculated the combined fuzzy degree for every registered person, and it identified walking person as a registered person with the highest fuzzy degree. In verification, we calculated the fuzzy degree for the target person. When the fuzzy degree is higher than a threshold, we verified the walking person as the target person. In the experiments, we identified 0.0% in FRR and 0.0% in FAR, and we verified with 2.52% in EER by the weighted sum operator on 20 subjects. We did with 35.0% in FRR and 0.39% in FAR, and we verified with 8.85% in EER on 90 subjects. Thus, this system achieved good performance on small number of subjects. In it, we consider the six combination operators. The mean operator obtained the lower error rates in authentication. We consider the mean operator is an optimal operator for combining left and right sole pressures for biometric security. In comparison with the other methods by walking data, our method achieved the lowest FRR.

Health monitoring for walking condition is also important research for human healthcare. In the feature, we will improve the performance by optimizing the fuzzy membership functions, and add other biometric feature to the method, and authenticate person by multimodal approach.

6 Conclusion

This dissertation introduced four personal classification systems aided by fuzzy logic. In these methods, human movement was measured to classify the human. To classify human, fuzzy degrees which represented a similarity degree of a category were obtained from developed fuzzy rules and fuzzy membership functions. Then, our systems classifies target objects by the fuzzy degree.

We firstly described the object classification method from distance distribution image as the home security system. In the security system, the TOF camera monitors front of entrance of a house in a day. The system required night vision, human detection and human classification system. For the night vision system, we employed infrared laser TOF camera to record distance distribution data. From the recorded data, the system detected moving objects by fuzzy *k*-means clustering method. The fuzzy *k*-means clustering method automatically determined cluster number *k* from distance and size of clusters. To classify the detected objects, height, thickness, aspect ratio and occupancy of a silhouette were extracted as human characteristics. The system classified the detected object by fuzzy degree determined from these characteristics. In the experiment, we set two TOF cameras to measure distance distribution images. The proposed method equally classified volunteers in the both TOF camera. Thus, we consider that our proposed algorithm is high availability to camera. As the result, the object classification method was good to use for home security system in both of daytime and nighttime.

We secondly described the foot-age estimation method from sole pressure distribution data as a diagnosis and advice system to improve our gait condition. To improve our gait, we need to know our gait condition. However, conventional estimation method such as sports test imposed big physical burden for us. For elderly people, we need to develop a novel estimation method which imposing few physical burden. The foot-age which is age-related indexes was estimated from sole pressure distribution while about 5m walking. The sole pressure data was acquired by portable mat-type load distribution sensor. By analyzing sole pressure data acquired 225 subjects, we found four gait features related to aging. Fuzzy degree of young age, middle age and elderly were decided by learned fuzzy membership functions. Then, the foot-age was estimated from these fuzzy degrees. We developed diagnosis and advice system by comparing the estimated foot-age and real-age. In our experiment, we showed our method estimated foot-age with better mean absolute errors. As the results, we consider that the foot-age estimation method automatic diagnoses and advises to improve our gait condition.

We thirdly described the gait level index estimation method from sole pressure distribution data as diagnosis support system for rehabilitation. In hospitals and medical welfares, an personalized rehabilitation program is made by medical doctors or physical therapists based on gait level of patients. In now, the gait level was evaluated by their experience and subjectively. For a quantitative evaluation, a novel index to evaluate gait level is needed. The system estimated gait level index as the quantitative index from sole pressure distribution while walking. Three gait features such as gait speed, time of double support and gait balance were extracted. We derived fuzzy if-then rules and fuzzy membership function

from deference between the features extracted from patients and commons. The gait level index was estimated by fuzzy MIN-MAX center of gravity method. In our experiments, we estimated gait level index of 10 patients with good correlations of real gait conditions. Moreover, the gait level index classified volunteers to patient and commons with better accuracy than the other classification method. As the result, we consider that estimation method developed a quantitative index to evaluate gait level for rehabilitation field.

We fourthly described the biometric security system based on walking. The walking is the most natural motion in our daily movements, and the system do not retardation us. As the biometric feature we acquired a pair of right and left sole pressure distribution. We extracted gait features based on shape of footprint and weight shift. From these features, fuzzy degree of similarity and effectiveness were determined by statistics learned fuzzy membership functions. The system authenticated person by combined fuzzy degree of right and left sole pressure. In our experiment, we employed 90 volunteers and authenticated them with better accuracy than the other biometric method based on walking. As the result, we consider that our method aided by fuzzy logic was good to use for security system.

Thus, it was established that the classification system is applicable for security systems and health condition estimation system. Furthermore, the four systems based on classification system aided by fuzzy logic obtained better accuracy than other method. From this fact, we consider that the fuzzy logic is good choice to develop a classification system for human.

References

[1] T. Moeslund, A. Hilton and V. Kruger, "A survey of advances in vision-based human motion capture and analysis," Computer Vision and Image Understanding, vol. 104, pp. 90-126, 2006.

[2] L. Herda, P. Fua, R. Plankers, R. Boulic and D. Thalmann, "Skeleton-based motion capture for robust reconstruction of human motion," Proc. of Computer Animation 2000, pp. 77-83, 2000.

[3] N. Dalal and B. Triggs, "Histograms of oriented gradients for human detection," Proc. of IEEE Computer Society of Conf. on Computer Vision and Pattern Recognition 2005, vol. 1, pp. 886-893, 2005.

[4] A. Hirono, T. Nakahara, H. Fujii and S. Hurukawa, "Measuring system for distribution of people in office," Journal of MEW Technical Report, no. 81, pp. 18-23 2003.

[5] T. Moeslund and E. Granum, "A survey of computer vision-based human motion capture," Journal of Computer Vision and Image Understanding, vol. 81, issue 3, pp. 231-268, 2001.

[6] J. Krumm, S. Harris, B. Mayers, M. Hale and S. Shafer, "Multi-camera multi-person tracking for easy living," Proc. of 3rd IEEE Workshop on Visual Sureillance, pp. 3-10, 2000.

[7] W. Niu, J. Long, D. Han and Y. Wang, "Human activity detection and recognition for video surveillance," Proc. of Multimedia and Expo, 2004. ICME '04. 2004 vol. 1, pp. 719-722, 2004.

[8] F. Chan, J. Chen and Y. W. Moon, "Fast construction of object correspondence in stereo camera system: an example to human face capturing system," Proc. of IEEE Workshop on Motion and video Computing, pp. 1-6 2008.

[9] S. Ikemura and H. Fujiyoshi, "Human detection by Haar-like filtering using depth information," Proc. of 21st Int. Conf. on Pattern Recognition, pp.813-816. 2012.

[10] K. Ho, K. Taniguchi, K. Asari, K. Kuramoto, S. Kobashi and Y. Hata, "Automated detection of people distribution by 3D camera," Proc. of 2010 World Automation Con., pp. 1-6, 2010.

[11] S. Morita, K. Yamazawa, M. Terazawa and N. Yokoya, "Networked remote surveillance system using omnidirectional image sensors," IEICE Trans. on Information and Systems, vol. J88-D-II, no. 5, pp. 864-875, 2005.

[12] H. B. Geoffrey and J. H. David, "Isodata: a method of data analysis and pattern classification," Stanford Research Institute, Menelo Park, United States. Office of Naval Research. Information Sciences Branch, 1965.

[13] Y. Ehara and S. Yamamoto, *Introduction to Clinical Gait Measurement*, 1st ed., Ishiyaku Publications, Inc., 2008 (in Japanese)

[14] D. A. Winter, Biomechanics and motor control of human movement, Wiley, 3rd Ed. 2004.

[15] T. Cloete and C. Scheffer, "Benchmarking of a full-body inertial motion capture system for clinical gait analysis," Int. conf. on IEEE, Engineering in Medicine and Biology Society, 2008, pp. 4579-4582, 2008.

[16] J. Mantyjarvi, M. Lindholm, E. Vildjiounaite, S. M. Makela, and H. A. Ailisto," Identifying users of portable devices from gait pattern with accelerometers," Int. conf. on IEEE, Acoustics, Speech, and Signal Processing, 2005, no. 2, pp. ii973-ii976, 2005.

[17] A. Fukayama, M. Sawaki, H. Murase, and N. Hagita, "Age estimation from dynamic features of gait," IEICE Trans. on Information and Systems, Pt.2, vol. J84-D-2-7, pp. 1522-1526, 2001 (in Japanese).

[18] M. J. Hessert, M. Vyas, J. Leach, K. Hu, L. A. Lipsitz, and V. Novak, "Foot pressure distribution during walking in young and old adults, " Jounal of BMC Geriatrics, 2005, vol. 5, 2005.

[19] K. Yonekawa, T. Yonezawa, J. Nakazawa, and H. Tokuda, "FASH: detecting tiredness walking people using pressure sensors," Proc. of MobiQuitous 2009, pp. 1-6, 2009.

[20] S. Shimada and Y. Aoyagi, "Quantitative evaluation of gait ability in elderly individuals based on foot contact area," IEICE Trans. on Information and Systems, Pt.1, vol. J82-D-1, no. 7, pp. 796-799, 2004 (in Japanese).

[21] K. Sudo, S. Shimada, S. Ohtsuka, and A, Tomono, "Analysis of differences in walking pattern, due to age, using a pressure sensor array," Technical report of IEICE, MBE96-84, vol. 96, issue 379, pp. 19-26, 1996.

[22] J. Yamato, S. SHimada, S. Ohtsuka, and A. Tomono, "Development of gait analyzer using large area pressure sensor array," IEICE Trans. on Information and Systems, Pt.2, vol. J84-D-2, no. 12, pp. 380-389, 2001 (in Japanese).

[23] L. A. Zadeh, "Fuzzy sets," J. of Information and Control, 8-3, pp. 338-353, 1965.

[24] L. A. Zadeh, "The role of fuzzy logic in the management of uncertainty in expert systems," Fuzzy Sets and Sysems, vol. 11, issue 1-3, pp. 199-227, 1983.

[25] R. Kruse, J. Gebhardt, and F. Kalawonn, Foundations of fuzzy systems, 1st ed. John Wiley & Sons Ltd. 1994.

[26] J. R. Gage, "An overview of normal walking," Instructional Course Lectures 39, 291-303, 1990.

[27] C. A. Downey, Observational Gait Analysis Handbook, 1989.

[28] Gabinet Office, Government of Japan, Annual report on the aging society in 2012, 2012 (in Japanese).

[29] J. H. Burridge, P. N. Taylor, S. A. Hagan, Duncan E Wood, Ian D Swain, "The effects of common peroneal stimulation on the effort and speed of walking : a randomized controlled trial with chronic hemiplegic patients," Clin Rehabil, vol.11, issue. 3, pp. 201-210, 1997.

[30] M. H. Granat, D. J. Maxwell, A. C. B. Ferguson, K. R. Lees, J. C. Barbenet, "Peroneal stimulator ; evaluation for the correction of spastic drop foot in hemiplegia. " Arch Phys Med Rehabil, vol. 77, issue. 1, pp. 19-24, 1996.

[31] H. Barbeau, M. Visintin, "Optimal outcomes obtained with body-weight support combined with treadmill training in stroke subjects." Arch Phys Med Rehabil, vol. 84, issue. 10, pp. 1458-1465, 2003.

[32] C. M. Dean, C. L. Richards, F. Malouin. "Task-related circuit training improves performance of locomotor tasks in chronic stroke：a randomized, controlled pilot trial." Arch Phys Med Rehabil, vol. 81, issue. 4, pp.409-417, 2000.

[33] C. Detrembleur, A. Renders, T. Willemart, A. V. D. Hecke "Usefulness of gait analysis combined with motor point block in a stroke patient." Acta Neurol Belg, vol. 100, issue. 2, pp. 107-110, 2000.
[34] Y. Kijima, "Definition of independence level for those who is independent for gait at indoor and outdoor -Evaluation of two action gait for hemiplegia by the wearable postural measuring system," Rigakuryouhougaku, vol. 37, 2010.
[35] M. Nakashima, "Relationship between gait level of independence and BMI, knee extension muscle strength, balance ability for the elder who has the knee osteoarthritis," Rigakuryouhou, vol. 13, pp. 21-26, 2006 (in Japanese).
[36] T. Narita, "Gait speed about gait independence in facility for hemiplegia patient," Rigakuryouhoukagaku, vol. 23, issue. 3, pp.419-424, 2008 (in Japanese).
[37] A. Hershkovitz, "Mobility assessment of hip fracture patients during a post-acute rehabilitation program" Arch Gerontol Geriatr, vol. 55, issue. 1, pp. 35-41, July 2012.
[38] J. E. Graham, "Walking Speed Threshold for Classifying Walking Independence in Hospitalized Older Adults," Physical Therapy, vol.90 no.11, pp.1591-1597, November 2010.
[39] E. A. Mamdani, “Application of fuzzy algorithm for control of simple dynamic plant,” Proc. of the Institution of Electrical Engineers, vol. 121, issue 12, pp. 1552-1558, 1974.
[40] N. Cristianini, and J. Shawe-Taylor, "An introduction to support vector machines and other kernel based methods." Cambridge University Press, Cambridge, 2000.
[41] G. Lanckriet, N. Cristianini, P. Bartlett, L. Ghaoui and M. Jordan, "Learning the kernel matrix with semi-definite programming." Proc 19th Int Conference Machine Learning, pp. 323-330, 2002.
[42] H. Abdi and L. J. Williams, "Principal component analysis." Wiley Interdisciplinary Reviews: Computational Statistics, vol.2, pp. 433–459, 2010.
[43] T. Jolliffe, "Principal Component Analysis," Series: Springer Series in Statistics, 2nd ed., Springer, NY, 2002, XXIX, vol. 487, pp. 28. 2002.
[44] S. Liu and M. Silverman, “A practical guide to biometric security technology,” IT Professional, vol. 3, issue 1, pp. 27-32.
[45] A.K. Jain, A. Ross, and S. Prabhakar, “An introduction to biometric recognition,” IEEE Trans. on Circuits and Systems for Video Technology, vol. 14 no.1,pp. 4-20, 2004.
[46] Biometrics security consortium (ed.), Biometric security technology handbook, 1st edn. ,Ohmhsa, Tokyo, Japan, 2006, (in Japanese)
[47] K. Ito, H. Nakajima, K. Kobayashi, T. Aoki, and T. Higuchi, “A fingerprint matching algorithm using phase-only correlation,” IEICE Trans. Fundamentals, vol. E87-A, no.3, pp. 682-691, 2004.
[48] X. Chen, J. Tian, and X. Yang, A new algorithm for distorted finger prints matching based on normalized fuzzy similarity measure, IEEE Trans. on Image processing, vol. 15, no. 3, pp. 767-776, 2006.
[49] A. Kholmatov and B. Yanikoglu, “Identity authentication using improved online signature verification method,” Patten Recognition Letters, vol. 26, no. 15, pp. 2400-2408, 2005.

[50] D.A. Reynolds and R.C. Rose, “Robust text independent speaker identification using Gaussian mixture speaker models,” IEEE Trans. on Speech and audio processing, vol. 3, no. 1, pp. 72-83, 1995.

[51] D.K. Wagg and M.S. Nizon, “On automated model-based extraction and analysis of gait,” Proc. of the 6th IEEE Int. Conf. on Automatic Face and Gesture Recognition, Korea, pp. 11-16, 2004.

[52] L. Wang, H. Ning, T. Tan, and W. Hu, “Fusion of static and dynamic body biometrics for gait recognition,” IEEE trans. on Circuts and Systems for Video technology, vol. 14, no. 2, pp. 149-158, 2004.

[53] J. Mantyjarvi, M. Lindholm, E. Vildjiounaite, S.-M. Makela, and H. A. Ailisto, “Identifying users portable devices from gait pattern with accelerometers,” IEEE, ICASSP’05, vol. 2, pp. ii/973-ii/976, 2005.

[54] J. W. Jung, Z. Bien, and T. Sato, “Person recognition method using sequential walking footprints via overlapped foot shape and center-of- pressure trajectory,” IEICE Trans. Fundamentals, vol. E87-A, no. 6, pp. 1393-1399, 2004.

[55] G. Qian, J. Zhang, and A. Kidane, “People identidication using gait via floor pressure sensing and analysis,” Proc. of the 3rd European Conf. on Smart sensing and Context, pp. 83-98, 2008.

[56] M.D. Addlesee, A.H. Jones, F. Livesey, and F. S. Samaria, “The ORL active floor,” IEEE Personal Communications, vol. 4, no. 5, pp. 35-41, 1997.

[57] R. J. Orr and G. D. Abowd, “The smart floor: a mechanism for natural user identification and tracking,” Proc. of the 2000 Conference on Human Factors in Computing Systems , 2000.

[58] T. Yamakawa, K. Taniguchi, T. Momen, S. Kobashi, K. Kondo, and Y. Hata, “Biometric personal identification based on foot pressure change,” Proc. of Int. Conf. on Soft Computing and Human Sciences, pp. 83-86, 2007.

[59] V. Conti, C. Militello, F. Sorbello, S. Vitabile, “A frequwncy-based approach for features fusion in fingerprint and iris multimodal biometric identification,” IEEE Trans. on SMC-C, vol. 40, no. 4, pp. 384-395, 2010.

[60] A. K. Jain, S. Prabhakar, and S. Chen, “Combining multiple matchers for a high security fingerprint verification system,” Patten Recognition Letters, vol. 20, no. 11-13, pp. 1371-1379, 1999.

[61] J. Kittler, Y.P. Li, J. Matas, and M.U.R. Sanchez, “Combining evidence in multimodal personal identity recognition system,” Patten Recognition Letters, vol. 18, no. 9, pp. 845-852, 1995.

[62] K. Nakajima, Y. Mizukami, K. Tanaka and T. Tamura, “Footprint-based personal recognition,” IEEE Trans. on Biomedical Engineering, vol. 47, no. 10, pp. 1534-1537, 2000.

[63] J. W. Jung, Z. Bien, S. W. Lee, and T. Sato, “Dynamic-footprint based person identification using mat-type pressure sensor,” Proc. of 25th Int. Conf. of the IEEE EMBS, pp. 17-21, 2003.

List of Publications of the Author

Chapter 2

1) T. Takeda, K. Kuramoto, S. Kobashi and Y. Hata, "A fuzzy moving object estimation using infrared TOF camera," Int. J. of Intelligent Computing in Medical Sciences and Image Processing, vol. 5, no. 2, pp. 147-160, 2013.
2) T. Takeda, K. Kuramoto, S. Kobashi, and Y. Hata, "A fuzzy human detection for security system using infrared laser camera," Proc. of IEEE 43rd Int. Symp. on Multiple-Valued Logic, pp. 53-58, 2013.

Chapter 3

3) T. Takeda, Y. Sakai, K. Kuramoto, S. Kobashi and Y. Hata, "Foot Age Estimation System from Walking Dynamics Based on Fuzzy Logic," Journal of Advanced Computational Intelligence and Intelligent Informatics. (Submitted in Oct. 2013)
4) T. Takeda, Y. Sakai, K. Kuramoto, S. Kobashi, T. Ishikawa and Y. Hata, "Foot age estimation for fall-prevention using sole pressure by fuzzy logic," Proc. of 2011 IEEE Int. Conf. on Systems, Man, and Cybernetics, pp. 769-774, 2011.
5) T. Takeda, Hong Ye, K. Taniguchi, K. Asari, K. Kuramoto, S. Kobashi, and Y. Hata, "Foot age estimation by gait sole pressure changes," Proc. of 2010 IEEE Int. Conf. on Systems, Man and Cybernetics, pp. 1204-1208, 2010.

Chapter 4

6) T. Takeda, Y. Sakai and Y. Hata, "Evaluation of autonomy walk by dynamic foot pressure analysis," Proc. of 2013 IEEE Int. Conf. on Systems, Man and Cybernetics, pp. 3408-3413, 2013.
7) T. Yagi, T. Takeda, K. Sueyoshi, Y. Oshiro and Y. Hata, "Fuzzy estimation system on gait independence level by footprint dynamics," Proc. of the 6th International Conference on Soft Computing and Intelligent Systems and 13th International Symposium on Advanced Intelligent Systems, pp. 1259-1264, 2012.

Chapter 5

8) T. Takeda, K. Kuramoto, S. Kobashi and Y. Hata, "Fuzzy-logic is precise -Its application to biometric system-," Jounal of Scientia Iranica, vol. 18, issue. 3, pp. 655-662, june 2011.
9) T. Takeda, K. Kuramoto, S. Kobashi and Y. Hata, "On optimal operator for combining left and right sole pressure data in biometrics security," Journal of Hindawi - Advances in Fuzzy Systems, vol. 2013, pp.1-10, 2013.

10) T. Takeda, S. Kobashi, K. Kuramoto and Y. Hata, "Biometrics personal identification by wearable pressure sensor," Proc. of 2012 Fifth Int. Conf. on Emerging Trends in Engineering and Technology, pp. 120-123, 2012.
11) T. Takeda, S. Kobashi, K. Kuramoto and Y. Hata, "A Challenge to Biometrics by Sole Pressure while Walking," Proc. of 2011 IEEE Int. Conf. on Fuzzy Systems, pp. 1430-1435, 2011.
12) T. Takeda, K. Kuramoto, S. Kobashi and Y. Hata, "Biometrics security by dynamics of left and right sole pressure while walking," Proc. of SPIE Defense, Security and Sensing 2011, pp. 805814-1-11, 2011.
13) T. Takeda, K. Taniguchi, K. Asari, K. Kuramoto, S. Kobashi, and Y. Hata, "Biometric personal identification by dinamics of sole pressure at walking," Proc. of 2010 World Automation Cong., 2010. (online)
14) T. Takeda, K. Taniguchi, K. Asari, K. Kuramoto, S. Kobashi, and Y. Hata, "Biometric Personal Authentication by One Step Foot Pressure Distribution Change by Fuzzy Artificial Immune System," Proc. of 2010 IEEE World Congress on Computational Intelligence, pp. 844-849, 2010.
15) T. Takeda, K. Taniguchi, K. Asari, K. Kuramoto, S. Kobashi, and Y. Hata, "Biometric personal authentication by one step foot pressure distribution change by load distribution sensor," Proc. of 2009 IEEE Int. Conf. on Fuzzy Systems, pp. 906-910, 2009.

Award

1) World Automation Congress, Best Paper 2nd place Award in IFMIP, Takahiro Takeda, Kazuhiko Taniguchi, Kazunari Asari, Kei Kuramoto, Syoji Kobashi, and Yutaka Hata, 2010.